2010

FIELD SCALE BROMIDE TRANPORT AS A FUNCTION OF PRECIPITATION AMOUNT, INTENSITY AND APPLICATION TIME DELAY

Vicente Vasquez
University of Kentucky, vicente.vasquez@agrsci.dk

ABSTRACT

FIELD SCALE BROMIDE TRANPORT AS A FUNCTION OF PRECIPITATION AMOUNT, INTENSITY AND APPLICATION TIME DELAY.

Rapid and deep transport of solutes in soils can potentially pollute groundwater resources. Field estimates of solute leaching depth based on randomized sampling provide extremely variable field average estimates that confound the treatment effects of the leaching study with the high spatial variation of soil hydraulic properties. The purpose of this study was to investigate the spatial scale of variation of solute (Bromide) leaching depth, and apply this scale of variation to study the leaching depth of Bromide as a function of a sinusoidal application of transport causing factors, i.e., rainfall amount, intensity and application time delay. Solute leaching depth varied over different spatial scales. The deepest leaching was observed on plots where the Br center of mass ranged from 19-30 cm depth. Deep leaching occurred with large quantities of low intensity precipitations (5.5 to 6 cm/day) and short time delays ($\leq$ 17 hours), respectively. The hydraulic gradient presented cyclic variation at 8 m wavelength across the 10-30cm depth compartment. Spectral analysis indicated that spatial variation of the leaching depth was mainly affected by precipitation amount and intensity and only a small portion of the leaching depth variation was caused by time delay. Cross-spectral analysis identified common cyclic variation between the Br leaching depth and precipitation amount, intensity and time delay over 32, 32 and 8 m wavelengths, respectively. Simulated Br concentration over depth and horizontal distance and soil water matric potential ψ_m were in good agreement with experimental observations, the latter revealing a satisfactory Br and water mass balance.

KEYWORDS: Bromide Leaching Depth, Application Time Delay, Solute and Water Transport, Variation Scale, Spectral Analysis.

Vicente Vasquez

November 10, 2010

FIELD SCALE BROMIDE TRANSPORT AS A FUNCTION OF PRECIPITATION AMOUNT, INTENSITY AND APPLICATION TIME DELAY

By

Vicente Vasquez

Dr. Ole Wendroth
Director of Thesis

Dr. Charles Dougherty
Director of Graduate Studies

November 10, 2010

RULES FOR THE USE OF THESES

Unpublished theses submitted for the Master's degree and deposited in the University of Kentucky Library are as a rule open for inspection, but are to be used only with due regard to the rights of the authors. Bibliographical references may be noted, but quotations or summaries of parts may be published only with the permission of the author, and with the usual scholarly acknowledgments.

Extensive copying or publication of the thesis in whole or in part also requires the consent of the Dean of the Graduate School of the University of Kentucky.

A library that borrows this thesis for use by its patrons is expected to secure the signature of each user.

Name Date

_____

_____

_____

_____

_____

_____

_____

_____

_____

THESIS

VICENTE VASQUEZ

The Graduate School

University of Kentucky

2010

FIELD SCALE BROMIDE TRANPORT AS A FUNCTION OF PRECIPITATION AMOUNT, INTENSITY AND APPLICATION TIME DELAY.

THESIS

A thesis submitted in partial fulfillment of the
requirements for the degree of Master of Science in the
College of Agriculture
at the University of Kentucky

By
Vicente Vasquez
Lexington, Kentucky

Director: Dr. Ole Wendroth, Associate Professor of Soil Science

2010

ACKNOWLEDGEMENTS

The following thesis was made through a combined effort involving many persons within the Department of Plant and Soil Sciences at the University of Kentucky but special thanks should be given to my advisor, Dr. Ole Wendroth, for his constant encouragement, guidance and dedication to this project both on the field work, and on the writing process. I am also very thankful to Dr. Chris Matocha for his unconditional collaboration during the chemical analysis and the design of the lab protocol for the sample analysis. My deep appreciation is given to Dr. Karathanasis and Dr. Witt for all their helpful suggestions on the early stages of this project.

Financial support of this project and my assistantship through the University of Kentucky College of Agriculture SB 271 Water Quality Program is greatly appreciated.

I owe a debt of gratitude to many technicians involved in this project but especially to Martin Vandiviere, Jim Crutchfield, Tami Smith and Jason Walton because of their enormous patience and helpful comments during the many sample analysis in this project.

To my fellow graduate students, Paul Schumaker, Jarrod Miller, Jared Edwards, Eduardo Rienzi, Susmitha Nambuthiri, and Andres Nunez, Nathan Hamilton and Soraya Alvarado for all their support, encouragement and collaboration on the most stressing moments of this project.

To my wife Ana and sister Samantha, whose unconditional support and encouragement were fundamental in the culmination of this project.

Table of Contents

List of Tables

List of Figures

List of files

Field scale Bromide transport as a function of precipitation amount, intensity and application time delay (1.5 Mb)

1. Introduction

The sustainability of modern agriculture relies heavily on the application of herbicides, pesticides and fertilizers to the bare soil surface or to crop stands at various stages. The appropriate timing of agrochemical application may benefit from an adequate soil moisture content to allow solute redistribution in the soil, facilitate hydrolysis, nitrification and other important soil processes to activate the solutes applied. However, an inherent risk to contaminate surface and ground water bodies is associated with agrochemical applications to soils and crop stands. Moreover, it is commonly assumed that a heavy rainfall shortly following an application will cause the majority of the solute applied to be washed out of the targeted zone to greater depths in the soil profile and into ground and surface waters (Evans et al., 1998; Shipitalo et al., 2000; Walker et al., 2005).

The main mechanisms by which water and solutes are infiltrated and possibly transported out of the intended domain are according to Beven and German (1982): 1. Overland flow or runoff for superficial water bodies, 2. leaching into deep layers and out of the root zone, and 3. preferential or non-equilibrium flow.

These mechanisms have the potential to contaminate superficial and groundwater bodies when the applied agrochemicals quickly bypass the soil matrix where biodegradation, plant uptake, and other mechanisms could decompose these pesticides to less harmful metabolites or possibly make them irreversibly adsorbed to the soil matrix (Brady and Weil, 2003).

In this study, the potential risk of groundwater contamination is determined by the leaching depth of a solute (Center of Mass) assuming that solute leaching depends on the

coincidence of surface application of an agrochemical and the subsequent amount, intensity and timing (time interval between solute application and precipitation) of precipitation, as well as the spatial variation of soil transport properties and the current soil profile moisture conditions.

2. Literature Review

The literature review in this thesis is divided in two sections. The first section reviews a basic concept to describe water and solute transport phenomena in soils, and research efforts that have demonstrated the importance of the precipitation amount, intensity and application time delay (Mc Lay et al., 1991) on the leaching depth of solutes. In the second section the impact of field scale spatial variability of soil hydraulic properties on the quantification of solute leaching depth is reviewed. It also highlights the opportunity to provide site specific estimates of field scale solute transport with spatially designed experiments and the use of statistical techniques focusing on spatial coordinates and covariance structure of observations, rather than on the traditional randomized layout underlying ANOVA.

2.1. Water and Solute Transport Phenomena

Beven and German (1982) describe transport phenomena and their dependence on precipitation intensity and soil infiltration rate by dividing the pore domain into micro and macropores. Three different scenarios are presented in their work:

a) Precipitation $P(t)$ < Infiltration $I_1(t)$

where $I_1(t)$ denotes the maximum infiltration rate into surface connected micropores that can absorb all the incoming precipitation. Therefore no surface ponding, macropore flow or runoff occurs.

b) Precipitation rate exceeds the infiltration into micropores

$I_1(t) < P(t) < I_1(t) + S_1(t)$

In this case, micropores cannot take up all the incoming precipitation and small scale surface runoff and ponding occur. Infiltration occurs through micropores as well as surface connected macropores $S_1(t)$. Once macropore flow is substantial, lateral micro and macropore infiltration will be initiated.

c) Onset of Runoff

$P(t) > I_1(t) + S_1(t)$

Precipitation is larger than infiltration into micro and macropores.

The effect of rainfall intensity and application timing in relation to the three case scenarios above is not well understood. For instance, on a study characterizing the movement of herbicides in different tillage systems on a Maury Silt loam soil, Sanders (1990) observed that more than 90% of the initial mass of Atrazine, Cyanazine and Simazine applied were lost through surface runoff when a 26-mm-rain fell one day after herbicide application. Comparable results of herbicide loss (90%) were obtained when the same study was replicated a year later, i.e., one month after herbicide application

when the first 13 mm rain fell 7 days after application and three 40 mm rain events followed within that month. However, initial soil water content was not measured in this study. These findings (Sanders, 1990) suggest that the time between application and following rainfall (application time delay) is critical for herbicide loss through runoff. Moreover, the combined effect of rainfall intensity (rainfall capable of producing runoff) and application timing in the first week after application determines the fate and transport of pesticides in soils and its partitioning to either runoff or infiltration (Sanders 1990).

Non-equilibrium transport or macropore flow (Beven and German, 1982) has been reported in experiments by Ehlers (1975) who noticed faster response of tensiometers deeper in the soil profile under No-till compared to tilled plots shortly after rainfall, suggesting that water and solute transport bypassed large portions of the soil matrix probably due to greater stability and connectivity of macropores in the no-till soil.

Studying the main factors governing preferential flow in a forest soil, Legout et al. (2009) identified both the initial soil water content and the precipitation intensity as the main factors controlling the onset of preferential flow. They also concluded that preferential flow and convective flow coexist in the soil matrix, and despite the fact that only 11% of the total porosity was involved in preferential flow, this fraction was responsible for the rapid transport of more than 17% of the solute mass applied.

In leaching studies by Kung et al. (2000 a; b), it was suggested that the pore spectrum responsible for preferential flow became hydraulically more active as the soil water content SWC increased, and that preferential flow dynamics shifted towards this larger pore spectrum as the soil became wetter during precipitation.

In a column study (30 cm diameter and 90 cm long) evaluating the water table depth and rainfall time delay effect on leaching of Br^- and NO_3^-, Jiang et al. (1997), concluded that water table depth affected the breakthrough curve patterns BTCP for both solutes. In this experiment a shallower water table had larger solute concentration peaks and caused earlier arrival than deeper water table initial conditions. This latter finding was attributed to the unsaturated hydraulic conductivity function, which increases with increasing soil water content. However, rainfall time delay had no effect on the BTCP in the study by Jiang et al. (1997) probably due to the dominating effect of the water table depth which for all treatments was not deeper than 35 cm. However, several leaching studies with a variety of initial soil profile conditions, precipitation amounts and intensities have encountered that short time delays cause deeper transport of chemicals in the soil than long delays (McLay et al., 1991; Evans et al., 1998; Shipitalo et al., 2000; Walker et al. 2005). The latter findings have been suggested to be a result of both macropore flow produced by high precipitation intensities (case b and c in the above infiltration scheme by Beven and German, 1982) and the reduced availability of solutes for rapid and deep transport due to greater solute diffusion from inter-aggregate pore space (larger pores) into the intra-aggregate pore space (smaller pores). For instance, longer application time delays cause greater solute diffusion into the intra-aggregate pore space, which in turn makes a significant amount of solute not available for rapid and deep transport through macropore flow (McLay et al., 1991).

In summary, it is necessary to explore the effects that application time delay combined with precipitation amount and intensity have on the leaching depth of solutes under different initial soil water content conditions.

The hypothesis of this project is that shallower leaching is caused by long time delays when precipitation amount and intensities remain invariable, i.e., the longer the time between solute application and the next rainfall event, the less available the solute is for deep leaching.

2.2. Spatial Variability of Soil Transport Parameters

Soil water and solute transport modeling through the vadose zone is complex because of temporal and spatial variability of soil hydraulic properties and transport characteristics that usually change over orders of magnitude at field scale (Netto et al., 1999). Geostatistical analysis of the spatial heterogeneity of soil transport parameters is widely used to investigate their spatial correlation structure (Netto et al., 1999). The identification and modeling of a spatial covariance structure of hydraulic parameters is the basis for stochastic simulations of the mass transfers in soil including preferential flow (Ünlü et al., 1990; Neto et al., 1999).

For instance, the statistical parameters of the semivariance (sill, nugget) and the correlation scale (range) of the natural log of saturated hydraulic conductivity, pore size distribution parameter α (slope of the natural log-transformed unsaturated hydraulic conductivity function) and the specific water capacity C were successfully described by Ünlü et al. (1990), demonstrating its application in stochastic modeling of field scale transient unsaturated flow.

Kazemi et al. (2008) described the spatial variability of soil transport parameters in a Udipsamment soil using the convection-dispersion equation to describe Bromide and

Atrazine unsaturated transient flow over a 0.1 ha field. They found spatial correlation ranges of 20 and 12 m for the Bromide pore water velocity ***(v)*** and dispersion coefficient ***(D)***, respectively, when core samples were taken every 2 m in the North-South direction and every 4 m in the East-West direction inside a 28 by 28 m field.

Netto et al. (1999) studying the local variability of soil water content and solute concentrations on a glacial till soil found random behaviour of these two variables. Their findings were supported by the heterogeneity of both soil hydraulic properties and geochemistry of the experimental site. However, their sampling design had only 10 observations along a 1.2 m trench in 10 cm depth increments down to 110cm. This sampling procedure was repeated six times, each time after 70-90 mm of precipitation. Moreover, each trench was located approximately 5-10 m apart of each other but observations of soil water content and solute concentration were combined in one dataset of 72 observations for each depth regardless of the time of sampling. Not surprisingly, random spatial variation for solute concentration and water content were reported.

Hassan et al. (1983) compared a 2.1 and a 7.9 cm diameter core sample support for water content and chloride concentration sampled in 10 cm increments down to 150 cm depth in a Typic Torrifluvent. The 2.1 cm diameter cores resulted in approximately 2.4 to 4 times larger variance than the 7.9 cm diameter cores for the two variables when six 2.2 m^2 plots were sampled three times with each auger.

Zhang et al. (1990) investigated the effect of the sample support on the variance of five experimental datasets and concluded that both the support and the domain size are effectively combined in the semivariogram function, i.e., small sample support or point

observations will manifest an increase in the nugget and sill when compared to observations averaged over a small area. However, they pointed out that the semivariogram function is rarely known a priori.

In another paper by Zhang et al. (1994), the semivariogram function was successfully applied to determine optimum plot shape and size in terms of minimizing the sample variance and cost. They concluded that sample plots having their largest dimension in the direction of the largest variability will give more accurate results (less variable) than plots with other orientation relative to the direction of major variation.

A leaching study by Hosang (1993) found spatial correlation ranges of approximately 40 m distance for dispersivity λ, mean soil water content and mobile porosity in a typical loess soil when profiles of 100 cm depth were sampled in 10 cm depth increments. Each core was taken at 20 m distance of each other along a 400 m long transect on two sampling campaigns. However, a poor correlation between the spatially variable transport parameters and measured soil physical properties, i.e. % sand, % clay and bulk density prevented the estimation of soil transport parameters based on easily available soil physical properties for this experiment.

Wendroth et al. (1999b) developed a state-space prediction model for soil water content time series and found out that the prediction uncertainty increased for periods where precedent observations of soil water content showed either very short ranges of spatial correlation or no autocorrelation at all. Studying the spatial association among soil hydraulic properties, soil texture and geoelectrical resistivity, Wendroth et al. (2006) demonstrated that state-space models which incorporate observations of spatial

autocovariance behavior provide greater precision to describe the spatial process of hydraulic property coefficients than that achieved by pedo-transfer functions alone.

In conclusion, the scale of variation of soil properties affecting solute leaching is not known a priori. Describing solute leaching for a given scale of interest still remains a challenging task (Ellsworth and Boast, 1996). Therefore, for any leaching study conducted in the field, randomly assigning treatments to a spatially variable soil would confound the real treatment effect with the spatially variable soil transport parameters and would probably result in highly variable estimates of average leaching behavior for a field. An alternative approach to the randomization of treatments, even when the scale of spatial variation of soil transport parameters is not known, is the application of such treatments in a spatially continuous cyclic pattern. The imposed cyclic pattern of treatments would identify zones along the spatial domain where correlations between treatments and response variables, i.e. precipitation amount, intensity and application time delay with solute center of mass, can be identified.

3. Objectives

The objectives of this tracer leaching study were:

1. to quantify the impact of the application time delay, i.e. the interval between a solute pulse and the following irrigation, on the leaching depth of solutes (Bromide Br^- and 4-Fluorobenzoic acid 4-FBA),
2. to assess the impact of irrigation amount and intensity on the leaching depth of a Br^- and 4-Fluorobenzoic acid pulse,

3. to determine the impact of initial soil water pressure head on leaching depth of tracers, and
4. to study these three objectives based on the autocovariance structure of observed patterns of measured state-variables reflecting transport and to compare them with those of precipitation amount, intensity and time delay.

In order to quantify the spatial representativity (scale of variation) of observations of Br^- concentrations and soil water content in the experimental site, a pilot study was carried out in the same soil but in a parallel transect downhill from the main experimental site in 2007 before the main experiment.

4. Materials and Methods

4.1. Experimental Field Site

The field strips selected for both the main leaching study and the pilot study were located in a summit landscape position at the UK Agricultural Experiment Station Spindletop Farm, Lexington, Kentucky. The field site was managed as mixed grassland for at least four years prior to these experiments. According to the NRCS web soil survey, the predominant soil series is a well drained Maury Silt Loam. The taxonomic class is fine, mixed, semiactive, mesic Typic Paleudalfs with 2-6 % slope, a mean annual precipitation of 117 cm, and a mean annual temperature of 12.8 °C. The typical profile is described as a silt loam (Ap and AB horizons) from 0-40 cm depth, a silty clay loam (BA and Bt1 horizons) from 40-74 cm depth and a silty clay (Bt2 horizon) from 74 to >100 cm depth.

The experimental area was covered with tarps except for the times of pre-wetting, tracer application, irrigation, and soil sampling to avoid plant growth and related water uptake and evapotranspiration. The grass cover around the experimental site was routinely mowed to the shortest extent possible.

4.2. Plot Layout and Field Instrumentation

A pilot study described in detail below was conducted in 2007 to determine the minimum size of plots to be investigated in the main leaching study of 2008. The criteria to define the plot length was based on the correlation range of Br^- concentration observations taken along a transect in 2007. The spatial correlation range λ identified in the pilot leaching study was 1 m for the 10-cm increments between 10 and 40 cm depth. Therefore, the distance represented by a single Br^- observations in both directions was 2λ or 2 m for both directions. This length served as the minimum plot length dimension for the main leaching study of 2008.

In the main leaching experiment of 2008, a total of 32 plots of 2m length by 8 m width were distributed along a 64-m transect. In order to record the initial soil profile moisture status and to monitor the hydraulic gradient throughout the main leaching experiment, a total of 48 nests of tensiometers were distributed along the 64-m transect with a separation distance of 1 and 2 m for plots 1 to 16 and plots 17-32, respectively. Each tensiometer nest depicted in Figure 4.1 had 6 tensiometers installed at 10, 30, 50, 70, 90, and 110 cm depth distributed on the vertices of a hexagon of 25 cm sides. In summary, the distribution of tensiometer nests resulted in two nests per plot for transect distances

between 0-32 m (plots 1-16) and one nest per plot for transect distances between 32-64 m (plots 17-32), illustrated in Figure 4.1.

4.3. Irrigation Prior to Main Leaching Study

The 64-m long transect was divided in two halves to investigate the influence of different initial soil moisture conditions, one half with higher and the other with a lower initial soil water content. To create these initial conditions and raise the soil water matric potential ψ_m above the lower field tensiometer measurement range ($\psi_m \geq$-650 cm), the area had to be irrigated across the whole transect due to a very dry summer in 2008. One half of the transect received more irrigation than the other half. Both halves were irrigated frequently and always with water filtered with a Reverse Osmosis System (GE). In between irrigations, the area was covered with plastic tarps.

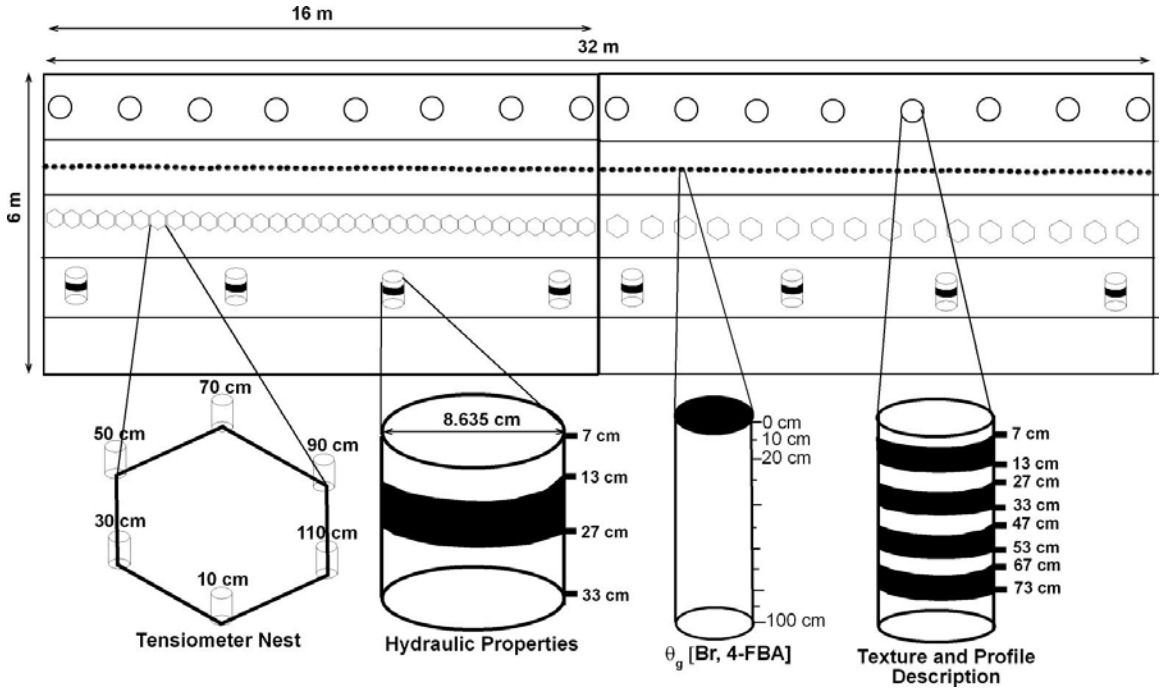

Figure 4.1. Distribution of field tensiometer nests along the 64 m long transect, locations for tracer concentration and soil water content sampling in Oct-31-08 and for cores taken for textural analysis, for profile descriptions and for soil hydraulic property core cylinders in summer 2009.

4.4. Pulse Input Tracer Application

Bromide was applied as a pulse with a field sprayer to each plot in seven paths within two minutes delivering in total 0.107 cm of a 0.3362 mmol/cm^3 Br^- solution for every plot of 2 m length and 4.5 m width. The application rate corresponded to 28.74 g Br^-/m^2. The calibration of the field sprayer revealed a coefficient of variation of 16 % among 5 nozzles separated by a distance of 50.8 cm (20 inches).

The timing of the Br^- pulse was managed for each plot individually since it was easier to schedule the Br^- spray applications with the field sprayer rather than managing the subsequent irrigation events individually for each plot. The irrigation equipment available for this study restricted the uniform water irrigation treatments to groups of four adjacent plots at any single time. Therefore, the beginning of irrigating groups of four plots was the time reference from which the Br^- pulses were scheduled ahead.

The 4-FBA due to its low solubility (<1gr/L) was mixed with the irrigation water at an estimated concentration of 0.0022 mmol/cm^3. However, the total dissolution of 4-FBA was never possible even with mechanical stirring, and undissolved, solid phases of this tracer were observed in the water and at the bottom of the mixing tanks. Measured concentrations of the 4-FBA pulse input solution by Ion chromatography indicated a 0.001285 mmol/cm^3 concentration which is 58% of the intended concentration. The intention was to apply 4-FBA with the irrigation water to enable us to investigate two different tracers under two different application boundary conditions. For the solubility problems we faced with the 4-FBA, its transport behavior could not be quantified.

4.5. Time-Variable Upper Boundary Conditions

This section deals with the different precipitation amounts, intensities and Br^- application time delays distributed across the upper boundary of the 2008 main leaching study.

The three factors affecting leaching depth of solutes, irrigation amount, intensity and the application time delay were studied in four different levels for each factor. Irrigation amounts were 2 and 4 cm of water and intended intensities were 4 and 2 cm/hr and 4 and 2 cm/day. Application time delays to be tested were 1, 4, 24, and 96 hours.

Four adjacent plots were grouped for the same precipitation intensity for managing the spatial irrigation pattern. In order to apply the irrigation of the intended intensity at the same time, the Br^- pulse application had to be scheduled plot-specifically ahead of irrigation. The schedule for the planned and executed Br^- pulses and irrigations for the main leaching study of Oct-08 are presented in the Appendices 8-19.

The first four neighboring plots were irrigated at an intensity level of 4 cm/hr with application time delays corresponding to 1 hour, 24 hours, 96 hours and 4 hours respectively (Figure 4.2). Next to the first four plots irrigated at an intensity of 4 cm/hr, four plots with 4cm/day followed. Then four plots of 2cm/day and lastly four plots of 2cm/hr completed the first cycle reaching across the first half of the transect. It is important to remember that each group of 4 plots under the same precipitation intensity consisted of plots that each had a different time delay. The second half of the transect is a replicate of the first half described, and only differs with respect to the initial soil moisture profile.

The sinusoidal patterns of irrigation intensity and application time delay displayed in Figure 4.2 were meant to create distinctive spatial patterns on the leaching depth of Br^-. It is believed that the combination of the shortest application time delay (1 hour) with the highest rainfall intensity (4 cm/hour) will result in the deepest leaching of solutes and vice versa. However, any findings not following this behavior could still be further investigated with respect to the spatial variability of soil hydraulic properties, as the exact location of these observations would be known.

The actual time variable boundary conditions (TVBC) imposed in the experiment differ from the originally intended TVBC in Figure 4.2 for two reasons: a) the low available supply of filtered water delayed the irrigation scheduled for plots 1-4 and 13-16 by approximately two days and b) natural rainfall occurred in Friday Oct-24-08 (1.52 cm from 8:40 AM to 5:00PM). This rainfall added 1.52 cm to the total precipitation of plots 5-12 and 21-28 and also increased the precipitation amount for plots 2, 3, 14, 15, 17-20 and 29-32 by different amounts depending on the timing of the Br^- pulse (see appendix for scheduled Br^- pulse application and irrigations). Intended and actual TVBC are presented in Figure 4.2 where the left y axis (precipitation amount and intensity) is drawn in logarithmic scale.

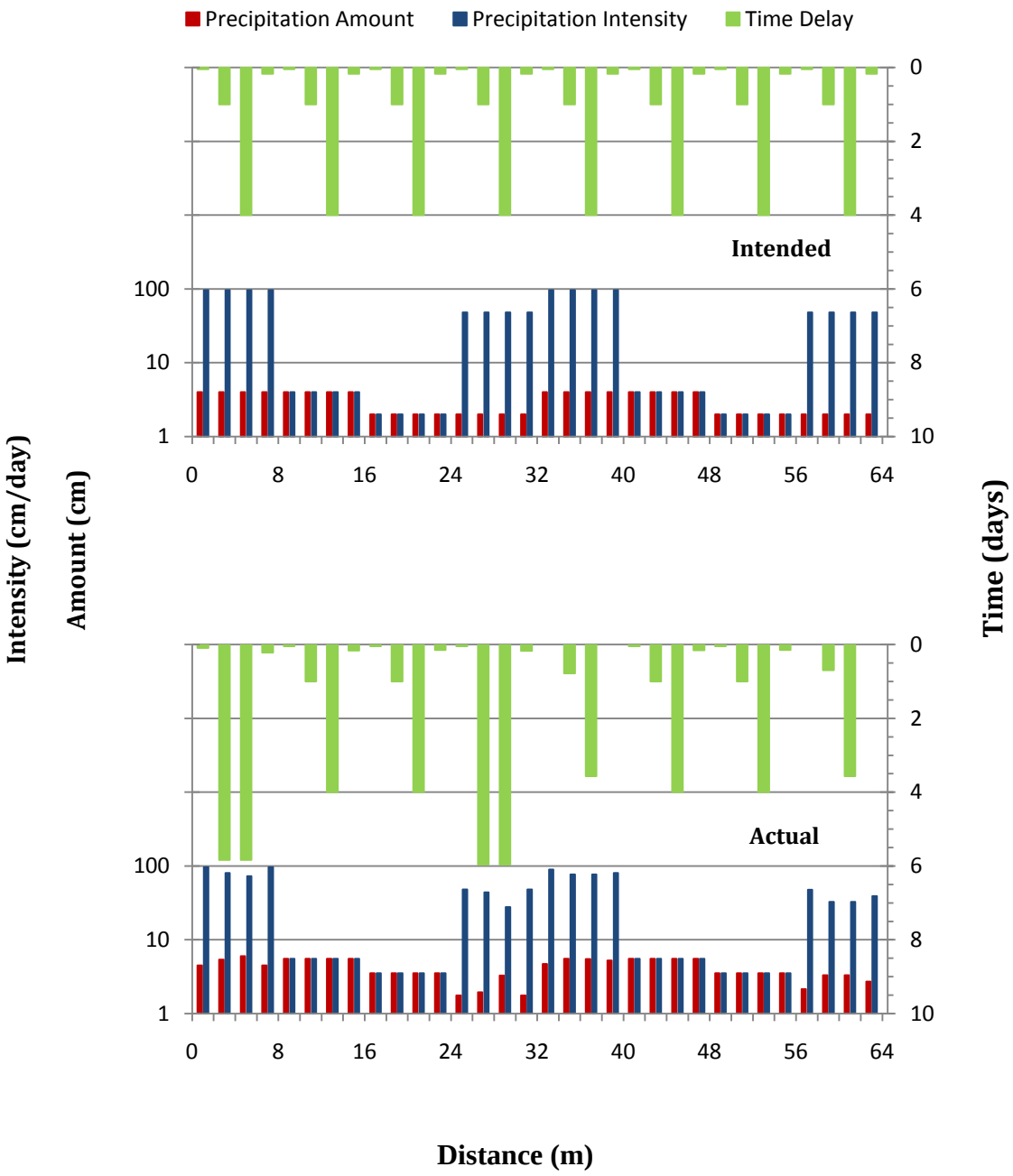

Figure 4.2. Time variable boundary conditions (TVBC) for the upper boundary, intended and actual. Each vertical bar along the distance axis represents precipitation amount, intensity and application time delay, respectively, in one plot.

Finally, the effect that the TVBC for the upper boundary would have on the leaching depth of Br^- was studied under the assumption of zero flux for the time when no precipitation or evaporation was allowed across the soil surface. The upper zero flux boundary was controlled through plastic tarps that covered the entire field transect over an area of 68 m length by 6 m width. The tarps limited evaporation for the time periods between Br^- pulse application and following precipitation, and from the last precipitation to the tracer soil sampling on Oct-31-08.

4.6. Calibration of Irrigation Equipment

A garden sprinkler system was used for the irrigation treatments. Each sprinkler delivered a total of 1cm/hour (24cm/day) discharge at 25 PSI over an area of 8m by 6m. The low intensity treatments of 4 and 2 cm/day for plots 5-8, 21-24 and plots 9-12, 25-28, respectively, were obtained through short five-minute-long irrigation pulses applied every hour for a 24 hour period between noon of Oct-23 and Oct-24. The different irrigation amounts, i.e., 4 and 2 cm were obtained using 2 and 1 sprinklers, respectively. The high intensity irrigations of 4 and 2cm/hr were obtained using 4 and 2 sprinklers over one hour for plots 1-4, 17-20 and plots 13-16, 29-32, respectively.

4.7. Tensiometer Readings and Soil Water Matric Potential Calculation

Tensiometer readings were taken using a tensimeter, which is a handheld manometer that measures the pressure in the air bubble in the upper perspective part of the tensiometer shaft. The tensiometer readings were taken in each of the 48 nests and for each of the 6

depths on Oct-19-08. These readings provided the initial soil water matric potential ψ_m after a series of pre-wetting irrigations had been applied and before the Br^- pulse was applied and the main leaching study began. Readings were also taken on Oct-25-08, after the Br^- pulses and irrigation treatments were applied to plots 5-12, and 17-32. The third and last complete set of tensiometer readings for the whole transect was obtained at the day of soil sampling for tracer analysis on Oct-31-08.

The time between Oct-23-08 at 1PM and Oct-24-08 at 8AM was a period of continuous irrigation for plots 5-12 and 21-28 with short five minute irrigation pulses being applied every hour (see 4.6). During this period ten series of tensiometer readings were taken approximately every 2 hours to monitor the hydraulic gradient in these plots, treated with irrigations of 4 and 2cm/day respectively.

In order to account for the temperature effect on tensiometer readings, a control tensiometer was placed in a sealed bucket with soil at 30 cm depth and then, the sealed bucket was completely buried in the soil site to allow equilibration with surrounding soil temperature. Since the manometer reading of this sealed bucket tensiometer was known to be -150 cm at 20 Celsius, regular readings of the cont rol tensiometer allowed for temperature based corrections on readings taken at the same time for the field tensiometers.

The manometer readings were corrected for the present deviation of the tensiometer reading in the control bucket from -150 cm for six sets of observations taken in Oct-23 5PM, Oct-23 7PM, Oct-24 3AM, Oct-24 5AM, Oct-24 8AM, Oct-25 and Oct-31 with correction factors of +18, -27, +2, +8, +9, +1, and -15 cm respectively. Temperature

based correction were obtained only for these sets of observations because the control tensiometer readings were only available for these times. Soil water pressure head values were calculated by adding the shaft length of the respective tensiometer to the corrected or non-corrected sets of manometer readings.

4.8. Hydraulic Gradient Calculation

The vertical hydraulic gradient $\Delta H/\Delta z$ between adjacent readings of ψ_m was calculated with the formula:

$$\frac{\Delta H}{\Delta z} = \frac{H_2 - H_1}{z_2 - z_1}$$

where:

H = Total soil water potential or hydraulic head (cm)

z = Depth (cm)

and,

$$H = \psi_m - \psi_z$$

for the z axis defined positive downward. The reference level was set at the soil surface and

ψ_m = Soil water matric potential (cm)

ψ_z = Gravitational potential (cm)

A positive hydraulic gradient $\Delta H/\Delta z$ indicates upward directed flow and a negative $\Delta H/\Delta z$ indicates downward directed flow.

4.9. Soil Measurement Methods

A percussion corer 2.5 cm in diameter and 1 m long, driven into the ground by a hand held electric hammer (Hilti USA) was used to take samples at 10 cm depth increments down to 100 cm depth. Cores were taken at 0.5 m intervals along the 64 m long transect for a total of 128 locations in Oct-31-08 (Figure 4.1). Samples were immediately stored in sealed specimen cups and taken to the lab to be divided into two subsamples, one for the determination of gravimetric water content and the other to air drying and processing it for tracer analysis and air dry soil water content.

4.10. Chemical Analysis of Br^- Concentration With Ion Chromatography

Two grams of air dried soil were extracted with 10cc of DI water in a test tube, shaken for one hour, and left to settle overnight. The solution extract was collected and passed through a 45 μm filter before injecting the sample into the Metrohm 792 Basic ion cromatograph (IC) in the Environmental Soil Chemistry Lab.

A total of 640 filtered soil extracts (128 locations down to 50 cm depth) were manually injected to the IC equipped with a Metrosep A Supp 5 column of 150/4.0 mm dimensions.

The eluent and acid were constantly pumped through the IC column during analysis and contained 1.6 mM $NaCO_3$ and 0.5 mM $NaHCO_3$ and the acid used was a 100 mM H_2SO_4. The amount of soil extract injected each time was 2 cm^3 to ensure that left-overs of previous samples were flushed out of the system before the following sample was injected. The actual amount analyzed by the IC was only 20 µl. Standard curves for Br^-, 4-FBA were developed and the elution times for each of these tracers were 8.5 and 18 min, respectively. A sample passed through the IC-column during a period of 30 min. The Minimum Detection Limit MDL calculated with the Student *t*-test standard deviation method was 0.086 and 0.05 for the 4-FBA and Br^-, respectively. Minimum Quantification Limits MQLs were established at 10X the MDL values, corresponding to≈1 and 0.5 ppm of 4-FBA and Br^-, respectively.

Only Br^- was quantifiable in the IC due to the fact that only 58% of the intended 4-FBA pulse input could be applied, which in turn was a result of its low water solubility and is explained under 4.4.

Bromide was analyzed for the 128 locations down to 50 cm depth and it was assumed that Br^- leaching did not move deeper because only very small concentrations were found in the 40-50 cm depth interval, for instance, only 8 values at this depth (40-50 cm) were below the detection limit MDL.

Bromide extract concentrations were then expressed in [mg Br^-]/[kg oven-dry soil] by the following conversion:

- **Readings**

mg Br/kg dry soil = IC reading * Dilution Factor DF*Conversion from g to kg soil basis* air-dry water content correction.

$$\frac{\text{mg Br}^-}{\text{kg ovendry soil}} = \frac{\text{mg Br}^-}{1000\ \text{cm}^3\ \text{water}} \times \frac{10\ \text{cm}^3\text{water}}{2\text{g airdry soil}} \text{ so} \frac{1000\ \text{g airdry soil}}{1\ \text{kg airdry soil}}$$

$$\frac{1\ \text{kg airdry soil}}{1\ \text{kg airdry soil} \times (1 - \text{airdry water content})}$$

4.11. Soil Hydraulic Properties

A total of 16 intact cores of 8.62 cm diameter and 6 cm height were taken along the transect at the center of plots 1, 5, 9, 13, 17, 21, 25, and 29. Two depth intervals for each plot were considered for core sampling: 7-13 cm and 27-33 cm depth (Figure 4.1). The intact core samples were taken in the spring of 2009 after the tracer experiment had been completed. Samples were wrapped in saran film, weighed and placed in a refrigerator at 4˚C until processing. Gravimetric soil water content samples were taken at the same time of core sampling for determining the dry bulk density ρ_b of core samples.

Unsaturated hydraulic properties were measured using the evaporation method according to Wendroth and Simunek (1999). For obtaining hydraulic conductivity in the range close to soil water saturation, the intact cores were removed from the refrigerator and placed on a double plate membrane permeameter (Wendroth and Simunek, 1999). This device included Mariotte devices to control the upper and lower pressure head boundaries (Figure 4.3).

The unsaturated hydraulic conductivity coefficients were obtained for three soil water pressure heads close to soil water saturation, i.e., ψ_m = -10, -5, and -1 cm. Each core was allowed to slowly saturate from the bottom up for a period of one to two days at a lower boundary of ψ_m = -2 cm (Figure 4.3). After the saturation period, the lower boundary was set to ψ_m = -1cm.

The upper boundary was immediately set to -1 cm with another Mariotte device (Figure 4.3). U-manometers were attached to the upper and lower porous plates to verify the intended ψ_m on each boundary. Once the upper and lower boundaries were set to ψ_m = -1 cm, flux across the soil core cross section was measured as a decrease in water level in the upper boundary reservoir. Steady state water flux was assumed after six consistent readings of water flux over the same time interval were obtained consecutively. The same procedure was followed for ψ_m = -5 and -10 cm.

Figure 4.3. Double plate membrane permeameter for measuring unsaturated hydraulic conductivity coefficients close to soil water saturation at ψ_m = -10, -5 and -1 cm.

For -10 > ψ_m > -650 cm, the laboratory evaporation method (Wendroth and Wypler, 2007) was used to measure unsaturated hydraulic conductivity and soil water retention curve.

The electronic transducer tensiometers used for the evaporation method were calibrated for 0 > ψ_m > -100 cm in -10 cm increments using a hanging water column device. For -100 > ψ_m > -700 cm, the water column device was connected to a sealed water reservoir in which vacuum was applied and monitored by manometer readings (tensimeter) to steadily decrease ψ_m in -50 cm increments.

Horizontal holes of 5.5 cm length and 0.5 cm diameter were drilled in the soil core samples to install two tensiometers at 1.5 and 4.5 cm depth, respectively. The mass of soil removed during drilling was carefully collected in specimen cups and added to the soil mass in the core after drying. Tensiometers were used to record ψ_m every 1 min with a dataloger; however sample weights were recorded at 2 to 4 hour intervals on a scale manually by disconnecting the pressure transducer cables (Figure 4.4).

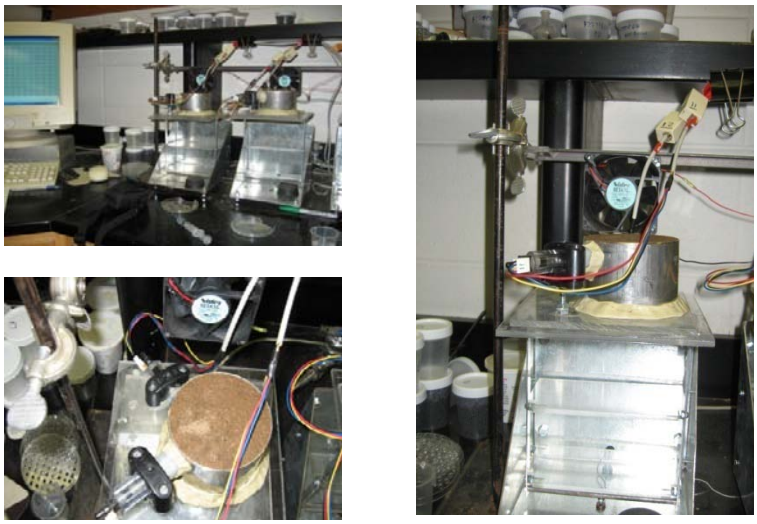

Figure 4.4. Laboratory evaporation method with two tensiometers for unsaturated hydraulic property measurement for soil cores at 7-13 and 27-33 cm depths for -10 > ψ_m> -650 cm.

Soil water retention curve parameters θ_s, θ_r, α, and n (van Genuchten, 1980) were iteratively estimated based on the Wind (1968) method using a FORTRAN computer program (Wendroth, 2009)1. Subsequently $K(h, \theta)$ was calculated based on Wendroth and Wypler (2007). Finally, soil water retention curve and unsaturated hydraulic conductivity function parameters were fitted using RETC (van Genuchten et al., 1991). These fitted parameters were used to run water and solute transport simulations with HYDRUS 1D (Simunek et al., 1998).

4.12. Water Mass Balance

The water mass balance for the duration of the experiment (Oct-19 to Oct-31) was calculated for each of the 128 locations sampled on Oct-31. The water mass balance calculation was based on the soil water storage over 100-cm-deep soil profile for Oct-19, plus the height of irrigation, rainfall and solute application from Oct-19 to Oct-30. The calculated the total soil water storage for Oct-31 was compared to the measured soil water storage of the same day, which was obtained from gravimetric water content observations (Oct-31) assuming ρ_b values of 1.12, 1.35 and 1.5 g/cm^3 for the 0-10, 10-50 and 50-100 cm depth increments, respectively. For the initial conditions on Oct-19, ψ_m readings were used in the water mass balance and converted to volumetric water content θ_v and storage based on the parameters of the Van Genuchten (1980) model obtained for each plot under 4.11.

1 Wendroth, 2009 Personal comunication

The parameters for the Van Genuchten (1980) model used for the estimation of θ_v for each plot were derived as described in 4.11. Soil water storage across the 100-cm-deep profile was calculated as follows: ψ_m observations in Oct-19 were linearly interpolated for 1.5-cm-depth increments and their corresponding θ_v was obtained. Subsequently, soil water storage values were calculated for each 1.5 cm depth interval and integrated to obtain the soil water storage over 100 cm depth. It should be noted that initial values (Oct-19) of soil water storage were calculated on a plot basis and therefore, the ψ_m observations of Oct-19 for plots 1-16 were the average of two available ψ_m readings per tensiometer depth.

Gravimetric water content θ_g was converted to θ_v, with:

$$\rho_b * \theta_g = \theta_v$$

The assumed dry bulk density ρ_b values discussed above were 1.35 g/cm^3 for the 10-50 cm depth, obtained from samples processed for hydraulic properties under 4.11, for 50-150 cm depth, a ρ_b of 1.5 g/cm^3 was assumed and finally, for the 0-10 cm depth, the ρ_b value of 1.12 g/cm^3 was estimated from the total dry soil mass recovered from the tracer sampling of Oct-31 and divided by the volume sampled with the percussion corer over the 0-10 cm depth increment.

4.13. Bromide Mass Balance and Center of Mass Calculation

The Br^- mass balance was based on the comparison between Br^- applied over 1 m^2 of surface area and Br^- recovered throughout the profile under 1 m^2 surface area. For this purpose Br^- concentrations given for each 10-cm layer on a gravimetric basis (mg Br^-/kg

soil) were multiplied by the dry soil mass in the control soil volume (0.1 m depth x 1 m^2 area = 0.1 m^3) to obtain the mass of Br^- present in a depth increment under 1 m^2 surface area. The total Br^- mass in each layer was integrated between 0-50 cm depth for each location. The dry soil mass present in the control volume was obtained for each 10-cm-layer using the same ρ_b estimates as those for the water mass balance under 4.12 by:

$$mass\ of\ dry\ soil\ = \rho_b\ *\ volume\ of\ soil$$

Next, the mass of Br^- for each control volume integrated between 0 and 50 cm depth for each location was compared to the application rate of 28.74 g Br^-/m^2 and a percent % Br^- mass recovery was obtained. The Br^- center of mass was calculated for each of the 128 locations sampled in Oct-31 from 0 to 50 cm according to Olson and Cassel (1999):

$$Bromide\ Center\ of\ mass = \frac{1}{M}\sum_{i=1}^{n} m_i * r_i$$

where:

M = Total Br^-mass recovered on a single core

m_i = Br^- mass recovered on an individual depth compartment

r_i = Center of individual depth compartment

4.14. Statistical Analysis

Initially, a fractile diagram for each variable was calculated to verify its normal distribution (Nielsen and Wendroth, 2003). Based on the fractile diagrams (see appendix), all variables considered were assumed normally distributed. Observations of hydraulic gradient, Br^- concentrations and θ_g were spatially analyzed with two public domain computer software packages:

a) Applied statistical time series methods (Shumway and Stoffer, 2000) were used for spatial analysis in the frequency domain, i.e., power, co-, quadrature, phase and coherency spectra.

The frequency domain techniques were chosen based on the experimental design to identify characteristic cyclic variation components of Br^- leaching and its underlying periodically varying factors, i.e., precipitation amount, intensity and time delay. Spectral analysis was used to identify the characteristic wavelengths over which cyclic behavior of the Br^- leaching occurred. Cospectral analysis determined the common frequencies at which Br^- leaching and the transport causing factors were correlated, the Quad and Phase spectrum determined if the series of Br^- leaching and transport causing factors were in phase or were shifted against each other by a lag.

Finally the squared coherency spectrum is a measure of the frequency-bound relationship between two series (Nielsen and Wendroth, 2003), similar to the coefficient of determination in correlation analysis with values between 0 and 1 for different frequency components. Coherency spectrum values > 0.69 indicate a highly significant (95%)

correlation whereas smaller values indicate no significant correlation. The program package WinASTSA was used for computations.

b) Geostatistical methods were used to calculate the experimental semi- and cross-semivariograms for all transport causing factors and variables investigated in this study. This form of the autocovariance function was used to verify if the observations of Br^-, θ_g, Br^- center of mass, water and Br^- mass balances and $\Delta H/\Delta z$ reflected a structured or random variability. Moreover, spatial association of different variables and their covariance behavior was quantified with cross-semivariograms. For illustration purposes, all semivariance values presented from this project were normalized by dividing the semivariance value for each lag distance by the sample variance of each data series. This normalization of semivariance values facilitates the comparison of spatial structures between different variables.

The nugget variance component, according to Journel and Huijbregts (1991), is associated with small scale variation, i.e., the amount of variability that can be attributed to spatial variation that exists at the sampling location, including measurement errors (Nielsen and Wendroth, 2003). The sill component of any spatially structured dataset indicates the level at which increasing lag separation distance does not result in a further increase of the semivariance. Therefore it is an important parameter to identify the range of spatially dependent observations. For geostatistical computations, the program package SGEMS was used.

A comprehensive review of the statistical methods applied in this study can be found in Nielsen and Wendroth (2003) and Shumway and Stoffer (2000).

4.14.1. Frequency-Based Analysis for $\Delta H/\Delta z$ and Br^- Center of Mass

In order to arrange the $\Delta H/\Delta z$ observations at regular sampling intervals, which are required for spectral analysis, the average of the two observations of $\Delta H/\Delta z$ for each plot within 0-32 m distance was calculated. A new data-series with 32 observations of $\Delta H/\Delta z$ taken 2 m apart from each other and each one representing one plot was created for each depth compartment and time for a total of 480 observations of $\Delta H/\Delta z$ (32 locations x 5 depth compartments x 3 reading times). There was, however, a total of 11 missing values of $\Delta H/\Delta z$ in this 480-observation dataset for which eight out of 11 missing observations occurred on transect distances between 0-32m. The eight missing values within 0-32 m distances occurred within eight different plots and therefore, the estimation of the $\Delta H/\Delta z$ for these plots is not an average value of two observations of $\Delta H/\Delta z$, but corresponds to the one and only observation of $\Delta H/\Delta z$ available for that particular plot, depth compartment and reading time. The remaining three missing observations of $\Delta H/\Delta z$ occurred between 32 and 64m distances, where only one tensiometer nest per plot was available to calculate $\Delta H/\Delta z$. In order to replace these three missing values, the average $\Delta H/\Delta z$ calculated for all 47 (48 nests minus missing value) observations for each reading time and depth compartment was used to complete the dataset and run the frequency analyses. The average was chosen because no spatial structure was found in the original dataset (48 gradient values per depth times five depths) for the $\Delta H/\Delta z$ at any depth or time in agreement with the semivariogram analyses and therefore, for a randomly distributed $\Delta H/\Delta z$ data series, the average of the series for each depth compartment at one single time is a reasonable estimation of a missing value.

The plot average Br^- center of mass was calculated with the three values of the Br center of mass obtained from the Br^- concentration profiles of core samples located within each plot. The Br^- center of mass values from cores taken at the plot boundary were not considered for this plot average Br^- center of mass calculation as it would be difficult to allocate this value to either one of the neighboring plots. The frequency analyses was based on 32 observations for each of the series of $\Delta H/\Delta z$, Br^- center of mass series and the transport causing factors. Signals for sixteen frequencies were calculated with a smoothing constant set to 1, no cosine taper and 2 degrees of freedom for all the frequency based analyses of this section.

4.14.2. Frequency-Based Analysis of Transport Causing Factors and Bromide Center of Mass

Different types of spectra were calculated considering 128 observations for each variable, 64 spectral estimates, smoothing constant set to 1 and no cosine taper for each of the three transport causing factors. However, for the coherency spectra between hydraulic gradient vs. Br^- center of mass and the transport causing factors vs. Br^- center of mass, the smoothing constant was set to three to distinguish significant correlations at common frequencies. The assignment of the transport causing factors to each plot and space coordinate was done by taking the first four point coordinates, i.e., 0.5, 1, 1.5 and 2m distances and assigning them to plot 1, next, by taking the 2.5, 3, 3.5 and 4 m distances point coordinates and assigning them to plot two, and following the same procedure successively for the entire dataset.

4.15. Profile Description and Soil Textural Analysis

A total of 16 intact cores from 0-100 cm depth along the transect were taken in spring of 2009 with a hydraulic Giddings probe auger mounted to a tractor. Each core was taken at the center of plots 1, 3, 5, 7, 9, 11, 13, 15, 17, 19, 21, 23, 25, 27, 29, and 31 corresponding to transect distances of 1, 5, 9, 13, 17, 21, 25, 29, 33, 37, 41, 45, 49, 53, 57, and 61 m. The intact cores were wrapped in saran film and then transported to the lab where profile descriptions were made by Mr. Nathan Hamilton.

After the soil horizon designation, color, structure and approximate textural class were determined. The intact cores were dissected into a total of 64 samples (16 locations and 4 depths) for soil texture determination. This dissection resulted in a spacing of 4 m distance between each location or core (Figure 4.1). The depth intervals analyzed for texture were: 7-13, 27-33, 47-53 and 67-73 cm depths (Figure 4.1).

A modified pipette method (sand was determined by sieving after the sample for clay was drawn from suspension) was used for rapid determination of the sand and clay fraction as follows: Each sample was air dried for 5 days and then sieved through a 2mm sieve. Next, 40 grams of air dried soil were mixed with approximately 5-10 ml of Deionized water (DIW) and then with 20 ml of 50% Hydrogen Peroxide (H_2O_2) applied in 5 ml steps every 2 hours to avoid excessive effervescence. Once the H_2O_2 had destroyed the organic matter, 50 ml of Sodium Hexametaphosphate were added to disperse the clay fraction. The resulting paste was stirred for 5 min with an electric mixer and then transferred quantitatively to a 1000 cc graduated cylinder which was brought up to the intended volume of 1000 cc with DIW.

A blank solution on a separate 1000 cc graduated cylinder was used to account for the Sodium Hexametaphosphate added to the suspension. This blank was prepared with 50 ml Sodium Hexametaphosphate and was brought up to volume with DIW. A thermometer was placed inside the blank graduated cylinder to get the reference temperature at which the settling of different particle sizes occurs after ideal suspension. This is to adjust the time at which the 5 cm deep 25 ml sample for the clay fraction < 2um needs to be taken. The temperature reference and sampling times used for the clay determination are shown on Table 4.1.

Table 4.1. Particle size distribution protocol. Reference sampling times for a pipette sample at 5 cm depth according to blank temperature for particles <2µm diameter used for soil particle size analysis by a modified Pipette method.

Temperature ˚C	Hours	Minutes
20	3	53
21	3	47
22	3	42
23	3	37
24	3	32
25	3	27
26	3	22
27	3	18
28	3	14
29	3	10
30	3	6

Before plunging of the samples in the graduated cylinder, readings of the blank temperature were taken to determine the sampling time for clay for each set of samples to be analyzed. Plunging was done for one minute on each sample to get all the particles in

suspension. After plunging and according to Table 4.1, a timer was set to take the clay fraction sample at the appropriate time of settling.

To account for the Sodium Hexametaphosphate added to disperse the clay fraction, a 25 ml sample was drawn from the blank and then oven-dried and weighed following the same routine as the clay and sand fraction. The dry mass of Sodium Hexametaphosphate was substracted from the clay dry mass to get the true mass of dry clay in the sample. Once the clay sample was drawn, it was transferred quantitatively to a beaker and oven-dried at 105˚C for 24 hours. The dry clay mass was weighed.

The sand fraction was determined by sieving after the clay sample was drawn. For this purpose, the suspension in the graduated cylinder was transferred quantitatively to a sieve # 270 (0.05 mm size) and the sieved material rinsed in a beaker and oven dried at 105˚C for 24 hours. The dry mass of the sand fraction was then determined.

Finally, the silt fraction was calculated as the difference between the fractions of sand and clay with 100%. However, since the soil texture protocol started with 40 g of an air dried sample, a correction had to be made to account for the air dry water content. Air dry water content was measured on a remainder of the air dried samples not used. These samples were oven-dried at 105˚C for 24 hours to get the gravimetric soil water content of the air dry sample. The air dry water content was used to correct the clay and sand fraction percentage and consequently, the silt fraction as well.

Also, textural composition was determined manually during soil profile description. This method is known to be within ±5 % accuracy and is based on the manual estimation of sand and clay particles. Sand particles are estimated by the roughness of the sample felt

by hand and the clay particles are estimated by the maximum length of the ribbon that can be formed for a gently saturated sample.

This method is used in this study as a rough field estimation of texture only and is compared with lab analysis on the same samples.

4.16. Simulations of Water and Br^- Transport using Hydrus 1D

Bromide movement was simulated based on the soil hydraulic properties to compute soil water dynamics and Br^- transport for the time from tracer application to sampling in Oct-31 and to compare simulation results with field measurements.

In order to run the simulations, several parameters needed to be given to define the soil profile system to be simulated. These parameters included:

a) The initial soil water profile conditions,

b) the soil materials with their respective depth intervals, bulk densities ρ_b, dispersivities λ and soil hydraulic property parameters of the Van Genuchten (1980) model,

c) the upper and lower boundary conditions, and

d) solute reaction parameters.

4.16.1. Initial Soil Profile Moisture Conditions

For each plot, the simulation began on Oct-19-08, the time when a tensiometer reading for all plots was taken just before the application of Br^- tracer. The ψ_m values were processed to run the simulations as follows:

a) For transect distances between 0-32 m, i.e., plots 1-16, where two tensiometer readings per plot and depth were available, the average of these two readings was taken to represent the initial soil profile ψ_m in that particular plot.

b) For transect distances between 32-64 m, i.e., plots 17-32, only one observation of ψ_m per plot and depth was available and consequently used with no processing to run the simulations, and

c) each resulting ψ_m plot profile with observations at 10, 30, 50, 70, 90, 110 cm depths for Oct-19-08 was downscaled to nodal values of ψ_m every 1.5 cm depth down to a 150 cm deep grid. This downscaling was accomplished by linear extrapolation of the initial ψ_m plot profile observations at 10, 30, 50, 70, 90, and 110 cm depths assuming that equilibrium conditions existed between 10, 30, 50, 70, 90 and 110 cm. The surface nodal points above 10 cm depth were assumed to follow the same linear slope obtained for the measured ψ_m at 10 and 30 cm depth. The deep nodal points below 110 cm depth were set to the ψ_m value measured at 110 cm depth

4.16.2. Soil Material Information

The soil hydraulic property parameters needed for simulations were obtained from the intact soil cores as described under 4.11. The hydraulic property parameters derived from

samples taken at 7-13 and 27-33 cm depth are assumed to represent the 0-13.5 and 15-49.5 cm depth on the simulation grid. The soil hydraulic property parameters for the 50-150cm depth were not experimentally determined but were assumed to be correctly estimated by the default Loam textural parameters obtained from the program Rosetta database incorporated in Hydrus 1D. These hydraulic property parameters are presented under 5.2.13.1 in Table 5.6.

Moreover, the spatial representation of each set of soil hydraulic property parameters (7-13 and 27-33cm depth) was arbitrarily assigned to four plots, i.e., hydraulic property parameters obtained for plot 1 represented plots 1-3, parameters obtained for plot 5 represented plots 4-7, and successively until the parameters of plot 29 represented plots 28-32.

At last, the dispersivity parameter λ defined as the scale over which water flux and solute convection are averaged (Jury and Horton, 2004) was set to 10 cm for all three soil materials.

4.16.3. Upper and Lower Boundary Conditions

A time-dependent variable flux for the upper boundary condition UBC and free drainage for the lower boundary at 150 cm depth were given to run simulations. All the UBCs simulated for each plot are included in the appendices 8-19 under Time variable boundary condition tables for each individual plot. The time variable boundary conditions in the appendix include the time intervals over which water and Br^- tracer were applied to the individual plots from Oct-19 to Oct-31. The Br^- mass balance was checked for all the

plot simulations and was found to be between 99.5 and 99.9% of the applied Br^- mass, validating the simulations.

4.16.4. Solute Reaction Parameters

Since Br^- is assumed to be a conservative non-reactive tracer in most soils with pH >2.5, adsorption and retardation were neglected. In the simulations, the diffusion coefficient of Br^- in water was set equal to 1.8 cm^2/sec.

4.17. Pilot Leaching Study Methods (2007)

The purpose of the pilot leaching study was to determine the spatial correlation length *a* over which observations of Br^- concentration were related to each other. This spatial correlation length is the criterion we used to define the size of plots and the separation distance between individual sampling locations for the main study in 2008.

By locating samples within *a*, i.e., sampling at shorter distances than *a*, we ensure that the Br^- leaching behavior observed within a plot of size 2*a* is mostly dependent on the effect of the transport causing factors (treatments) and to a less extent, an effect of the inherent soil spatial variability.

For this purpose, a 16-m transect of the same soil series and with the same management as described under 4.11 was allocated in a parallel strip located 10 m in the downhill direction (south) from the main experimental site investigated in 2008. Soil moisture was increased at 0-12 m transect distance by irrigation with two garden sprinklers and

evaporation was minimized with plastic tarps that covered the field after each irrigation. The irrigation water used was regular tap water. From 12-16 m distance, soil was left purposely without irrigation to create two initial soil profile conditions, i.e., high and low initial soil water content for the 0-12 and 12-16 m distance, respectively.

4.17.1. Initial Soil Profile Conditions (2007)

Samples for gravimetric soil water content were taken every 1 m along the 16-m-transect approximately 1 hour before the application of the Br^- tracer on Sep-14-07. These samples were taken with a 2.5 cm-diameter percussion corer down to 100 cm depth in 10 cm increments. Samples were immediately stored in sealed specimen cups and taken to the lab to obtain the ovendry weight at 105˚C after 24 hours of drying.

4.17.2. Bromide Pulse Input for Pilot Study (2007)

Bromide was chosen as tracer because its background is very small in most soils. Bromide was applied with garden sprinklers delivering a total 0.5 cm of a 0.067 $mmol/cm^3$ Br^- solution on Sep-14-07. Sprinklers were distributed at 3, 9 and 15 m distance for a uniform Br^- application.

The amount of tracer applied in the pilot study in 2007 was an average based on studies by Kung et al. (2000a, b), Caron et al. (1999), Olson and Cassel (1999) who used ion chromatography for Br^- analyses. In these studies KBr solution was applied to soils at rates ranging from 13- 56 g KBr/m^2 to investigate solute breakthrough curves on tile

drain facilities. The Br^- pulse applied in the pilot study of 2007 corresponded to 40 g KBr/m^2

4.17.3. Upper Boundary Conditions (2007)

Two irrigations of 2 cm each were applied on Sept-26-07 and Sept-28-07, 12 and 14 days after the Br^- pulse was applied on Sep-14-07. Plastic tarps covered the entire transect for the time intervals in between Br^- pulse, irrigations and tracer sampling (Oct-10-07). Therefore the UBC was assumed zero flux.

4.17.4. Tracer and Water Content Sampling on Sep-14-07

A total of 64 locations were sampled at every 0.25 m distance along the 16-m-transect. Each core sample was taken down to 100 cm depth in 10-cm increments. Sampling locations with odd numbers, i.e., locations 1, 3, 5, etc. were sampled with a 4.3 cm diameter Edelman auger. Even-numbered locations, i.e., locations 2, 4, 6, etc. were sampled with the 2.5 cm diameter percussion corer that was later used in the main study.

Samples were immediately stored in sealed specimen cups and taken to the lab to obtain the oven dry weight at 105˚C after 24 hours of drying.

4.17.5. Colorimetric Br^- Analysis

The Automated Ferricyanide method for Cl^- determination described in “Standard Methods for Examination of Water and Wastewater” published by APHA (1989) was

used for Br^- determination by introducing a 2.25 molar factor. This molar factor was used to apply the method originally developed for Cl^- analysis for colorimetric Br^- analysis.

The molar factor is given by:

$$\frac{Atomic\ weight\ of\ Bromide}{Atomic\ weight\ of\ Chloride} = \frac{79.9\text{g}}{35.5\text{g}} = 2.25$$

The molar factor approach was chosen over Br^- determination on the microplate reader based on Br^- standards because the Br^- standards did not show the same consistency on the microplate reader. The calibration curve on the microplate reader for Br^- standards was not optimum and using the Br^- standards calibration curve would have given larger measurement uncertainty.

Therefore, the molar factor approach was followed under the assumption that the majority (> 90 %) of the Cl^- signal picked up by the microplate reader is due to the Br^- ion and only a marginal fraction (< 10 %) was due to Cl^-.

The soil extracts analyzed for Br^- were produced using the protocol described under 4.10 but only a 1 cm^3 aliquot of the extract was drawn without filtering for chemical analysis. The 1 cm^3 aliquot was injected to a cluster tube to proceed with the Cl^- determination in the Microplate reader.

Chloride is determined colorimetrically at 480 nm using an adaptation of the Automated Ferricyanide method described in “Standard Methods for Examination of Water and Wastewater” APHA (1989). Reaction with mercuric thiocyanate in the presence of acidified ferric nitrate causes formation of $HgCl_2$ and colored ferric thiocyanate according to the equation:

$$3Hg(SCN)_2 + 6\,Cl^- + 2Fe(NO_3)_3 \longrightarrow 3HgCl_2 + 2Fe(SCN)_3 + 6\,NO_3^-$$

The intensity of the $Fe(SCN)_3$ is proportional to the chloride concentration of the sample. The working range is from 0-50 ppm using a 60 µl sample. There are no significant interferences with the method except sample turbidity (Standard Methods for Examination of Water and Wastewater APHA 1989)

4.17.6. Statistical analysis (2007)

Spatial autocorrelation length was analysed for the Br^- and soil water content observations taken on Oct-10-07 to determine their spatial representativity,i.e., the maximum distance beyond which observations were independent of each other.

Also, the Statistical Analysis System SAS was used to perform an ANOVA to evaluate differences between water content and Br^- results obtained from samples that were either taken with the Edelman or the percussion corer.

4.17.7. Water Mass Balance for Pilot Study 2007

Soil water storage over the 100-cm-deep profile was calculated with the gravimetric soil water content observations taken in Sep-14-07 (16 locations) and the 64 locations sampled for θ_g at tracer sampling on Oct-10-07. Each core sampled in Sep-14-07 was assumed to be representing 1 m distance for the calculation of soil water storage.

Soil dry bulk densities ρ_b of 1.24, 1.34 and 1.5 g/cm^3 for the 0-10, 10-40 and 40-100 cm depth were used to convert the gravimetric water content values into volumetric water

content and soil water storage. The ρ_b values for the 0-40cm depth were obtained from intact core samples investigated as an assignment of the Soil Physics Lab course PLS 576 of 2007. These samples were obtained approximately 10 m to the west from the site investigated in 2007. Soil water storage on Sep-14-07 + 0.5 cm of Br^- pulse on Sep-14-07 + 4 cm of irrigation water should account for all the inputs into the profile investigated in 2007. The soil water storage calculated at the time of tracer sampling on Oct-10-07 was divided by the soil water storage obtained on Sep-14-07 plus the 0.5 cm of the Br pulse and 2 cm of irrigation in order to calculate the water mass balance.

4.17.8. Bromide Mass Balance for Pilot Study of 2007

The Bromide mass balance was calculated following the description under 4.13 but the ρ_b values used for the calculation were those described under 4.17.7. Two sets of Br^- observations for the Br^- mass balance were considered, i.e., the original set obtained with the molar factor and described under 4.17.5 and another data set created by substracting the average Cl^- background concentration from the original Br^- concentrations. The Cl^- background concentrations were determined on samples taken for the initial soil profile conditions on Sep-14-07. The average Cl^- background concentration measured was 15.06, 11.1, 9.27, 6.9, 6.01, 8.02, 6.25, 6.13, 7.03, 5.91 mg/kg soil for the 0-10, 10-20, 20-30, 30-40, 40-50, 50-60, 60-70, 70-80, 80-90, 90-100 cm depth increments, respectively. However, for some depths below 60 cm, the Cl^- background exceeded the original Br^- concentration and therefore, these values were not considered for the mass balance or Br^- center of mass calculation.

4.17.9. Bromide Center of Mass

The Br center of mass was calculated for both datasets described under 4.17.8 following the method described under 4.13.

5. Results and Discussion

In this section, results are organized in two parts: First, the results of the pilot leaching study carried out in 2007 are presented because the pilot study was the basis for defining the plot size and sampling distance for the main leaching study of 2008. Second, the results of the main leaching study of 2008 are presented and then discussed.

5.1. Pilot Study (2007)

5.1.1. Bromide and Soil Water Content Profile Distribution in 2007

Bromide and gravimetric soil water content θ_g distributions for the pilot study in Figure 5.1 show a higher water content on the first 11 m of the transect as a consequence of irrigation water applied prior to the Br^- pulse. This pattern holds for the 0-50 cm depths. At depths beneath 50 cm, soil water content becomes nearly constant in space within a particular layer (Figure 5.1). The Br^- concentration series for each depth increment, derived from colorimetric analyses (Figure 5.1) suggest leaching deeper than 50 cm depth barely occurred. From 50-100cm depth increments, Br^-concentrations displayed in Figure 5.1 are < 10 mg Br^-/kg soil. The Br^- concentrations at depths below 50 cm are assumed to reflect, to a great extent, the native soil chloride background rather than Br leaching signal.

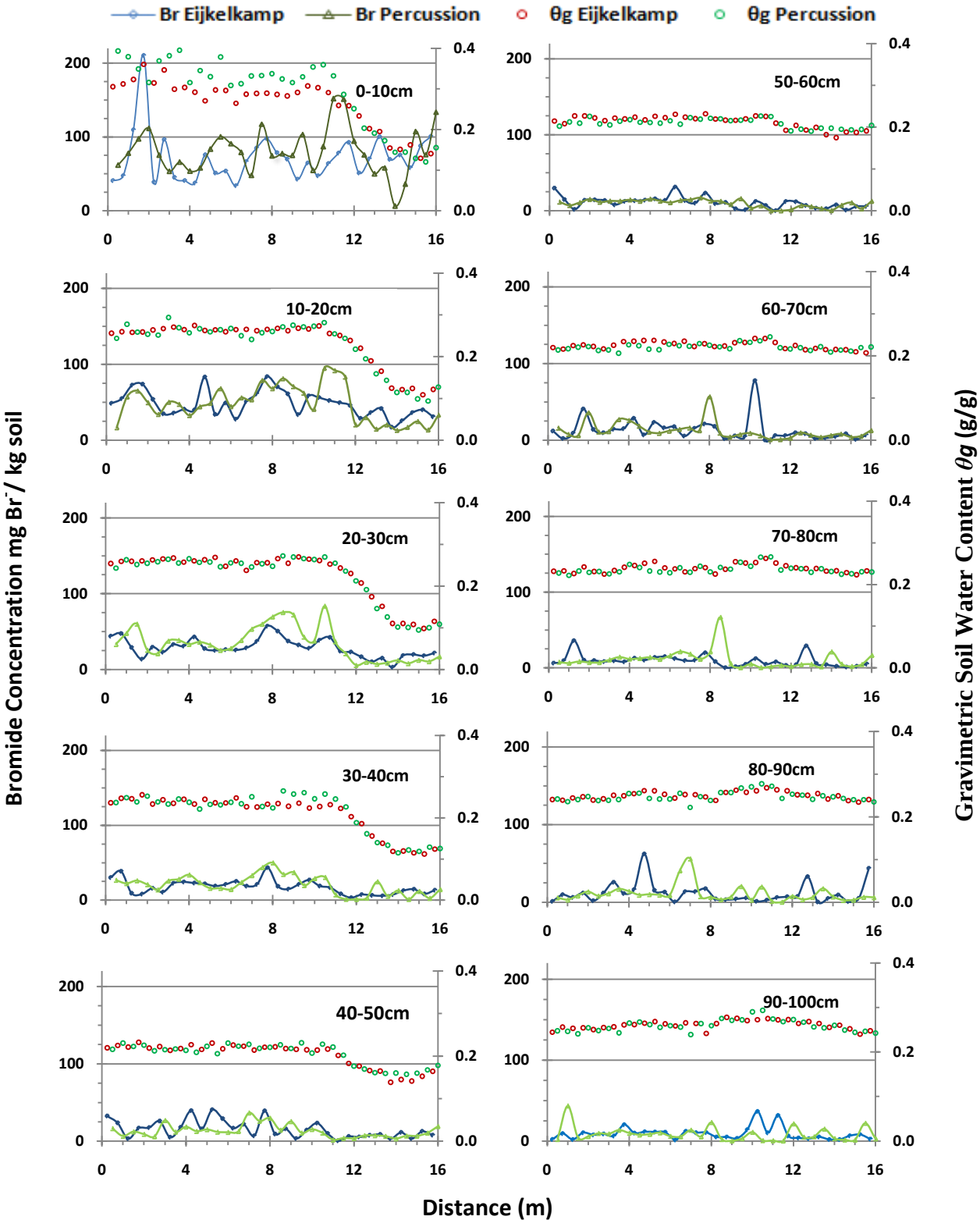

Figure 5.1. Spatial distribution of soil water content and Bromide concentration on Oct-10-07 sampled with Edelman and percussion cores. Pilot leaching study (2007).

Both Br^- and θ_g, at the moment of sampling were normally distributed. The two different sampling tools, Edelman auger and Percussion corer, showed small differences with respect to the mean and variance of Br^- and θ_g as displayed in Figures 5.2a and b. These differences were found not significant after an analysis of variance ANOVA (Table 5.1).

Regardless of the sampling tool, the overall tendency of the mean and variance of Br^- concentration is to decrease with increasing soil depth (Figure 5.2a). The mean of θ_g decreases from the surface to 50 cm depth and then increases from 50 to 100 cm depth (Figure 5.2b).

In summary, θ_g exhibits less variability than Br^- and this variability decreases with increasing depth, whereas Br^- variability is always greater than θ_g and increases with decreasing depth (Figure 5.2c). These findings suggest that water redistribution processes occur faster than solute redistribution.

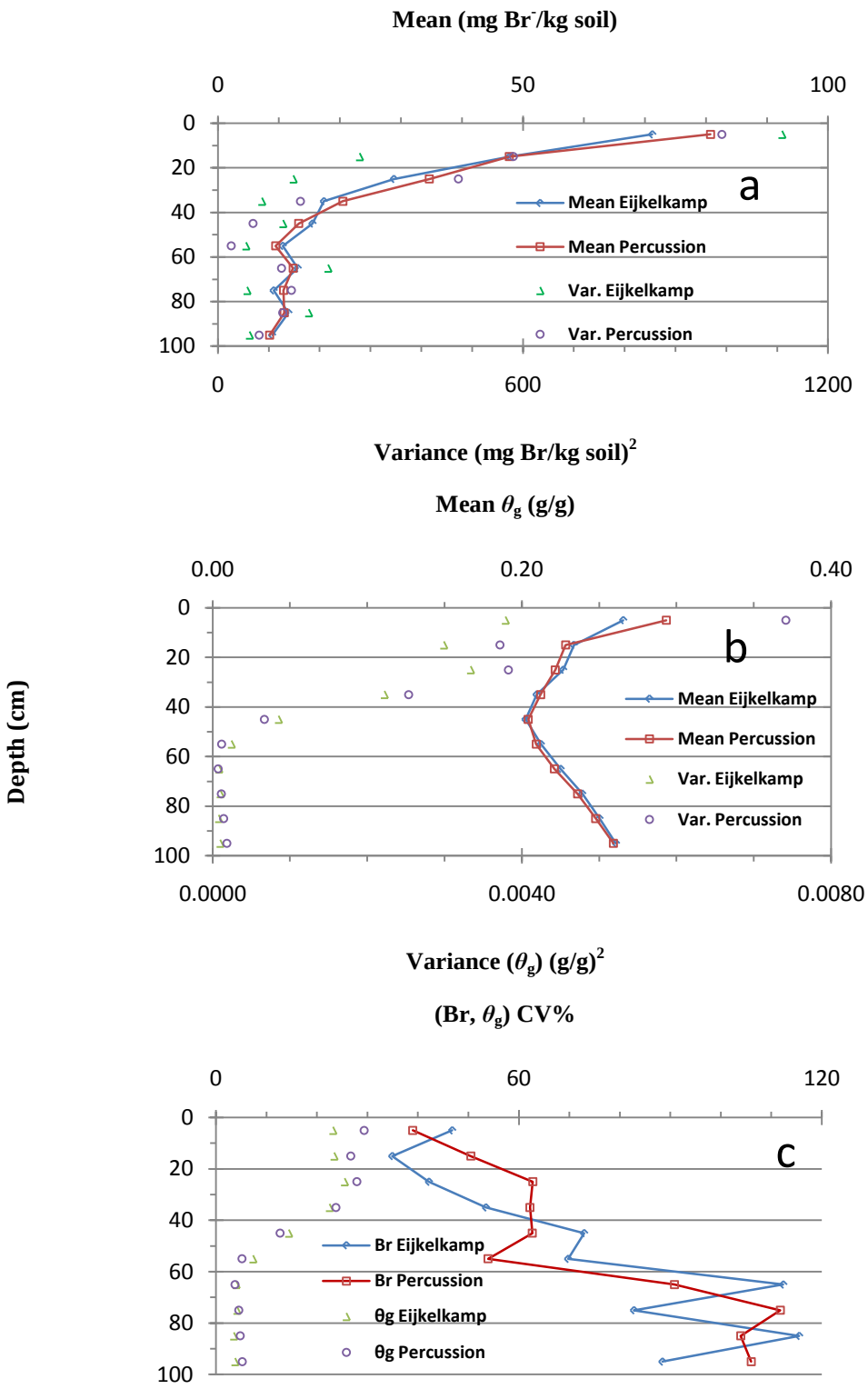

Figure 5.2. Bromide and soil water content descriptive statistics: mean, variance and coefficient of variation profiles for samples taken with Eijkelkamp and percussion cores on Oct-10-2007 (Pilot study).

Table 5.1. Probability values for F statistics comparing Eijkelkamp auger with Percussion corer samplers (Pilot study).

	Pr > F	
Depth (cm)	Br	θ_g
0 - 10	0.19	0.31
10 - 20	0.34	0.30
20 - 30	0.11	0.53
30 - 40	0.40	0.57
40 - 50	0.73	0.17
50 - 60	0.18	0.09
60 -70	0.78	0.39
70 - 80	0.50	0.43
80 - 90	0.83	0.10
90 – 100	0.85	0.39

5.1.2. Spatial Analysis of Br^- and Soil Water Content in 2007

The autocorrelation length λ indicates the distance over which observations are correlated to each other. However, the spatial representativity of one observation corresponds to 2λ. Spatial structure was found for Br^- from 10-40 cm depth as shown in Figure 5.3 for $\lambda \leq 4$ lags, i.e., 1 meter separation distance. Thus the spatial representativity of one Br^- observation along the transect from 10-40cm depth is 2 m. Variation for depth compartments from 0-10 cm and below 60 cm for Br^- was random (Figure 5.3). Soil water content presented spatial structure in all depth compartments investigated (Figure 5.3) probably as a result of the long trend in water redistribution after irrigations. The correlation length for θ_g is 10 lags (2.5 m) for the depth increments between 0-60 cm and $\lambda \leq 4$ lags (1 m) for all depth increments below 60 cm (Figure 5.3).

These findings suggest that the spatial scale of variation for Br^- transport in a Maury silt loam soil extends over 2 m length (10-40 cm depths), i.e., sampling locations at distances < 1 m along a transect yield Br^- observations that are correlated to each other. This very

important finding is the criterion used to design the maximum length of plots (2 m) and the separation distance of soil samples for the main Br^- leaching study of 2008, and constitutes a priori knowledge of the spatial scale of variation of Br^- and water transport in this Maury silt loam soil. Ellsworth and Boast (1996), identified the lack of *a priori* knowledge of the spatial scale of variation of water and solute transport as the main factor limiting their understanding of observed phenomena.

In conclusion, the spatial scale of variation of water and solute transport can be investigated at the field scale and furthermore can be applied in the spatial design of experiments, i.e., the spatial scale of variation of Br^- represented by the spatial autocorrelation length λ was used to define the maximum length of plots (2 m for this study) over which different treatment effects were planned for the main leaching study of 2008. This approach of designing the plot size for leaching experiments facilitates the identification of treatment effects because sampling is conducted at shorter distances than the known spatial scale of variation and therefore, observations sampled within this scale are expected to be correlated to each other.

These findings confirm that adequate field solute transport investigation requires a greater sampling effort than soil water content investigation, because observations for solute investigations were found to have shorter autocorrelation lengths λ than those of θ_g.

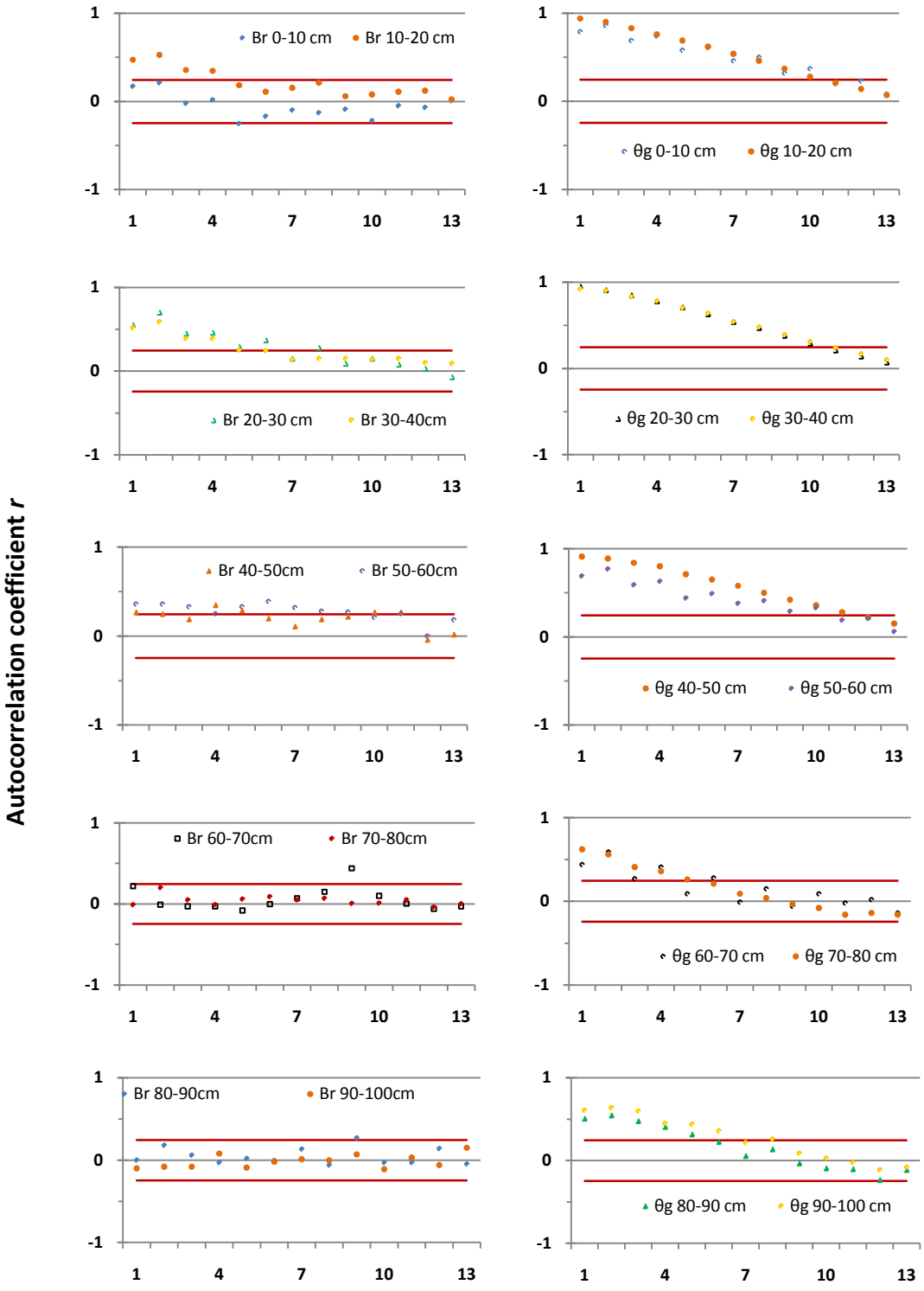

Figure 5.3. Spatial autocorrelation of Br^- (calculated with molar factor)and θ_g sampled in Oct-10-07 after 26 days of Br^- pulse on the pilot leaching study of 2007. Red lines are the 95% confidence intervals for the autocorrelation function.

5.1.3. Water and Br^- Mass Balances (2007)

Initial soil water content samples taken before the Br^- pulse were used to calculate the water mass balance for the pilot leaching study. The pattern of θ_g observations displayed in Figure 5.4 corresponds to the irrigation applied to the field transect to create different initial soil moisture profiles. These θ_g observations are the starting point for the water mass balance calculation.

The water mass balance was normally distributed with an average mass recovery of 83% throughout the transect as shown in Figure 5.5, and exhibited small variability (CV 3.5%). The 83% water mass recovery indicates a net water was loss in the transect profiles. The water loss is probably an effect of evaporation coupled with lateral redistribution during the 26 days of the pilot leaching study. However, water drainage to depths >100 cm cannot be discarded given the high θ_g status of the 50-100 cm depth increments (0.22-0.26 g/g) at the moment of sampling (Figure 5.4b). There is a slightly larger water mass balance for 12-16 m distance (Figure 5.4a) probably because the initial soil water status at these locations was smaller than that at 0-12 m distance, i.e., 0.25 g/g for 0-12 m distance and 0.15 g/g for 12-16 m distance down to 50 cm depth. Probably, the lower initial saturation at the 12-16 m distance favors smaller water fluxes out of these compartments.

The Bromide mass balance was normally distributed with an average mass recovery of 122 and 83 % for the original Br^- concentrations and those corrected for Cl^- background, respectively (Figure 5.5).

The excess Br^- mass recovery based on the original Br^- concentrations is probably an artifact caused by Cl^- background concentration of the soil (average Cl^- background was 11.6 mg/ kg soil for the 0-60 cm depth, see 4.17.8) whereas the 83 % mass recovery based on the Br^- concentrations that were corrected for Cl^- background suggests either that a) the average Cl^- background estimated for 11 observations along the transect was not an accurate representation of Cl- background at the experimental site, or b) there was Br^- flux out of the 0-100 cm depth profile which could be a reasonable assumption since the water mass balance was also 83%.

The Br^- center of mass (CoM) displayed in Figure 5.5 was normally distributed, with an average of 31 and 25.5 cm depth for the original Br^- concentrations and the Br^- concentrations corrected by Cl^- background, respectively. Consistently with the mass balance conclusion, the 100% Br^- signal had a higher mean CoM and exhibited less variation (CV = 23 %) than the Cl^- background corrected signal (CV = 39 %). Also, for transect distances 0-12 m where higher initial soil moisture conditions prevailed (Figure 5.4) deeper leaching of Br^- occurred (Figure 5.5). This is not surprising since the unsaturated hydraulic conductivity coefficient is known to increase with increasing soil water content (Jiang et al., 1997)

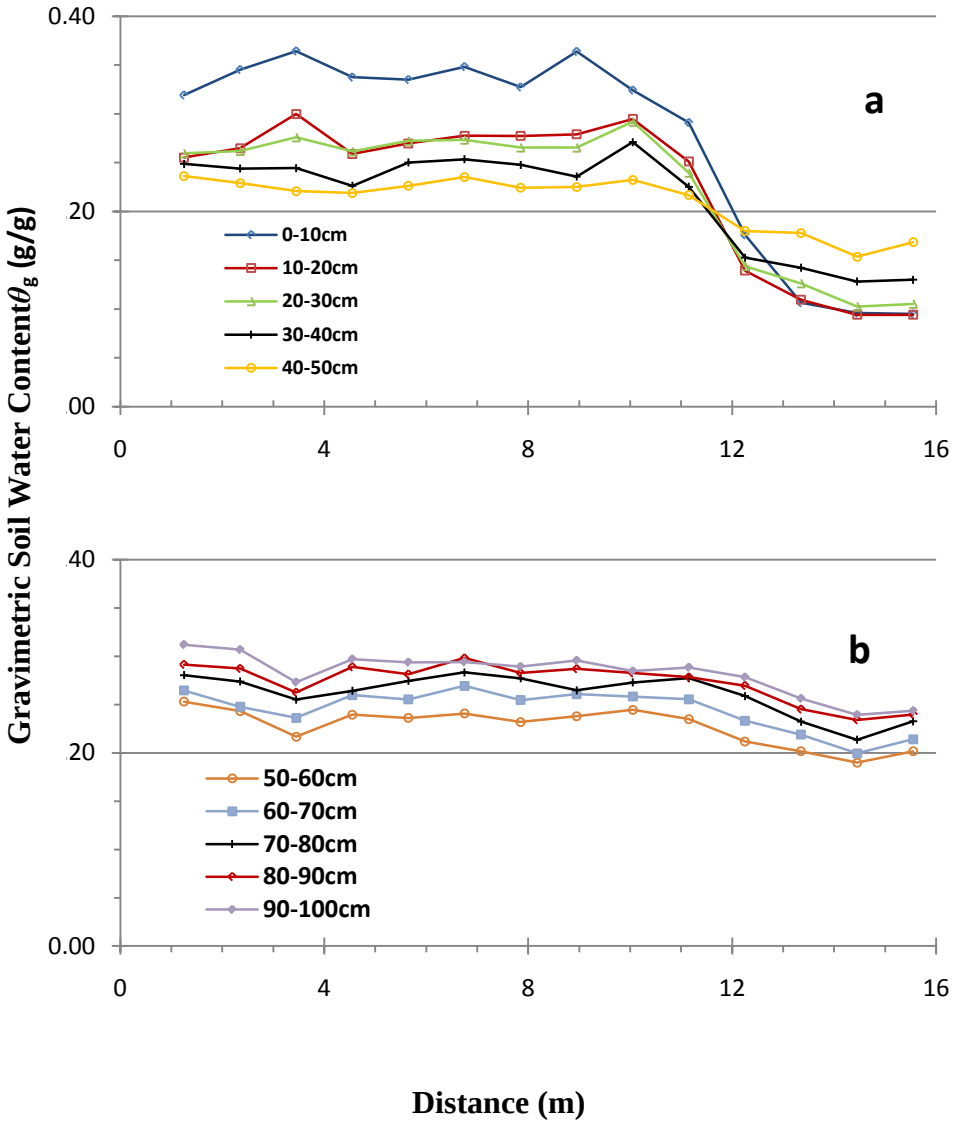

Figure 5.4. Initial soil water content on core samples taken on Sep-14-07 prior to Br^- pulse application in the pilot study.

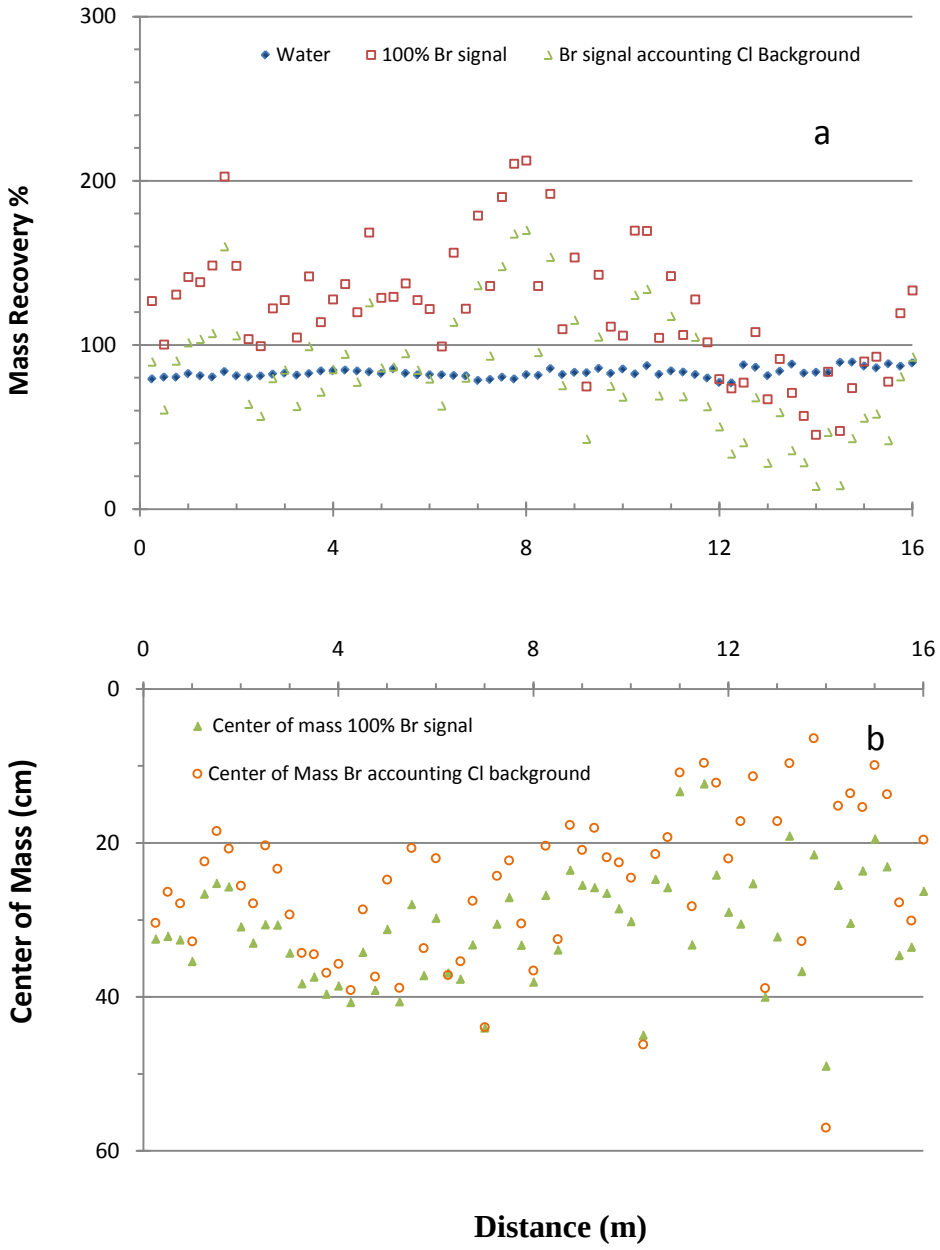

Figure 5.5. Bromide and water mass balances (a), Bromide center of mass (b) for the pilot study in 2007. Tracer and water sampled 26 days after the Br pulse application.

5.2. Main Leaching Study (2008)

5.2.1. Textural Analyses and Soil Profile Description

Soil particle size distribution determined in the lab for the 7-13 cm depth interval depicted in Figure 5.6 revealed little variation in soil texture as shown by the ranges for % sand, % silt, and % clay which were 6.9 to 10, 61.9 to 74, and 18 to 29 %, respectively. Because of this little variation of soil textural distribution at the 7-13cm depth, 15 out of 16 samples were classified as silt loam and only one sample, corresponding to the 45 m distance (plot 23) had enough clay to reach the silty clay loam classification. The profile descriptions for all 16 intact cores indicated that, for the 7-13 cm depth interval, the horizon designation corresponded to an Ap horizon with granular structure and a 10YR 3/3 matrix color and 10YR 2/1 concretions. These soil attributes, i.e., horizon designation, structure and color, were present in all the core samples taken at 7-13 cm depth and are consistent with the information for the experimental site provided by the NRCS Web-Soil-Survey database accessed on Oct-20-08. Continuing with textural laboratory analyses, the samples taken at the 27-33 cm depth interval showed a slightly greater variation in % silt and % clay than in the above layer as shown by their ranges of 51.6 to 73.72 and 19.76 to 39 %, respectively (Figure 5.6). Interestingly, the range of % sand at the 27-33 cm depth (5.87 to 9.12 %) was very similar to the one at 7-13 cm depth (6.9 to 10%). The ranges for the sand, silt and clay content at the 27-33cm depth classify these samples as silt loam and silty clay loam categories. Therefore, for the 27-33 cm depth interval and considering transect distances from 0 to 25 m, texture corresponded to a silty clay loam and the following observations along the transect for distances > 25m were classified as silt loam.

Profile descriptions made on six intact cores for transect distances between 0 and 25 m indicated that four out of six core samples presented a Bt1 horizon at the 27-33 cm depth interval accompanied by a change in soil structure from granular at the 7-13 cm depth to sub-angular blocky at the 27-33 cm depth interval with 7.5YR4/6 matrix color and10YR 2/1 concretions.

Two core samples for the 27-33 cm depth interval, and 0-25 m transect distance were classified as an AB (Plot 3, transect distance of 4-6 m) and BA (Plot11, transect distance of 20-22 m) horizon with a 7.5YR 4/4 and 10YR 4/4 matrix color, respectively. And both horizon's structures were described as granular and sub-angular blocky structure according to the profile description. The finger test for both the AB and BA horizon at plot 3 and plot 11, respectively, indicated a silt loam texture for the AB horizon and a silty clay loam texture for the BA horizon. The finger test was consistent with the laboratory textural analyses for all samples but the one in plot 3, where a silty clay loam was reported by the lab method and a silt loam was reported from finger test. This is probably an error in the estimation of % clay or % sand in the manual determination of texture.

For transect distances > 25 m at the 27-33 cm depth interval, ten cores were taken and described as transitional horizons, either an AB or a BA horizon and eight out of ten of these cores presented a matrix color of 10YR 4/3 and only two (Plot 13, 15 on transect distances 24-26 m and 28-30 m) out of these ten core samples presented a matrix color of 7.5YR 4/4. For transect distances > 25 m and for the 27-33 cm depth, the manual determination of texture was consistent with the lab determination and corresponded to a

silt loam. Also, the soil structure for transect distances >25 m at the 27-33 cm depth were granular to sub-angular blocky.

In conclusion, the description of the Bt1 horizon for the 27-33 cm depth interval for the 0-25 m transect distance, and the transitional AB or BA horizon description for transect distances >25 m at the 27-33 cm depth interval were consistent with the soil textural analyses. The change in textural classification for the 27-33 cm depth is due to the progressive increase in the range of % silt from 50 to 60 % for the 0-25 m transect distance, to a range of 60 to 74 % for transect distances > 25 m and also to a decrease in clay content range from 30-40 % for the 0-25 m transect distance to 20 to 28 % for transect distances > 25m (Figure 5.6).

In the following depth interval, from 47 to 53 cm depth and according to laboratory texture determination, it can be seen in Figure 5.6 that samples taken at 0-10 m transect distance fall into the clay category, followed by a silty clay from 10 to 20 m distance and finally to a silty clay loam texture for transect distances > 20 m. These domains of soil texture at 47-53 cm depth were mostly the result of the change in clay and silt distribution along the transect as can be deducted from Figure 5.6. Horizons Bt1 and Bt2 with matrix color of 7.5 YR 4/6 and 5YR 4/4, respectively, were found for the 47-53 cm depth interval. However, the finger test for the profile description at the 47-53 cm depth interval, classified all the 16 core samples at this depth as silty clay loam and did not reflect the small changes in texture found from lab analyses.

Finally, the soil textural distribution pattern observed for the 67-73 cm depth displayed in Figure 5.6 closely resembles that of the previous depth interval (47-53 cm). However, it

was described as either Bt2 or Bt3 horizons and this designation was sustained on small changes in color from 7.5 YR 4/6 on the Bt1 (47-53 cm depth) to a 5YR 4/6 on Bt2 and Bt3 horizons (67-73cm depth). Manual textural determination for the profile description identifies the samples taken from 67-73 cm depth and for transect distances between 0 and 10 m, at the limit between silty clay loam and silty clay whereas the lab determination establishes the same samples to be within the clay class. For the domain between 10 and 20 m transect distance, the profile description of texture changes from a silty clay to a silty clay loam to a clay at the 67-73 cm depth whereas the lab method identified all of these as a silty clay. Finally, for transect distances > 20 m, both the manual and the lab method for texture determination agreed to a silty clay loam category for the 67-73 cm depth interval.

Therefore, assuming these changes in texture promoted differences in soil drainage, as larger diameter pores are expected in coarser textural soils, it can be expected that drainage and hydraulic conductivity coefficients will be greater at transect distances >25 m for the 27-33 cm depth interval, because textural changes at this depth reached from a silty clay loam for the 0 to 25 m distance to a silt loam for distances >25 m. Deeper in the soil profile, at 47-53 and 67-73 cm depth intervals, it can be inferred that a larger drainage occurred at transect distances >20 m since the % clay decreases progressively from ≈50 % for the 0 to 10 m distances to 45% from 10 to 20 m distances and finally to≈ 30 % for distances >20 m (Figure 5.6) which corresponded to a textural determination of clay, silty clay and silty clay loam, respectively.

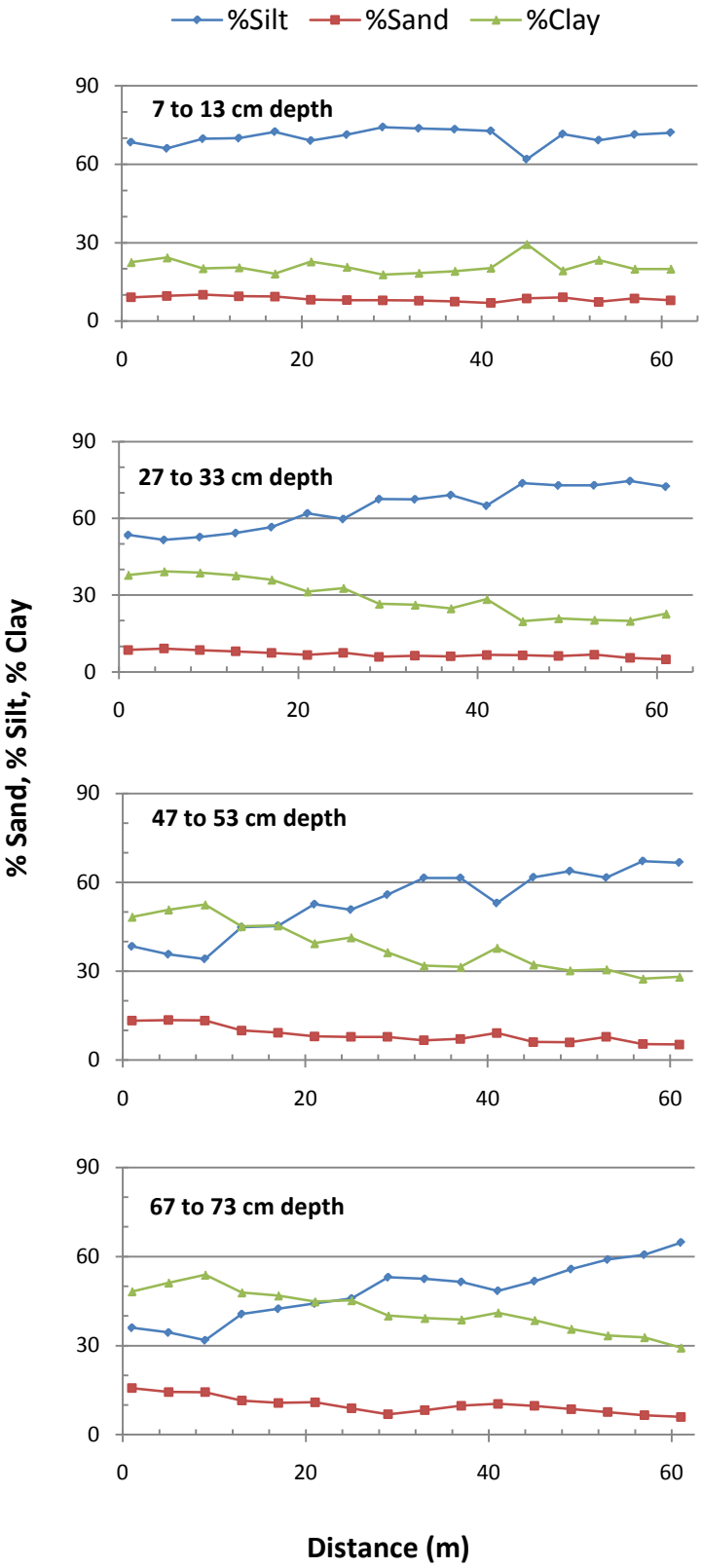

Figure 5.6. Soil particle size distribution along the investigated transect. Soil series is a Maury silt loam soil. Ticks on the x axis are distributed at 4 m intervals.

5.2.2. Soil Water Matric Potential ψ_m Readings During Main Leaching Experiment

5.2.2.1. Initial Soil Moisture Conditions on Oct-19-08

The initial ψ_m profile conditions for the beginning of the main leaching study are presented in Figure 5.7. All soil profiles on Oct-19-08 were reasonably moist, ψ_m >-300 cm and although the different moisture conditions intended for the 0-32 and 32-64 m distances were not achieved (Figure 5.7), the ψ_m profile for the beginning of the leaching study was a fundamental information for the hydraulic gradient ($\Delta H/\Delta z$) and water mass balance calculation as well as a starting point for the simulations of water and Br^- transport. There were however, some profiles in which perched water tables occurred for some depths as hydrostatic pressure was observed for the tensiometers installed at 10, 30 and 90 cm depth for transect distances between 16 and 40 m (Figure 5.7).

5.2.2.2. Soil Water Matric Potential Monitoring During Low Intensity Irrigations and at Tracer Sampling

The ψ_m readings taken between Oct-23 and Oct-31 are presented in Figures 5.8-5.11. The results obtained for the low irrigation intensity plots, i.e., plots 5-12 and 21-28 (Figures 5.8-5.10), could be interpreted as a larger drainage capacity for plots 21-28 (40-56 m distance) than plots 5-12 (8-24 m distance). Larger fluctuations in ψ_m observed for plots 21-28 can cause larger $\Delta H/\Delta z$ and fluxes in these plots and therefore could be associated with faster drainage for the tensiometers in plots 21-28 than in plots 5-12. In Figure 5.11, ψ_m measured on Oct-25 indicated values closer to saturation for most of the transect and all tensiometer depths, one day after irrigation treatments were applied to all the plots

with exception to plots 1-4 (0-8 m distance) and plots 13-16 (24-32m distance). In Oct-31, however, the ψ_m observations indicated that all the soil profiles investigated had reached conditions very close to hydraulic equilibrium (Figure 5.11), i.e., the only difference in ψ_m observations across depths corresponded to the gravitational potential ψ_z component of the total head *H*, and no net water transport occurred due to values of *H* very similar to each other across depths.

To better illustrate the magnitude and direction of flow in this study, the main focus of the analysis was the $\Delta H/\Delta z$ given that Darcian flow in porous media is defined by:

$$J_w = -\frac{\Delta H}{\Delta z} K(\psi)$$

where

J_w = Water flux [length/time]

$\Delta H/\Delta z$ = hydraulic gradient [length/length]

$K(\psi)$ = hydraulic conductivity for the average ψ_m in soil compartment [length/time]

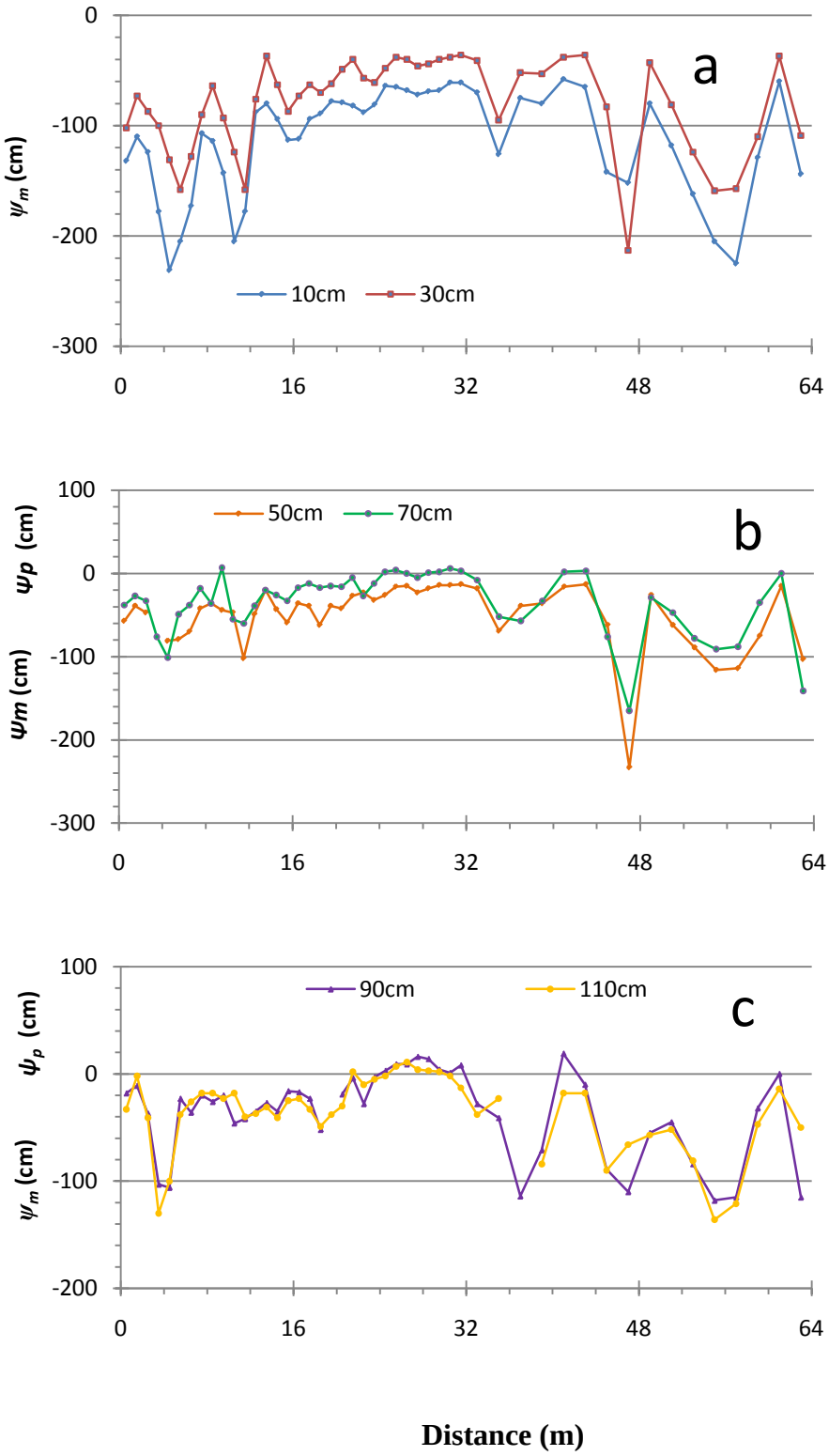

Figure 5.7. Initial soil profile conditions of the soil water matric potential ψ_m. ψ_p denotes hydrostatic pressure head. Readings were taken on Oct-19-08 for all 48 tensiometer nests along the investigated transect.

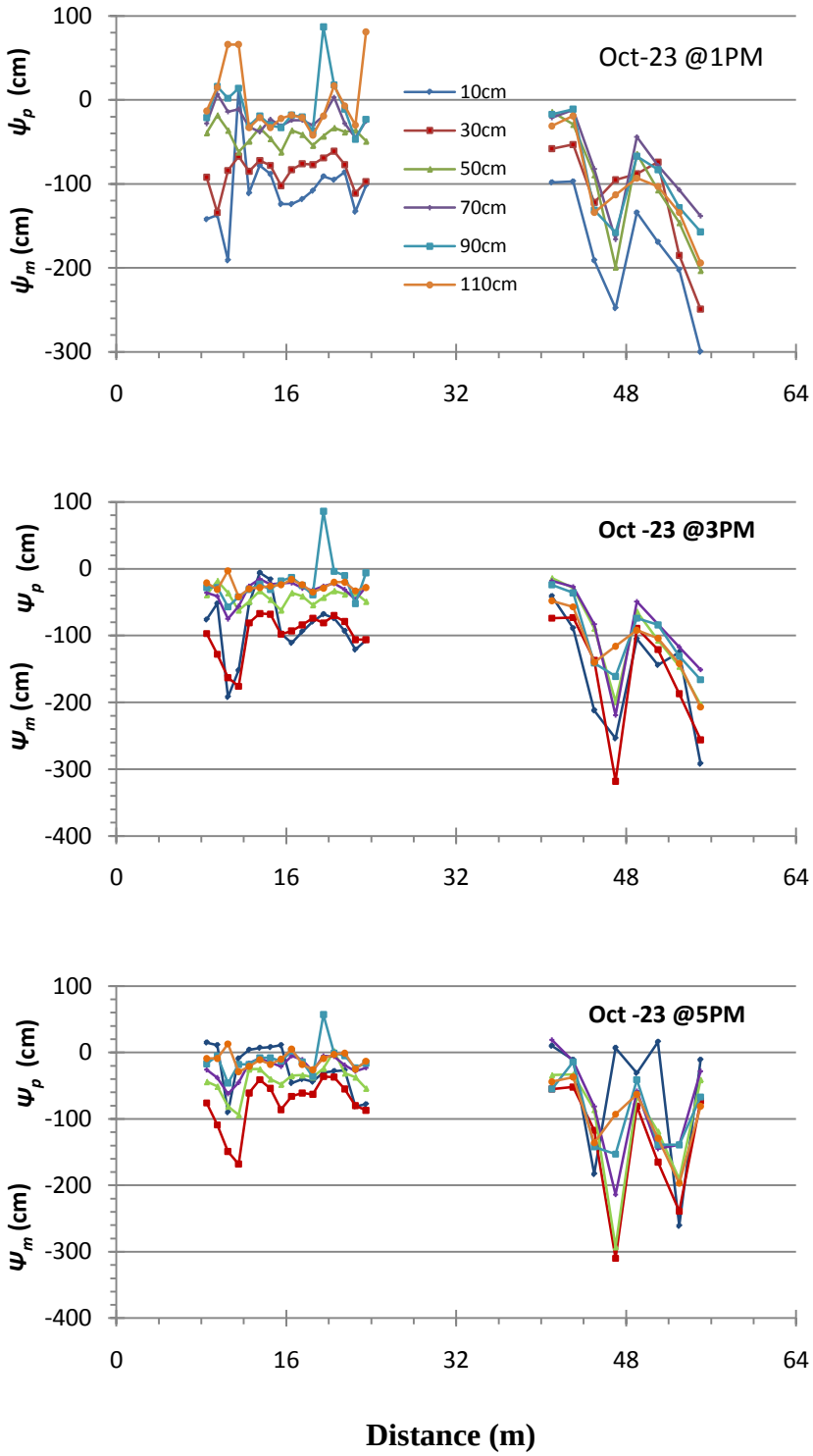

Figure 5.8. Soil water matric potential ψ_m and hydrostatic pressure head ψ_p readings during low intensity irrigations in plots 5-12 and 21-28 for Oct-23-08 between 1 and 5 PM.

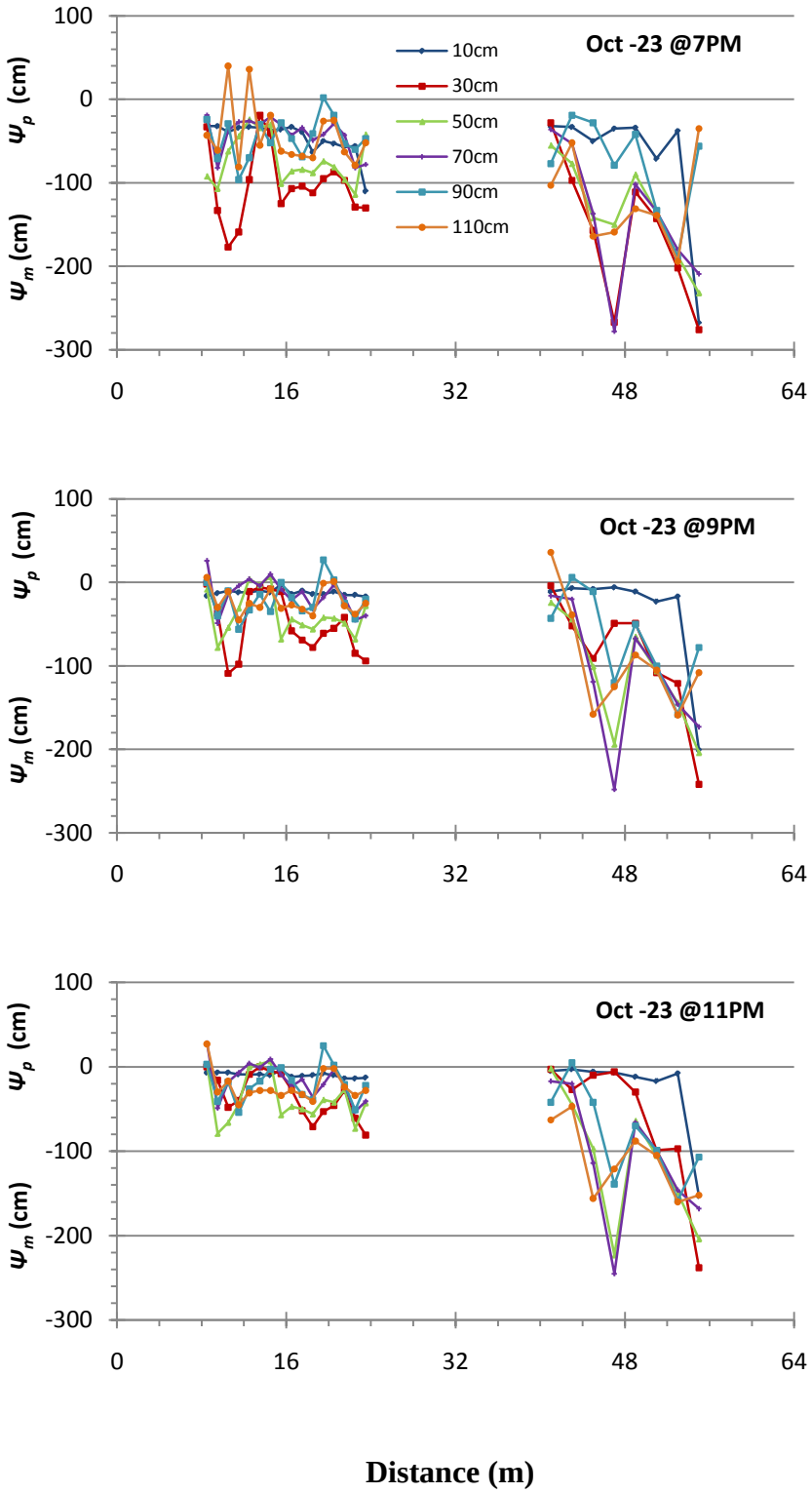

Figure 5.9. Soil water matric potential ψ_m and hydrostatic pressure head ψ_p during low intensity irrigations on plots 5-12 and 21-28 for Oct-23-08 between 7 and 11PM.

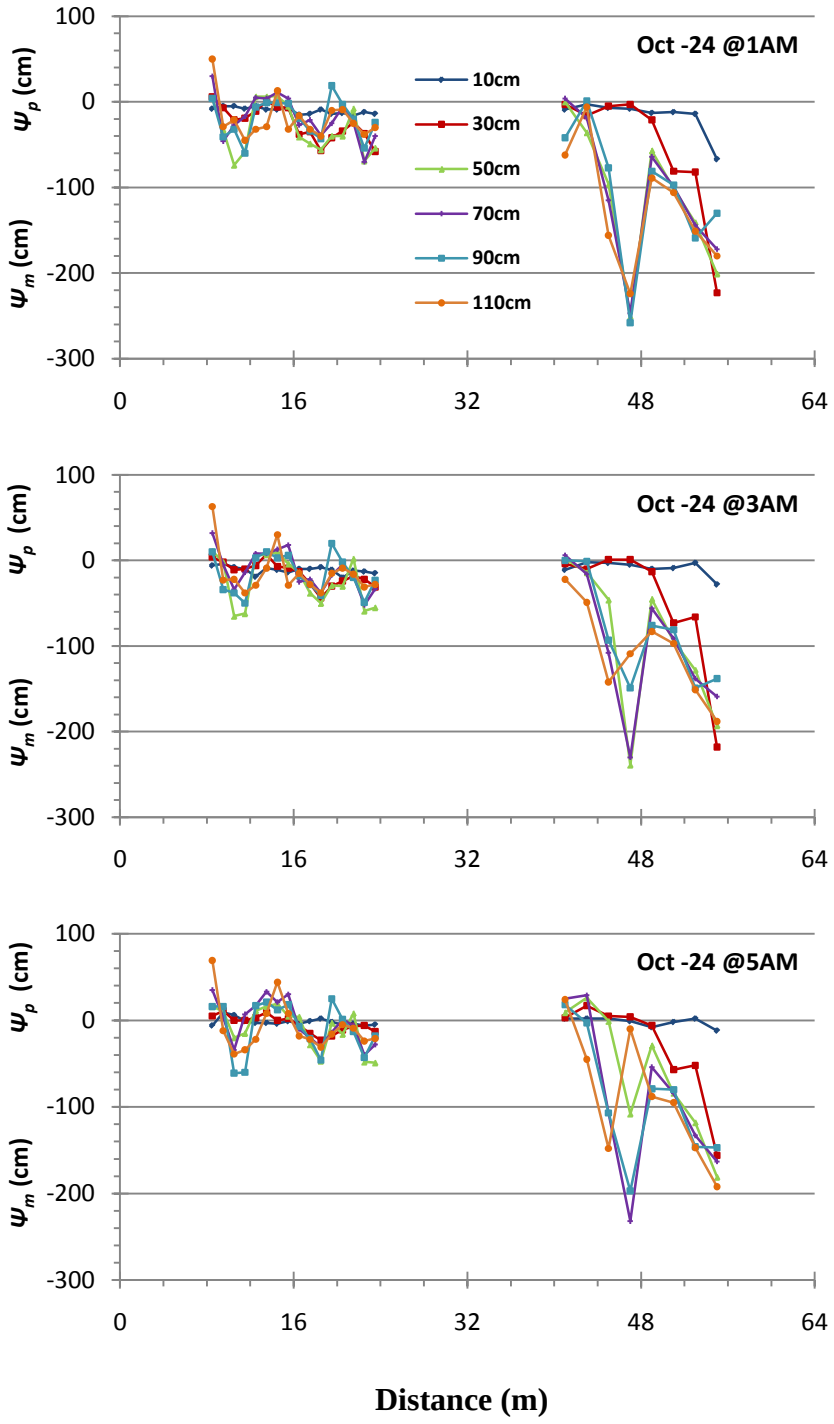

Figure 5.10. Soil water matric potential ψ_m and hydrostatic pressure head ψ_p during low intensity irrigations in plots 5-12 and 21-28 for Oct-24-08 between 1 and 5AM.

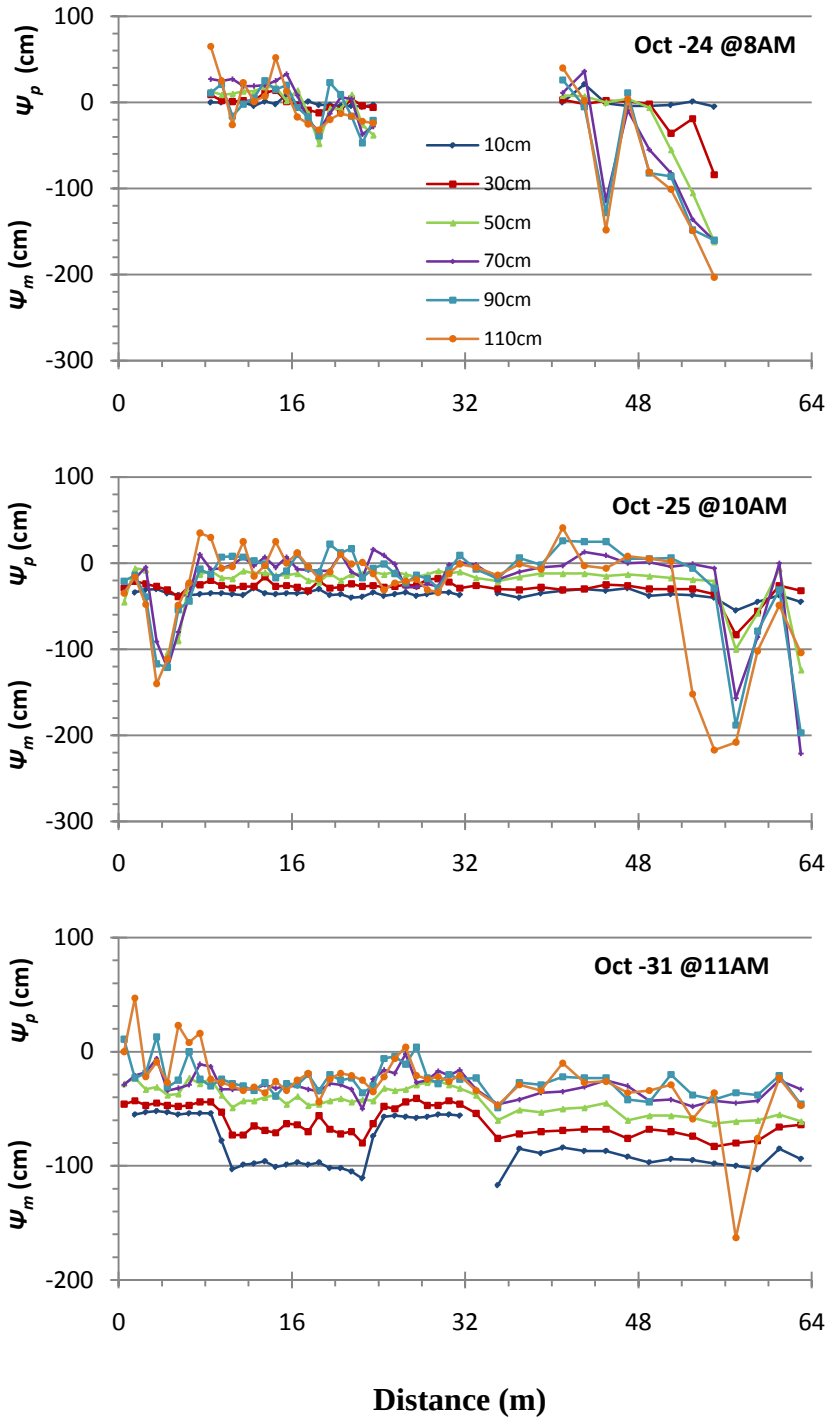

Figure 5.11. Soil water matric potential ψ_m and hydrostatic pressure head ψ_p during low intensity irrigations on plots 5-12 and 21-28 for Oct-24-08 at 8AM. Readings for Oct-25 and Oct-31 correspond to one day and 7 days after application of irrigation treatments.

5.2.3. Hydraulic Gradient Monitoring

Observations of the hydraulic gradient are presented in Figures 5.12-5.19 for the five depth compartments studied. The initial status of the hydraulic gradient of the experiment (Oct-19-10AM) indicated a slightly upward directed $\Delta H/\Delta z$ for transect distances between 0-24 m for the three depth increments shown in Figure 5.12. From 24 to 40 m distance, hydraulic equilibrium was observed across the three depth compartments (10-30, 30-50 and 50-70cm) at the beginning of the experiment on Oct-19-10AM (Figure 5.12). However, for transect distances >40 m and for the 10-30 and 30-50cm depth increments, a slightly upward directed $\Delta H/\Delta z$ was found whereas for the same transect distances (>40 m) in the 50-70cm depth increment, downward directed $\Delta H/\Delta z$ was present (Figure 5.12). This behavior of $\Delta H/\Delta z$ was probably the result of equilibration and redistribution processes in the soil triggered by pre-wetting irrigations applied prior to the beginning of the experiment.

For the lower depth compartments, at 70-90 and 90-110 cm, a downward directed $\Delta H/\Delta z$ was observed at the beginning of the experiment on Oct-19-10AM for the majority of locations along the transect (Figure 5.13).

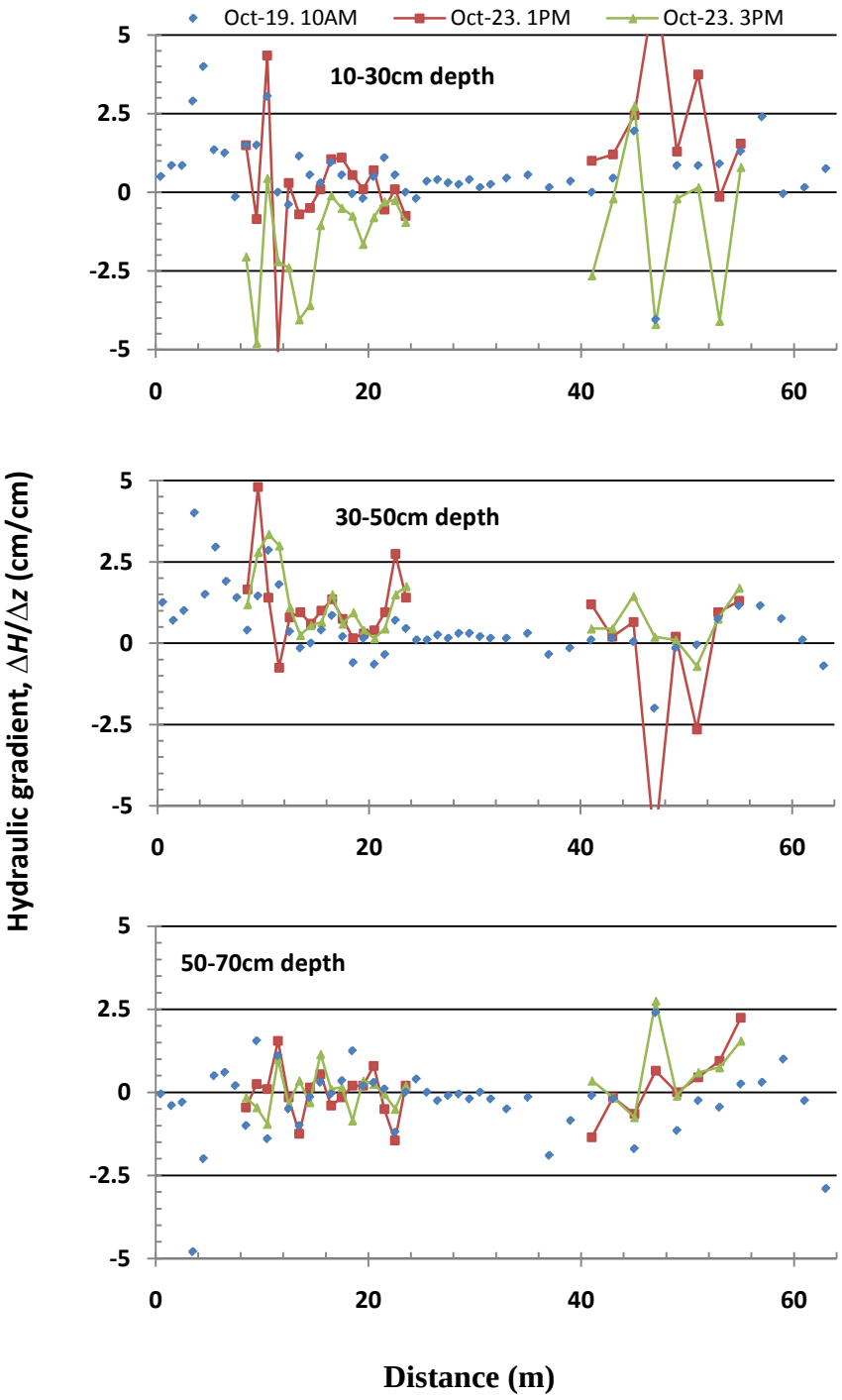

Figure 5.12. Hydraulic gradient at the beginning of the leaching study (Oct-19-08), and after 1 and 2 short irrigation pulses of the low intensity irrigation treatments (Oct-23 at 1 and 3PM). Upper depth compartments are shown.

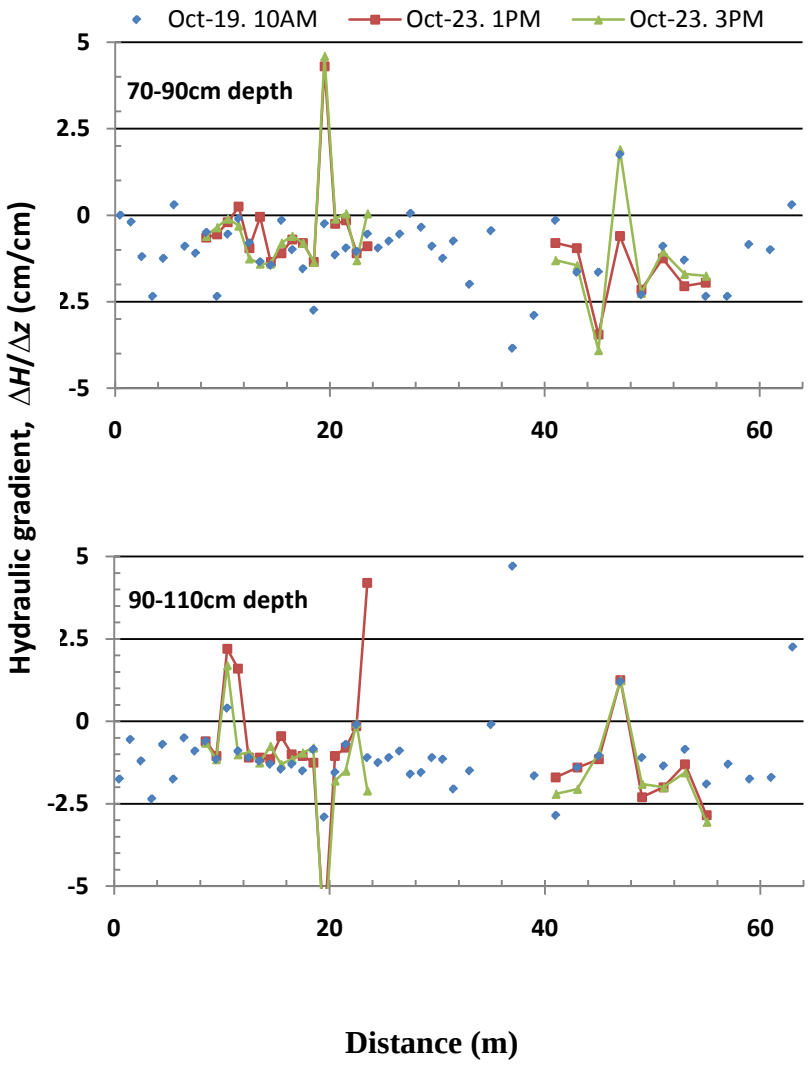

Figure 5.13. Hydraulic gradient at the beginning of the leaching study (Oct-19-08), and after 1 and 2 short irrigation pulses of the low intensity precipitation treatments (Oct-23 at 1 and 3PM). Lower depth compartments are shown.

After five short pulses of 0.16 and 0.08 cm the hydraulic gradients for plots 5-8, 21-24 and 9-12, 25-28 respectively, indicated consistently negative values suggesting downward directed water flux for the 10-30 cm depth compartment (Figure 5.14). Downward directed water flux was consistent for the same plots on Oct-23 at 7 and 9 PM for the 10-30 cm depth compartment as the cumulative precipitation added up to 1.12 and 0.56 cm, respectively.

The hydraulic gradient for the 30-50cm depth compartment remained at values around equilibrium with small spatial differences (Figure 5.14), leading to the assumption that the infiltrating water front had not reached the tensiometers at 30 and 50 cm depth by Oct-23 at 9 PM. It is interesting that at a transect distance of 47 m at the center of plot 24 and for the 30-50 cm depth compartment (Figure 5.14), $\Delta H/\Delta z$ had a faster response from nearly equilibrium on Oct-23 at 5 PM to a +5 cm/cm upward directed $\Delta H/\Delta z$ two hours later at 7 PM, and finally another quick response to a -8 cm/cm downward directed $\Delta H/\Delta z$ at 9 PM.

The fast changes, both in magnitude and sign of $\Delta H/\Delta z$ of this compartment (47 m distance, plot 24, 30-50cm depth compartment) could be attributed to either an erroneous ψ_m reading at the 50 cm depth (7 PM) or, to the presence of macropores connecting the domains of the 10 cm with the 50 cm depth tensiometers which could have caused a faster response of the tensiometer at 50 cm than the one at 30 cm depth. The unusually high ψ_m of the 50-cm-depth-tensiometer at 7 PM, -160 cm in Figure 5.9, is in contrast with the trend of increasing ψ_m observed for the neighboring tensiometers at 10 and 50 cm depths over the same time interval (5 and 9 PM) depicted in Figures 5.8 and 5.9.

The 50-70 cm depth compartment observations of$\Delta H/\Delta z$ shown in Figure 5.14 suggest conditions near hydraulic equilibrium in Oct-23 at 5, 7 and 9 PM with the exception of plot 24 (47 m distance) that still exhibited fast changes in $\Delta H/\Delta z$ being also a result of the unusually high ψ_m at 7 PM of the 50 cm depth tensiometer.

Finally, the 70-90 and 90-110 cm hydraulic gradients presented in Figure 5.15 indicate a predominant downward directed$\Delta H/\Delta z$ for observations taken on Oct-23 at 5, 7 and 9 PM.

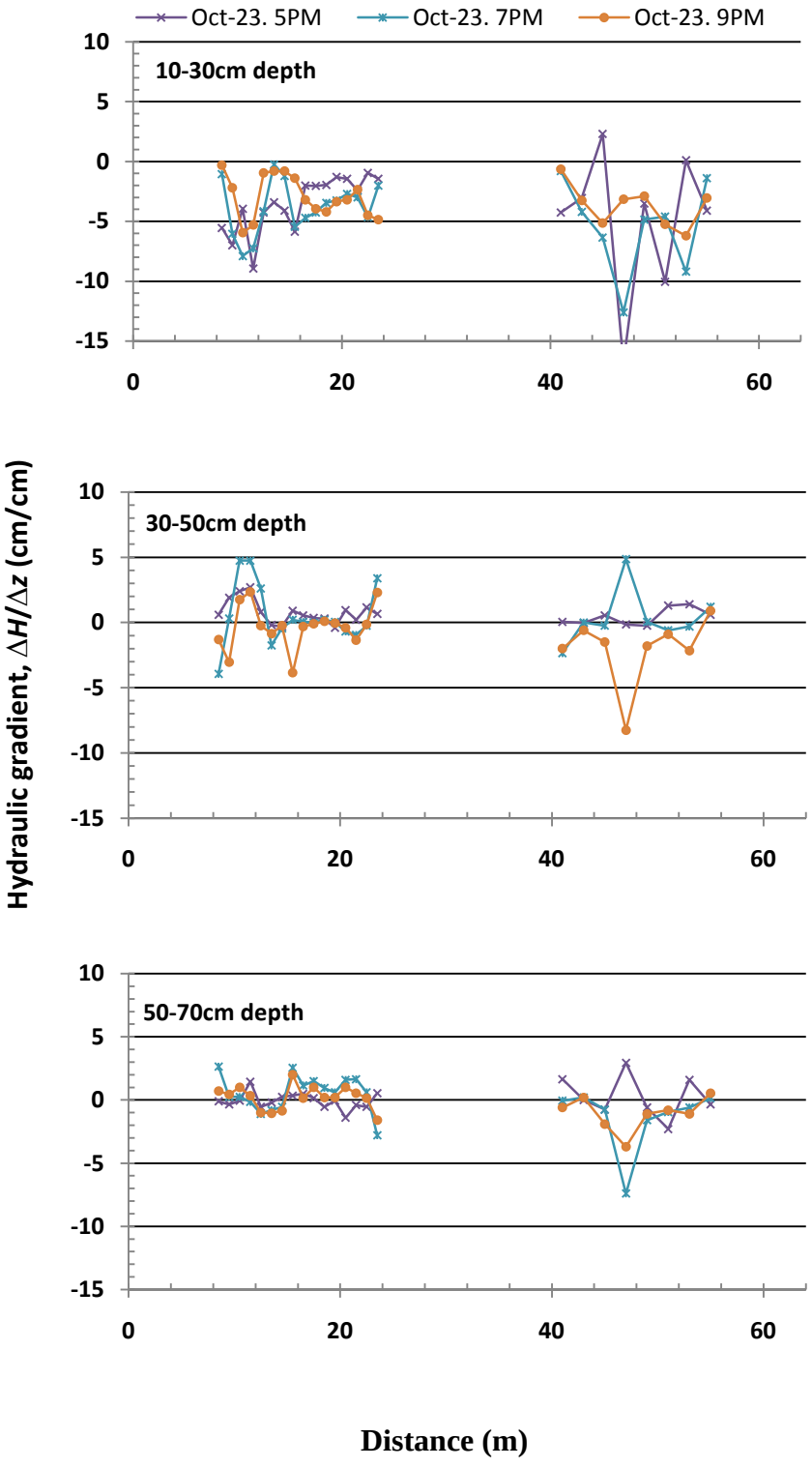

Figure 5.14. Hydraulic gradient monitored for upper three depth compartments on Oct-23-08 between 5 and 9 PM during the low intensity irrigation.

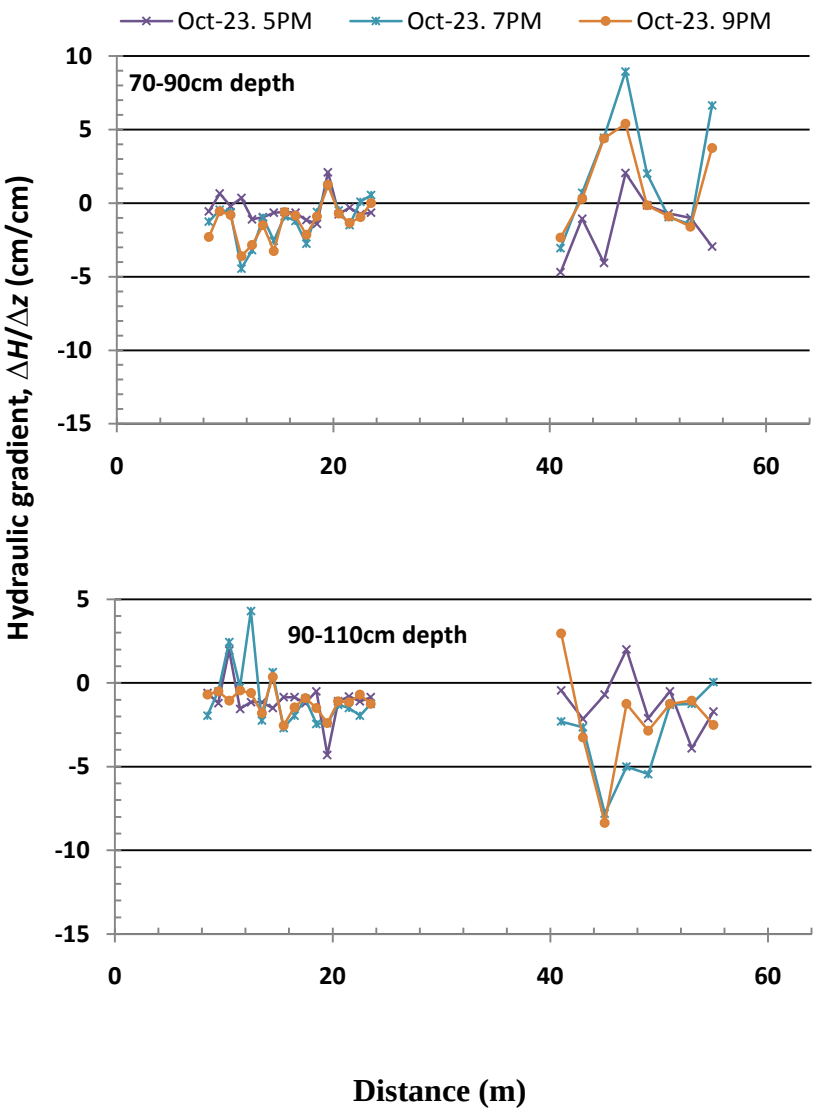

Figure 5.15. Hydraulic gradient monitored for lower depth compartments on Oct-23-08 between 5 and 9 PM during the low intensity irrigation.

Between Oct-23-08 at 11 PM and Oct-24-08 3 AM, little if any temporal changes on $\Delta H/\Delta z$ were observed for all six depth compartments shown in Figures 5.16 and 5.17.

However, the negative $\Delta H/\Delta z$ observed for plot 24 at a transect distance of 47 m across the 30-50 cm depth compartment (Figure 5.16) is two times larger than in its closest neighboring compartments. This larger $\Delta H/\Delta z$ in plot 24 was due to ψ_m readings very close to saturation ($\psi_m \geq$ -10 cm) at 30 cm compared to ψ_m readings of $-260 \geq \psi_m \geq -239$ cm being more than one order of magnitude smaller measured at 50 cm depth (Figures 5.9 and 5.10), and corresponding to the period between 11 PM Oct-23 and 3 AM Oct-24. Large temporal changes in $\Delta H/\Delta z$ were also observed before at the same location on Oct-23 between 5, 7 and 9 PM with abrupt changes in the direction of the $\Delta H/\Delta z$. However, for the observations made on Oct-23 at 11 PM and Oct-24 at 1 and 3 AM (Figure 5.16), the negative sign and magnitudes of $\Delta H/\Delta z$ and the consequently downward directed J_w were temporally stable suggesting that water infiltration did not reach deeper than the 30 cm tensiometer. This behavior could be attributed to the presence of a lower conductivity zone below 30 cm. Observations of $\Delta H/\Delta z$ shown in Figure 5.18 for Oct-24 across the 10-30cm depth compartment indicate larger hydraulic gradients in the plots receiving 3.52 cm/day; when compared to the 5.52 cm/day plots, i.e., plots 9, 10, 11, 12, 25, 26, 27 and 28 located at transect distances between 16 to 24 m and 48 to 56 m had larger hydraulic gradients than plots 5, 6, 7, 8, 21, 22, 23, and 24 located at transect distances between 8 to 16 m and 40 to 48 m. Also, these larger hydraulic gradients observed in plots that received the 3.52 cm/day precipitation intensity, had greater differences from the 5.52 cm/day plots where the texture at the 27-33cm depth was a silt loam (transect distances > 25m)

On Oct-25, the hydraulic gradient across the 10-30 cm depth displayed in Figure 5.18 was consistently downward directed with values between -0.05 to -2.4 cm/cm. On Oct-31 (Figure 5.18), values of $\Delta H/\Delta z$ fluctuated around equilibrium across the 10-30 cm depth compartment. In the 30-50 cm depth compartment shown in Figure 5.18, the behavior of $\Delta H/\Delta z$ was very similar to that described for the 10-30 cm depth compartment for all the readings. However, in plot 24 at a transect distance of 47 m on Oct-24 at 5 AM, a -6.6 cm/cm gradient was observed whereas three hours later at 8 AM, $\Delta H/\Delta z$ was reduced to -0.6 cm/cm. The behavior of plot 24 towards equilibrium in Oct-24 should be considered carefully because with a larger average soil water pressure head, a smaller $\Delta H/\Delta z$ is sufficient to conduct water downwards due to a higher hydraulic conductivity. In Plots 23 and 24 at transect distances of 45 and 47 m, the $\Delta H/\Delta z$ observations taken on Oct-24 at 5 and 8 AM for the 50-70 cm depth compartment in Figure 5.18 indicated a larger gradient for these two locations when compared to compartments in their closest neighborhood. These larger values of $\Delta H/\Delta z$ could possibly be attributed to the presence of macropore flow in plots 23 and 24 at the 50-70cm depth compartment. For the readings taken on Oct-25 and on the day of tracer sampling for the 50-70 cm depth compartment, the range of variation of $\Delta H/\Delta z$ was smaller and maintained a downward directed flux.

The observations of $\Delta H/\Delta z$ taken across the 70-90 and 90-110 cm depth compartments indicated a downward directed water flux for the entire transect and for all the readings taken between Oct-24 at 5 AM and Oct-31 at 11 AM (Figure 5.19). This downward directed flux was maintained, in part, due to the plastic tarps that covered the plots on Oct-24 at 5 PM to reduce evaporation.

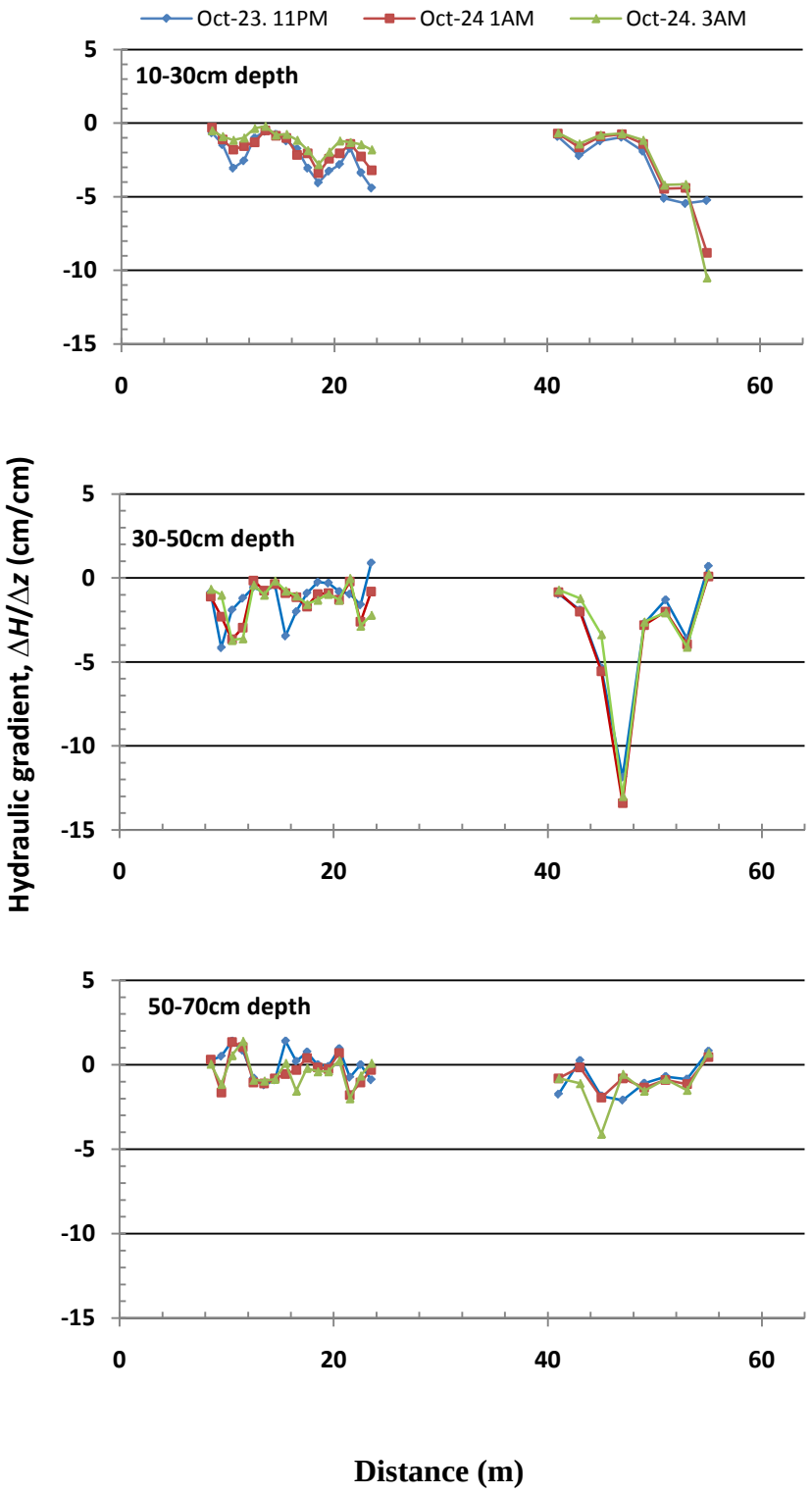

Figure 5.16. Hydraulic gradient monitored for the upper depth compartments between Oct-23-08 at 11 PM and Oct-24 3 AM during the low intensity irrigation.

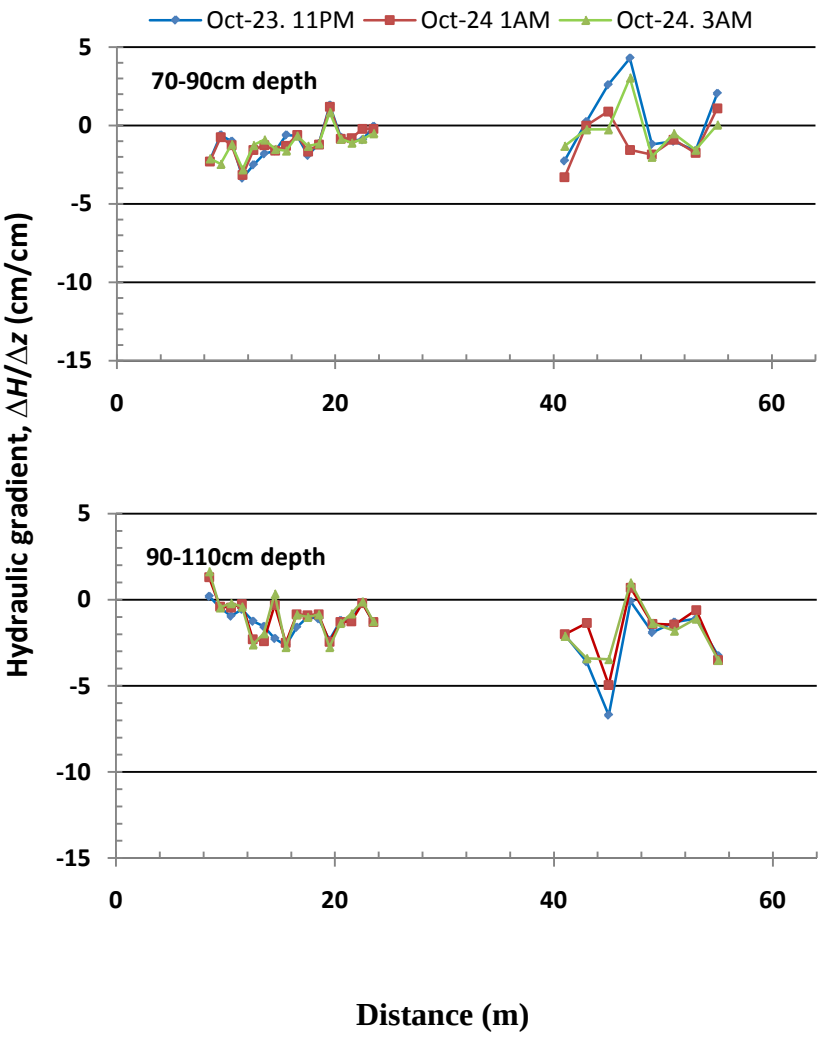

Figure 5.17. Hydraulic gradient monitored for the lower depth compartments between Oct-23-08 at 11 PM and Oct-24 3 AM during the low intensity irrigation.

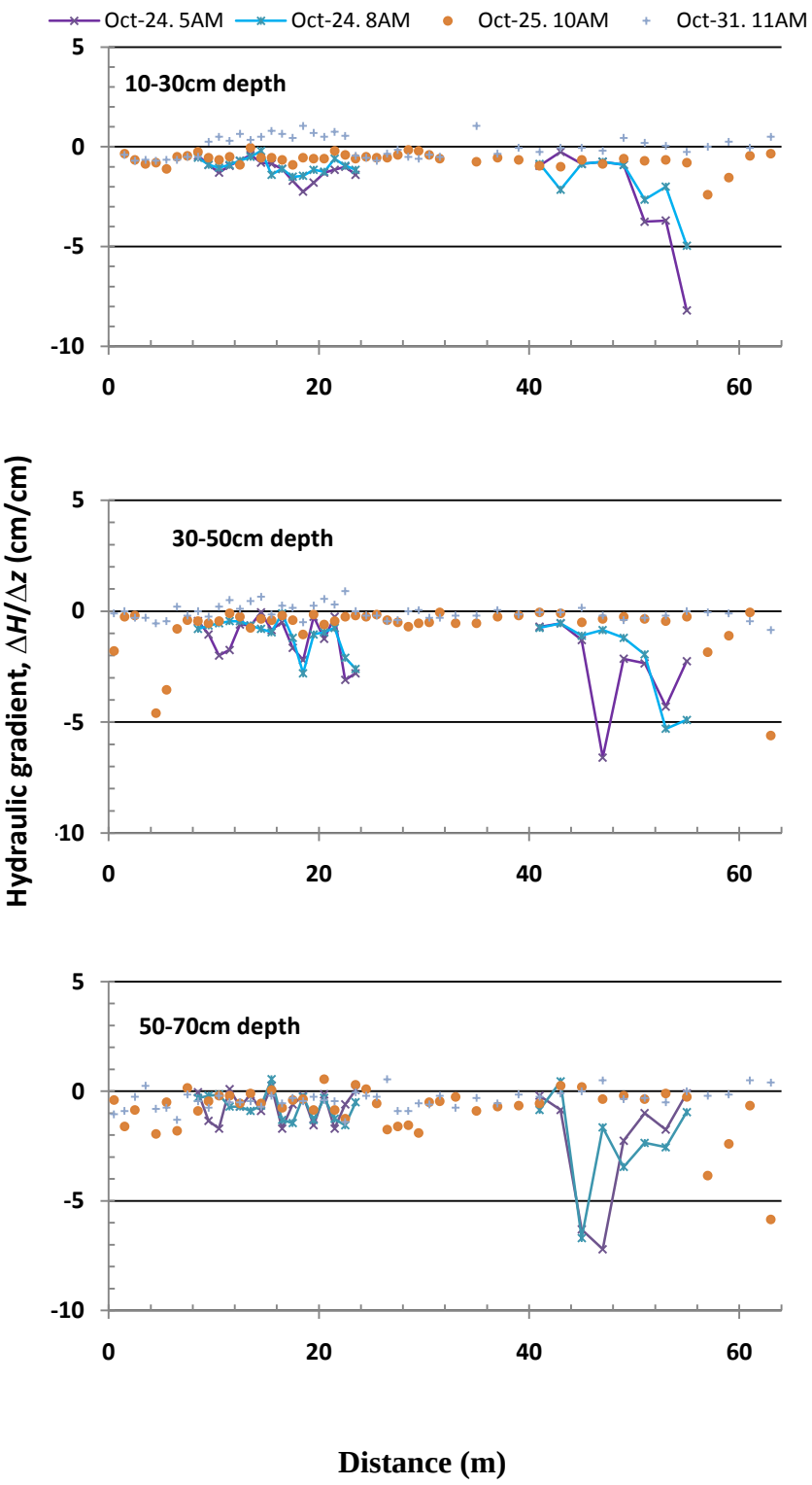

Figure 5.18. Hydraulic gradient monitored for the upper depth compartments between Oct-24, 5 and 8 AM during the low intensity irrigation. Hydraulic gradient readings for Oct-25-08 and Oct-31-08 are included.

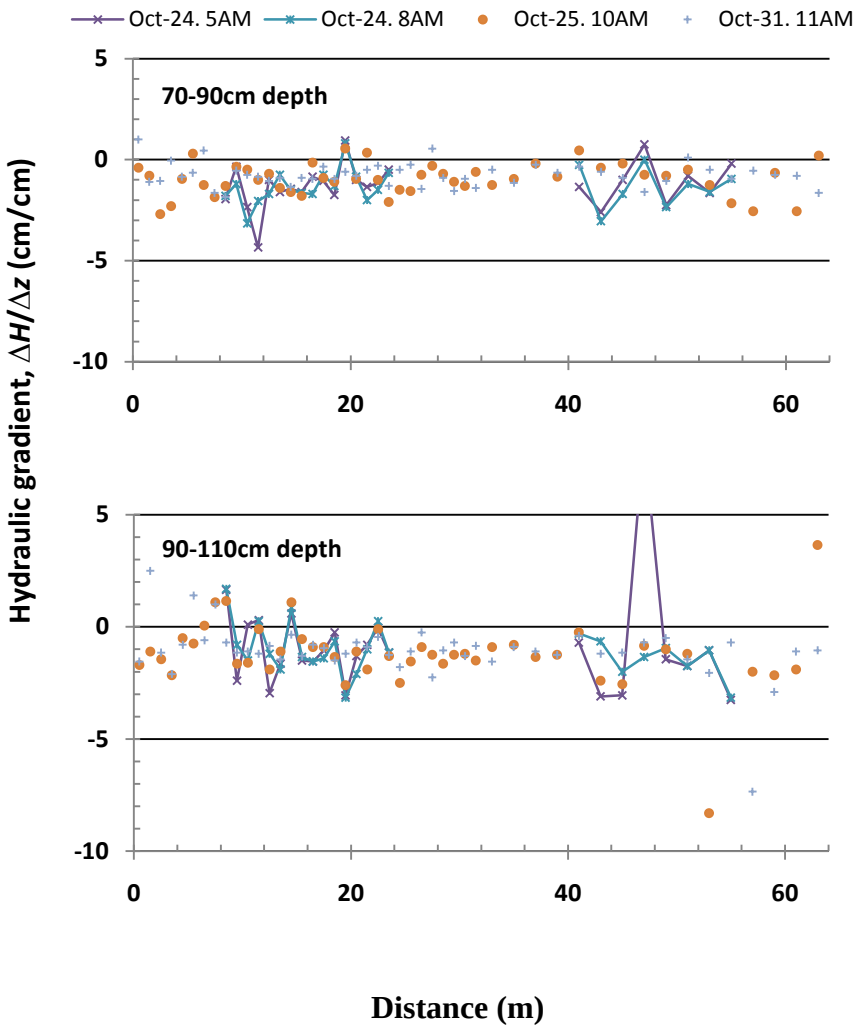

Figure 5.19. Hydraulic gradient monitored for lower depth compartments between Oct-24, at 5 and 8 AM during the low intensity irrigation. Hydraulic gradient readings for Oct-25-08 and Oct-31-08 are included.

In summary, larger downward directed hydraulic gradients at the 10-30, 30-50 cm compartments were observed for the plots receiving 3.52 cm/day but not for the ones receiving 5.52 cm/day. The monitoring of the hydraulic gradient revealed larger gradients present on plot 24 at a transect distance of 47 m as large temporal changes in $\Delta H/\Delta z$ (both magnitudes and signs) were observed at the 10-30 and 30-50 cm compartments, and these changes were assumed to be the result of macropore flow bypassing the 30 cm depth tensiometer at this location.

Assuming similar hydraulic conductivity functions for neighboring plots, larger temporal changes in hydraulic gradients in plot 24 suggested a larger drainage capacity. This larger drainage capacity in plot 24 was observed for the 5.52 cm/day irrigation in one out of 8 profiles along the transect that received the same 5.52 cm/day precipitation

Also, it can be interpreted that the plastic tarps allocated on the plots were successful in reducing evaporation because this physical barrier maintained a downward directed flux for 7 days (between Oct-25 and Oct31); after which soil core samples were taken.

5.2.4. Spatial Analyses of Hydraulic Gradient $\Delta H/\Delta z$

A summary of the descriptive statististics of the $\Delta H/\Delta z$ observations taken for the whole set of tensiometer nests along the transect is presented in Table 5.2 and serves as a reference for the spatial analysis of $\Delta H/\Delta z$. The coefficients of variation CV of hydraulic gradients found for the three sampling dates presented in Table 5.2 ranged from 62 to 371 %. In this range of CV, extremely high CVs caused by hydraulic gradients of 0 were not considered. This CV range was larger than the one reported by Reichardt et al (1993) of 19-254% when they investigated the spatial and temporal stability of hydraulic properties in a Brazilian Alfisol. They concluded that although soil water content and soil water matric potential could be estimated with relatively low CV of 3 and 8%, respectively, the application of this data to calculate Darcian flux densities at 150 cm depth had a prohibitive CV in the order of 60%. Their experimental design had 25- five by five m plots with two tensiometers (135 and 165 cm depth) and one water content acces tube per plot sampled at different intervals over a two year period.

Table 5.2. Descriptive statistics for hydraulic gradients sampled along the 64m long transect in 2008

	Oct-19-08			Oct 25-08			Oct-31-08		
Depth	Mean	Variance	CV	Mean	Variance	CV	Mean	Variance	CV
(cm)	(cm/cm)	$(cm/cm)^2$	%	(cm/cm)	$(cm/cm)^2$	%	(cm/cm)	$(cm/cm)^2$	%
10 to 30	0.656	1.268	171.6	-0.640	0.140	58.5	0.007	0.271	7982
30 to 50	0.454	0.764	192.4	-0.718	1.225	154.1	-0.065	0.111	515.5
50 to 70	-0.244	0.815	370.7	-1.007	0.991	98.8	-0.371	0.177	113.6
70 to 90	-1.178	0.876	79.5	-1.173	0.393	53.5	-0.811	0.251	61.8
90 to 110	-0.966	0.609	80.7	-1.393	3.719	138.5	-1.221	1.057	84.2

The $\Delta H/\Delta z$ observations taken on Oct-19, 25 and 31 were analyzed to check if the variation followed a random or a spatially structured behavior. The semivariograms in

Figures 5.20 and 5.21 indicate that at the beginning of the experiment on Oct-19 and one day after the low intensity precipitation treatments were applied on Oct-25, the $\Delta H/\Delta z$ varied randomly in the 10-30, 50-70, 70-90, 90-110cm depth compartments. Also spatial structure for a short 3-m-range was observed for the 30-50 cm depth compartment on Oct-19 and Oct-25. However, the assumption that spatial structure existed across the 30-50 cm depth compartment up to a 3-m-range on Oct 19 and 25 should be taken cautiously as only 48 observations of $\Delta H/\Delta z$ were included in the estimation of the semivariance.

This short range of spatial structure observed across the 30-50cm depth compartment on Oct-19 and 25; should rather be interpreted as a hint leading to increase the number of $\Delta H/\Delta z$ observations to strengthen the reliability of the autocovariance function. The latter could be done by reducing the sampling distance or by increasing the sampling domain. On Oct-31 at the moment of soil core sampling, the variation of the $\Delta H/\Delta z$ was random for the 30-50, 50-70, 70-90 and 90-110cm (Figures 5.20 and 5.21) probably due to soil water redistribution and equilibration processes. Moreover, the variance of ψ_m was found to be minimum at ψ_m ranges close to field capacity in a study by Wendroth et al (1999a). This finding is important because the ψ_m ranges observed on Oct-31 were >-100 cm, reducing the variability of ψ_m which is needed for the identification of spatial structure.

The pattern of semivariance observed for the 10-30cm depth compartment at the moment of sampling on Oct-31 (Figure 5.20), suggests that spatial structure was present over a range of 13 m. This range of spatial structure was probably due to equilibration and redistribution processes of the soil water total potential induced by the zero-flux upper boundary condition.

In summary, it is shown in Figures 5.20 and 5.21 that most of the $\Delta H/\Delta z$ observations were randomly distributed.

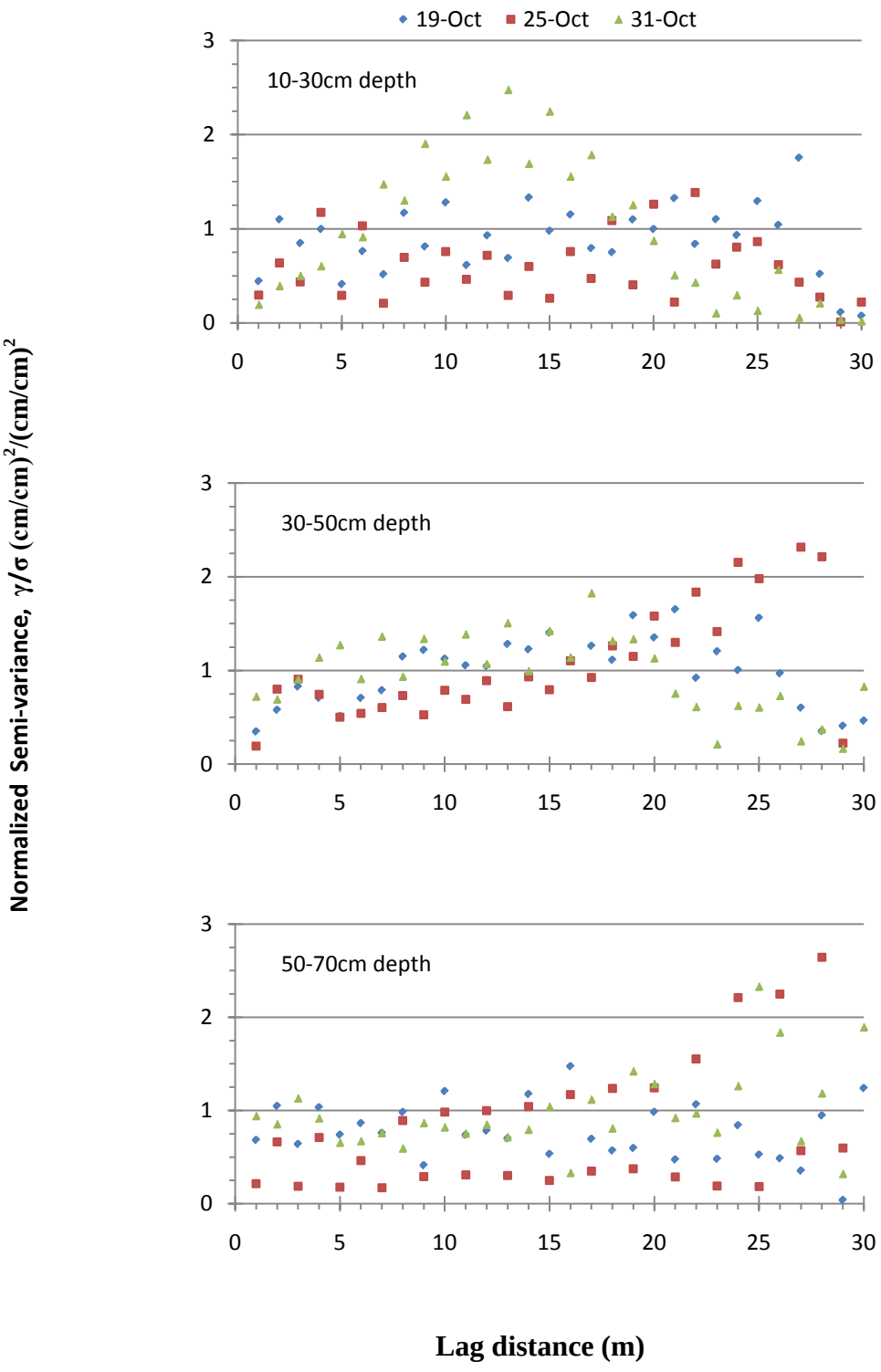

Figure 5.20. Normalized semivariograms of $\Delta H/\Delta z$ for upper three depth compartments during the main leaching study of 2008.

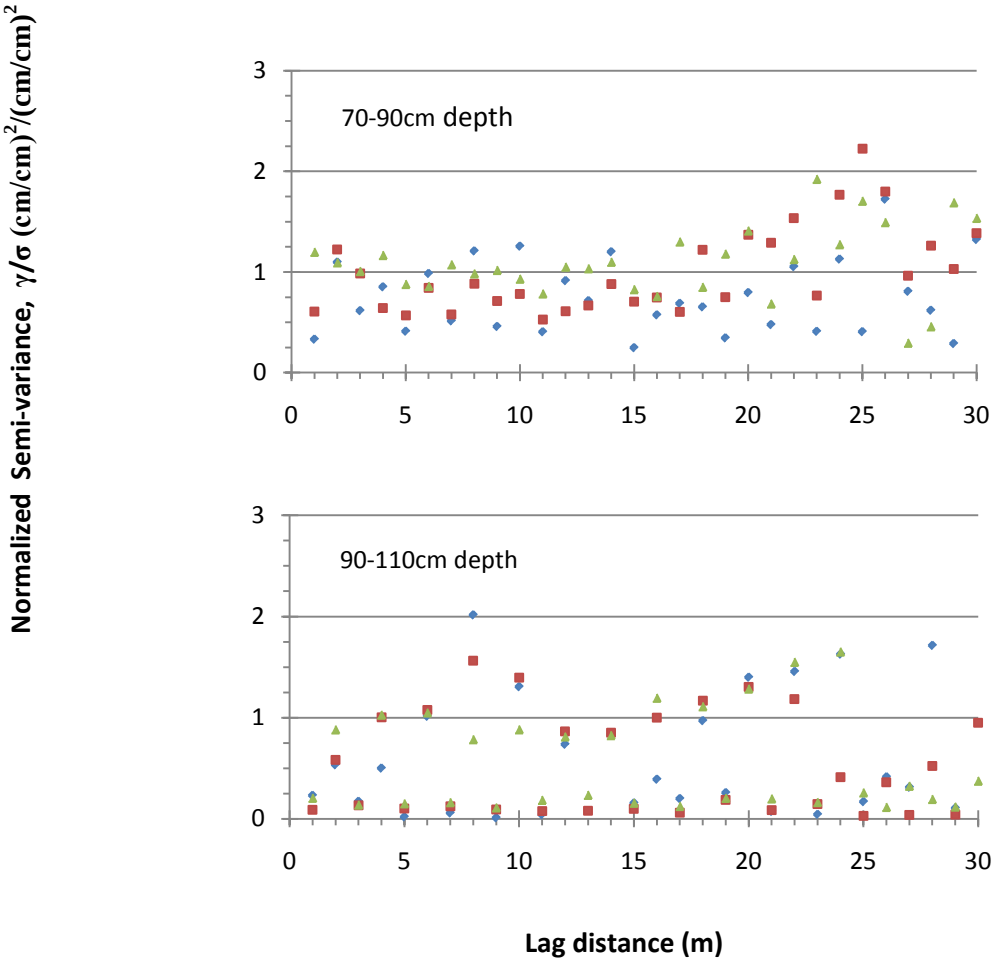

Figure 5.21. Normalized semivariograms of $\Delta H/\Delta z$ for lower two depth compartments during the main leaching study of 2008.

5.2.5. Cyclic spatial variation of hydraulic gradient $\Delta H/\Delta z$.

A first look at the dataset produced at regular sampling intervals in Figures 5.22 and 5.23 indicate that the highest precipitation amount combined with low precipitation intensities caused a deeper leaching of Br^- manifested in the Br^- center of mass than other combinations of precipitation amount and intensity.

However, the impact that the transport causing factors had on the hydraulic gradient and utterly on the plot average Br^- center of mass is not clearly evident on a first snapshot of the data provided in Figures 5.22 and 5.23. This is not surprising since water redistribution and equilibration of ψ_m were allowed to occur over a period of 1-6 days for the readings taken on Oct-25 and Oct-31.

The power spectra for the transport causing factors and Br^- center of mass presented in Figure 5.24 positively identified cyclic variations occurring every 32 m for the case of precipitation amount and intensity and every 8 m for the time delay. The plot averaged Br^- center of mass spectrum in Figure 5.24 revealed that the majority of the variance on the leaching depth of Br^- occurred at 32 m wavelengths and only a small fraction of the variance is due to regular 8 m cycles. These characteristic wavelengths correspond to frequencies of 0.0625 and 0.25 for which the main spectrals peak were found. Notice that the point distance was 2 m as plot average data were considered in this analysis.

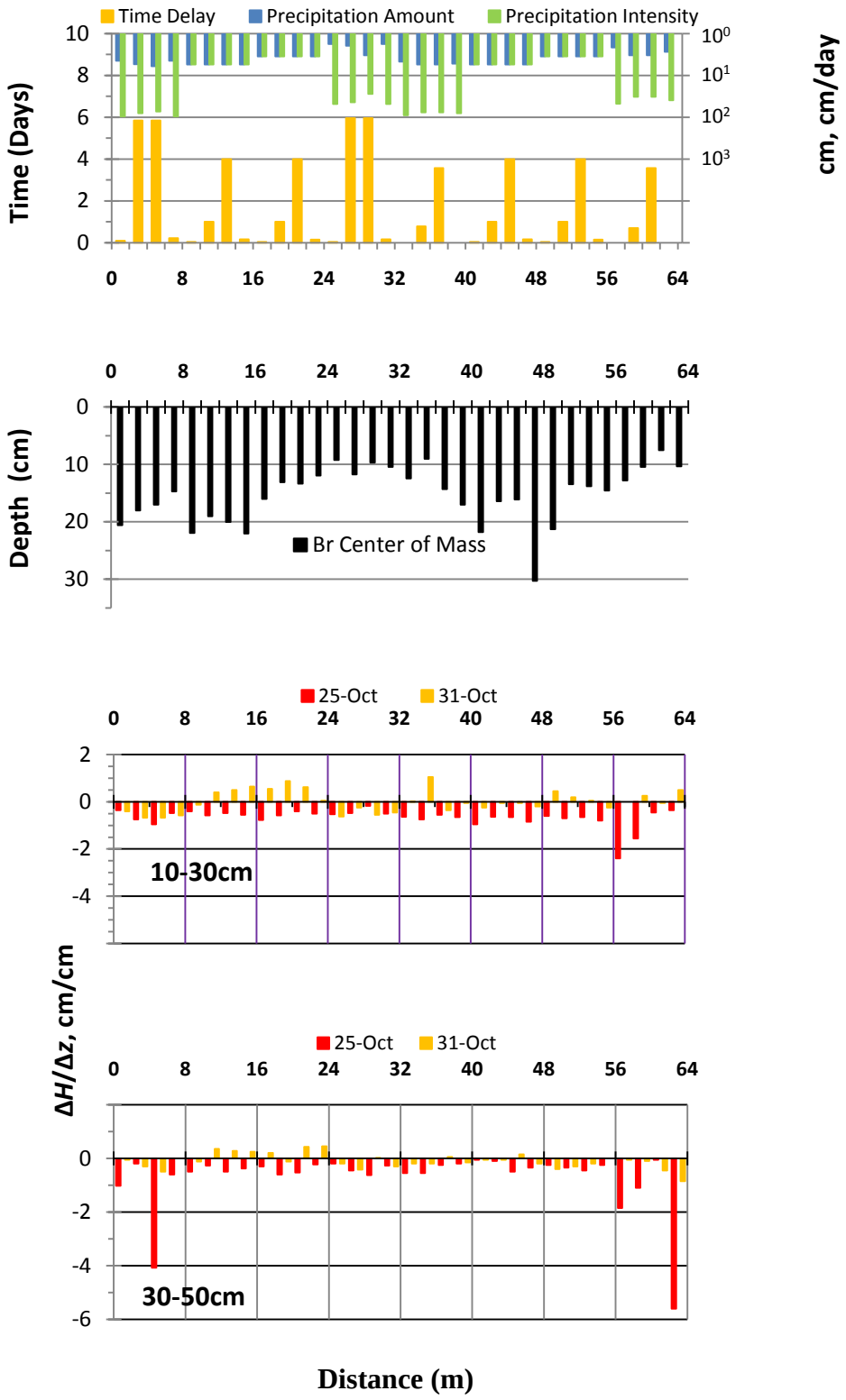

Figure 5.22. Transport causing factors, plot average Br center of mass and $\Delta H/\Delta z$ in the upper compartments for a 32 observation dataset created for each variable.

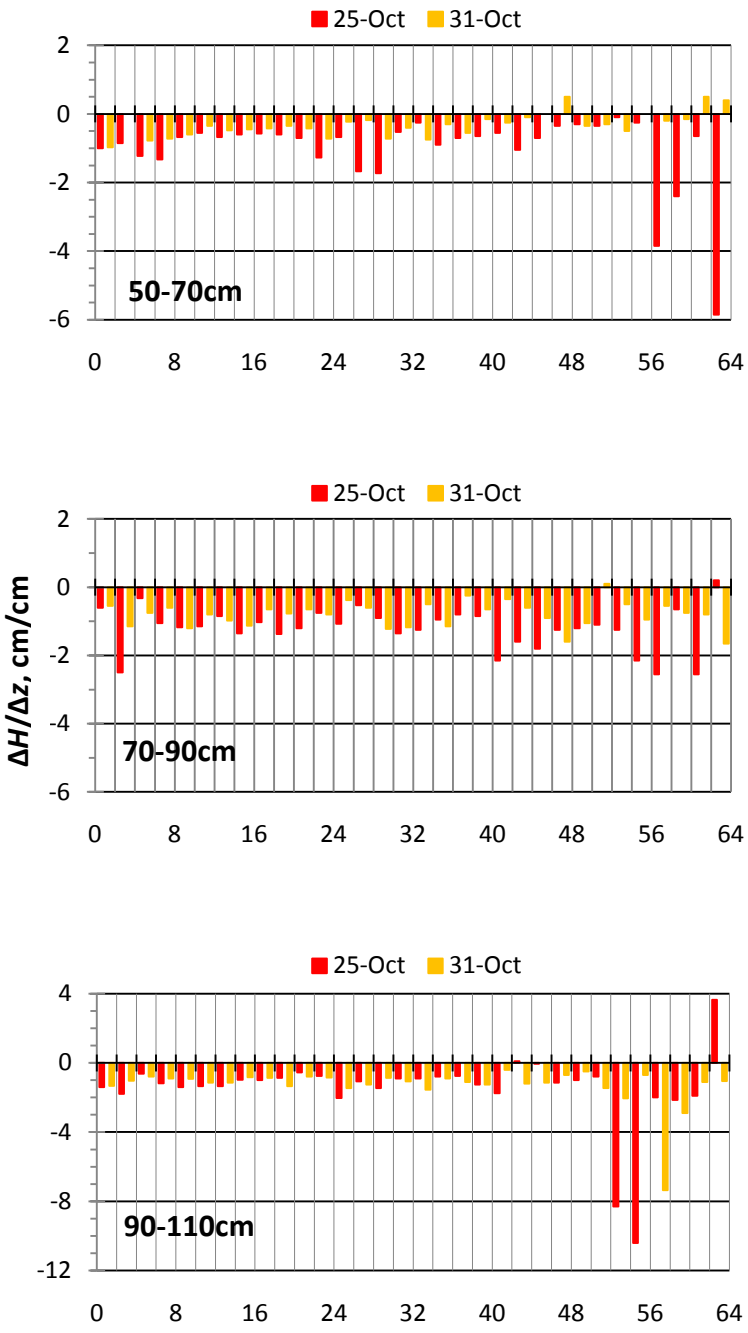

Figure 5.23. Plot-average hydraulic gradients for the lower depth compartments on Oct-25 and Oct-31-08.

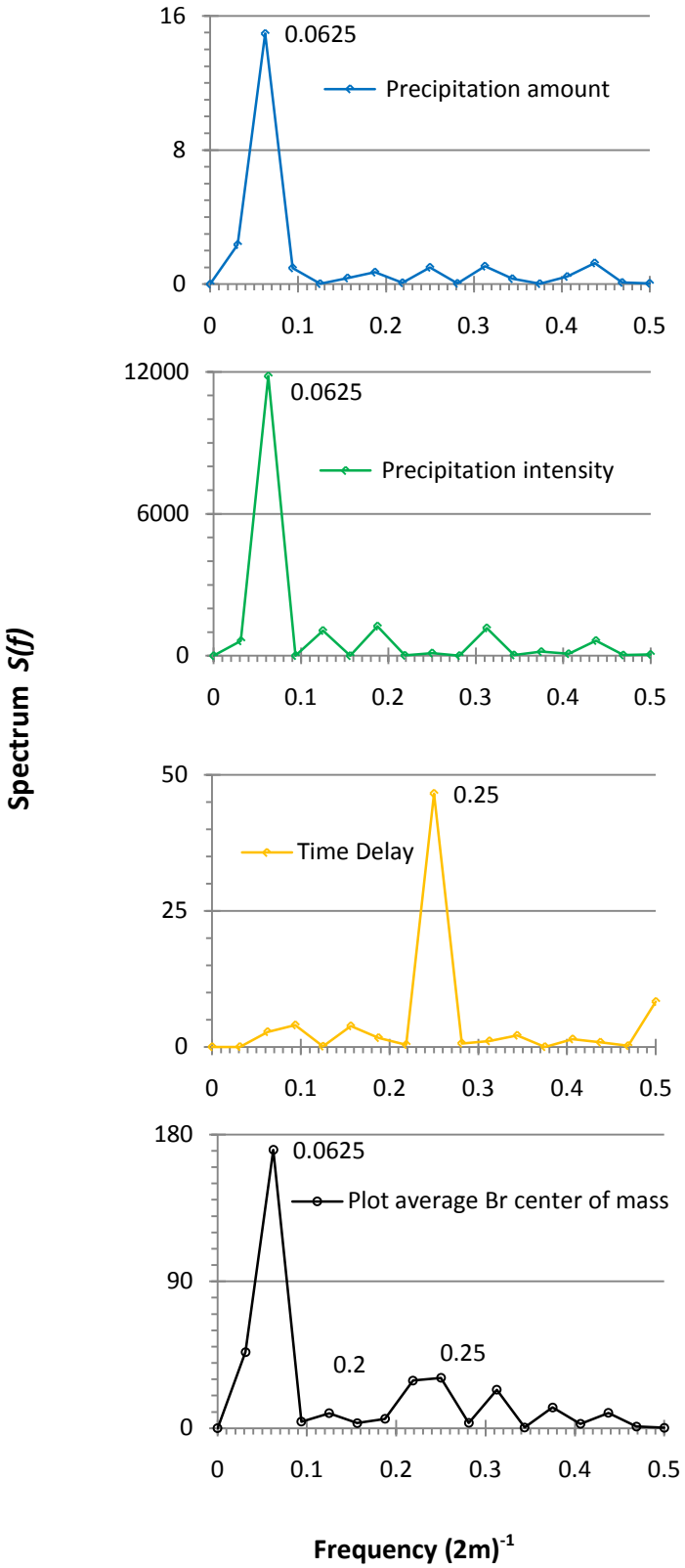

Figure 5.24. Power spectra of transport causing factors and plot-average Br^- center of mass measured on Oct-31.

The frequency analyses of $\Delta H/\Delta z$ considering two measurement times on Oct-25 and Oct-31 will follow the discussion. Spectral signals of $\Delta H/\Delta z$ measured on Oct-25 showed three peaks corresponding to 13, 11 and 8 m wavelengths (Figure 5.25). The 13 and 11 m wavelength cyclic variations at this time could be attributed to be a result of the precipitation intensity and amount treatments whereas the 8 m wavelength is clearly an effect of the application time delay of the Br^- pulse. It is worth to mention that by the time the $\Delta H/\Delta z$ readings were taken, most of the Br^- pulses were already applied and only plots 1, 4, 13 and 16 had not received the Br^- pulse.

For hydraulic gradient measurements on Oct-25 in the 30-50 and 50-70 cm depth compartment, spectral peaks at 6 m wavelength were observed probably due to the different timings of the incoming 0.107 cm applications of the Br^- pulse (Figure 5.25).

On Oct-31 at the moment of soil core sampling, the spectral signal of the $\Delta H/\Delta z$ displayed in Figure 5.25, reflected only a peak for larger scale variation at 21.33 m wavelength for the 10-30 and 30-50cm depth compartments. The power spectrum for the hydraulic gradient between 50 and 70 cm depth compartment measured at the same time showed two peaks corresponding to 7 and 5 m wavelengths, however these characteristic wavelengths could not be associated with any of the applied transport causing factors.

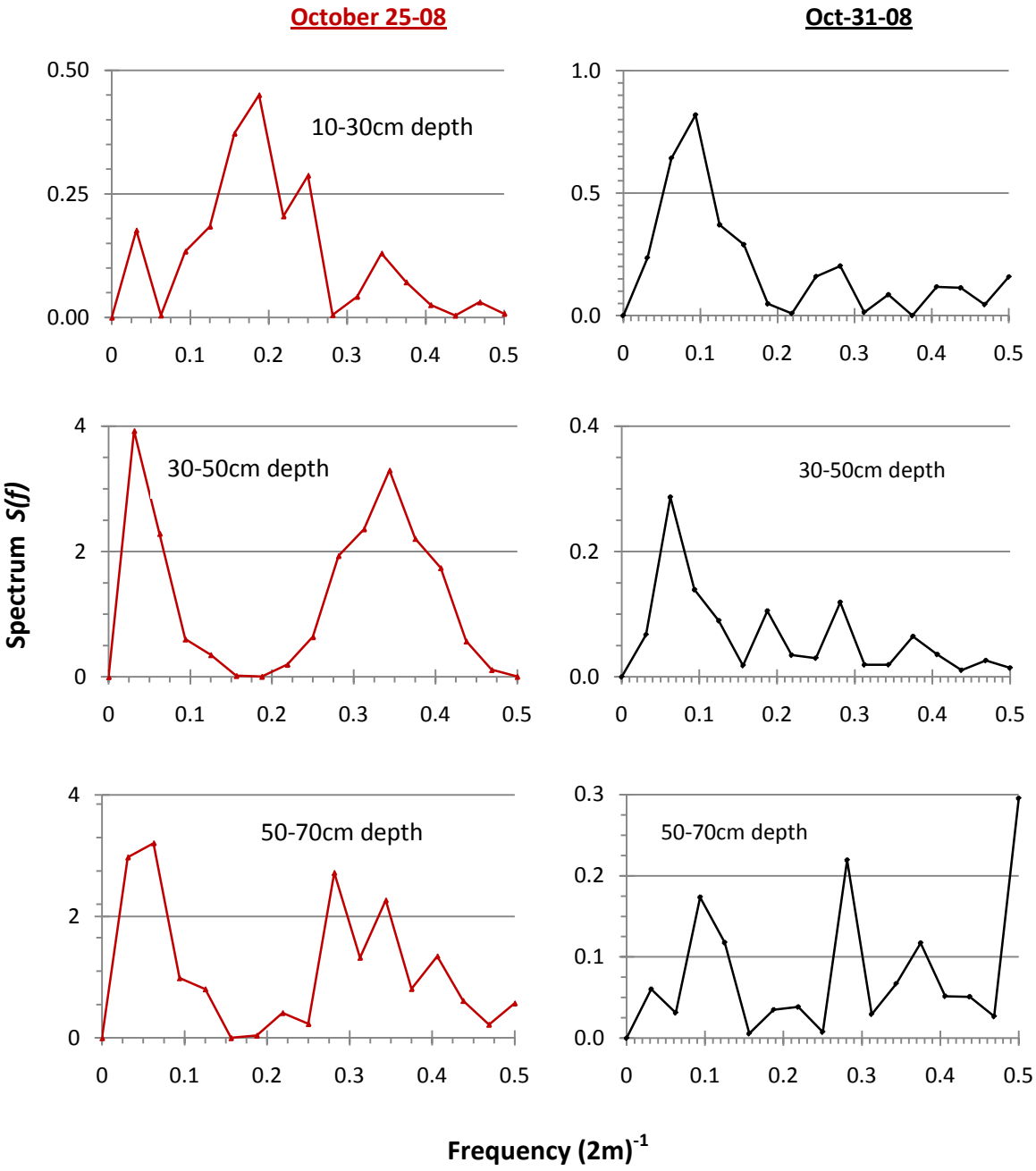

Figure 5.25. Power spectra of $\Delta H/\Delta z$ for the upper three depth compartments obtained from tensiometer readings taken on Oct-25 and Oct-31-08.

Cross-spectral analyses between the series of $\Delta H/\Delta z$ taken on Oct-25, and Oct-31 for the upper three depth compartments vs. the Br^- center of mass should indicate if in fact,

common cycles of variation between the two variables existed as a result of the different transport causing factors. It was anticipated that such a coincidence would exist if the two series compared exhibited common frequencies of variation.

In Figure 5.26, an inverse relationship with common periodic fluctuations at 64 m wavelengths between the $\Delta H/\Delta z$ on Oct-25 for the 10-30 cm depth compartment and the plot average Br^- center of mass was indicated in the cross-spectrum. The 64 m wavelength identified the variation over the whole transect distance and was not related to anything other than the whole variance of the dataset. The quad spectrum (Figure 5.26) for the 10-30 cm depth observations of $\Delta H/\Delta z$ on Oct-25 vs. plot average Br^- center of mass peaked at a corresponding wavelength of 8 m indicating cyclic variation was shared by both series at regular 8 m cycles. However, both series were shifted by 0.858 lags≈1 lag or 2m distance as quantified by the phase spectrum.

The 2m phase lag indicated that a typical 8m wavelength cyclic pattern of the plot average Br^- center of mass was inversely correlated with the same wavelength cyclic pattern behavior of $\Delta H/\Delta z$ (10-30cm depth compartment for Oct-25 in Figure 5.25) when the $\Delta H/\Delta z$ series was shifted by one lag, or 2 m to the left. The inverse correlation identified between these two variables is consistent with the definition of the z axis (positive downward) where a negative sign of $\Delta H/\Delta z$ indicated downward directed water flux; and the magnitude of ψ_m determined the magnitude of hydraulic conductivity prevailing at that time at that depth compartment.

The cross-spectrum between the $\Delta H/\Delta z$ in the 30-50cm depth compartment on Oct-25 vs plot average Br^- center of mass presented in Figure 5.26 peaks at 0.063, and 0.313 $(2m)^{-1}$

frequencies equivalent to 32 and 6 m wavelengths. This cyclic variation identified by common wavelengths at 32 and 6 m was associated with the precipitation amount and intensity (32 m wavelength) and could also be associated with the application time delay of the Br^- pulse (6.4 m wavelengths). Moreover, a positive correlation of these two variables at this depth compartment sustains the idea that larger values of $\Delta H/\Delta z$ at the 30-50 cm depth on Oct-25 were associated with greater depths to the plot average Br^- center of mass. This conclusion was sustained by the fact that the majority of the plot average Br^- center of mass values were found between 10 and 20 cm depth (Figure 5.22) and that a larger $\Delta H/\Delta z$ at the 30-50 cm depth compartment on Oct-25 would have decreased the rate of downward Br^- transport. The cross-spectrum of $\Delta H/\Delta z$ for the 50-70 cm depth compartment on Oct-25 vs. the plot average Br^- center of mass signaled a positive correlation between these two variables at a common 32-m-wavelength (Figure 5.26), and again, was associated with the sinusoidal patterns of precipitation amount and intensity shown in Figure 5.22. The same interpretation for the 30-50 cm depth compartment $\Delta H/\Delta z$ vs. plot average Br^- center of mass behavior as discussed above was valid for the cross-spectra between the $\Delta H/\Delta z$ at the 50-70 cm depth and.the plot average Br^- center of mass (Figure 5.26).

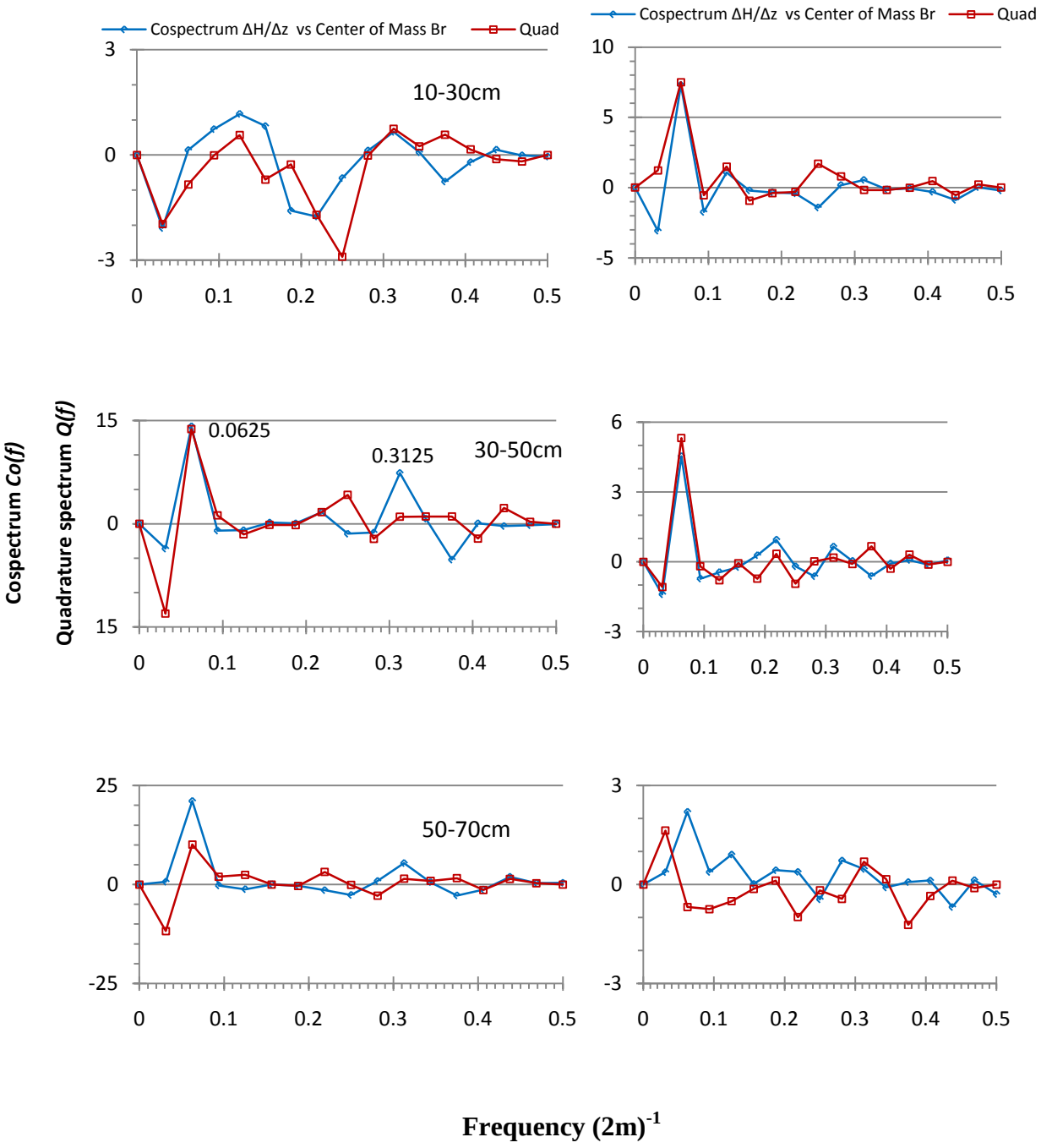

Figure 5.26. Cross spectra of $\Delta H/\Delta z$ for upper depth compartments on Oct-25 and Oct-31 vs. plot average Br center of mass.

The cross-spectrum of $\Delta H/\Delta z$ measured on Oct-31 for the 10-30 and 30-50 cm vs. the plot average Br^- center of mass indicated a positive correlation at a common cyclic variation observed for 32-m wavelengths (Figure 5.26). Despite this positive correlation found for the $\Delta H/\Delta z$ at these two depth compartments (10-30 and 30-50cm on Oct-31) with the plot average Br^- center of mass, the meaning of this correlation is difficult to explain since the readings of the hydraulic gradient on Oct-31 were affected by different phases during soil water redistribution and equilibration that occurred for period between 1 and 6 days before the $\Delta H/\Delta z$ readings were taken on Oct-31.

Also, the significance of the common cyclic variation between the $\Delta H/\Delta z$ readings and the plot average Br^- center of mass was quantified with the squared coherency spectrum (smoothing constant = 3) and shown in Figure 5.27. It was found that across the 10-30 cm depth, the cyclic variation of 8 m wavelength (0.25 $[2m]^{-1}$ frequency) in Oct-25 was significant and related to the application time delay of Br^- pulse. This cyclic variation was also significant for Oct-31 but across the 30-50 and 50-70cm depth compartments (Figure 5.27).

In conclusion, the common cyclic variations found in the cross-spectra (Figure 5.26) were highly significant when a coherency peak > 0.7 (95% confidence interval) was observed (Figure 5.27).

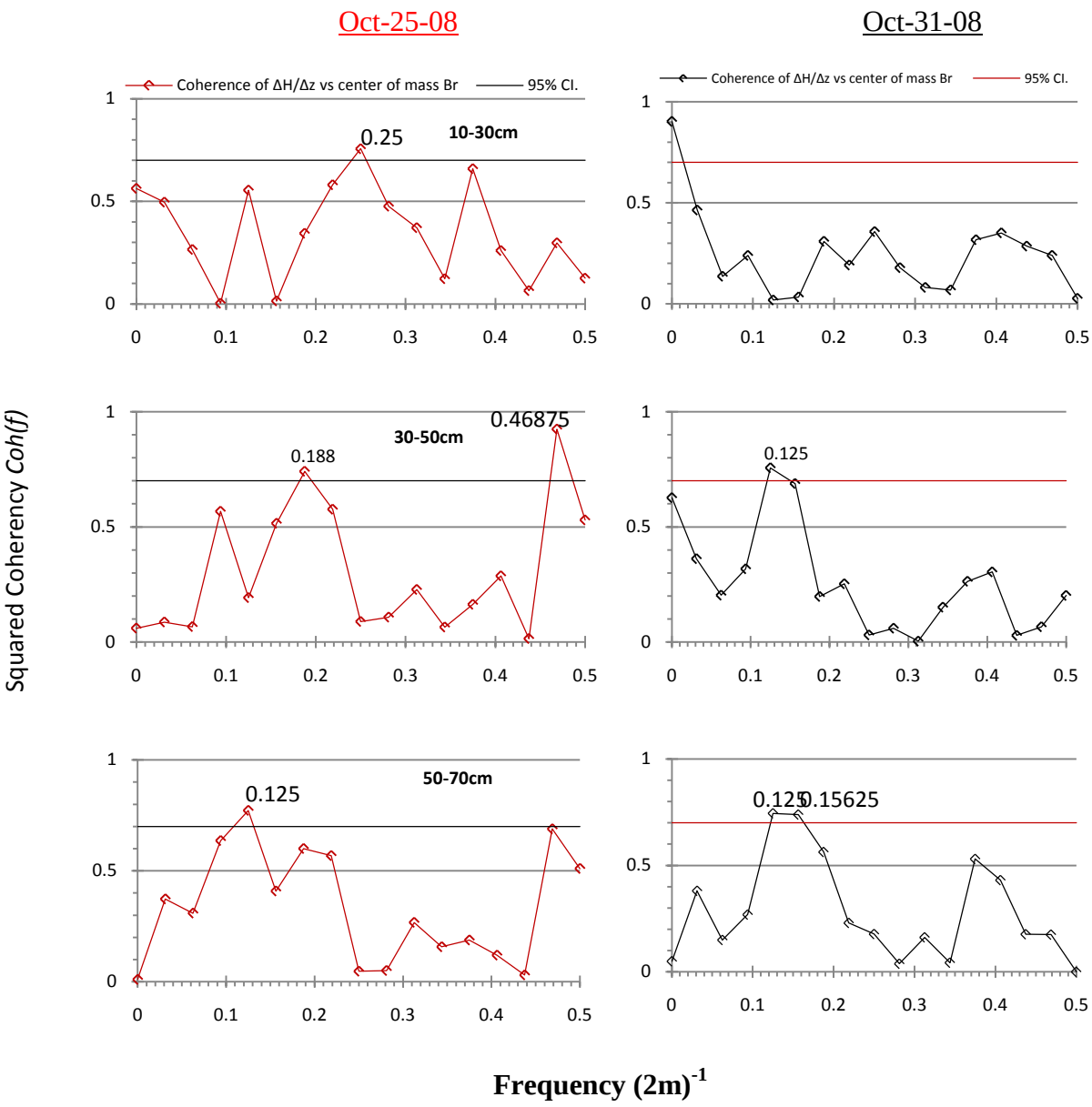

Figure 5.27. Squared coherency spectra between $\Delta H/\Delta z$ in the upper three depth compartments and the plot average Br^- center of mass.

5.2.6. Bromide concentration profiles and soil gravimetric water content θ_g at the day of soil core sampling (Oct-31-08).

The final result of the tracer experiment was reflected by the observations of θ_g and *Br-*$^-$ concentration at the moment of soil core sampling on Oct-31-08. The spatial Br^- concentration behavior was the result of the different transport causing factors, i.e., precipitation amount, intensity and KBr application time delay, combined with the initial soil profile moisture.

The Br^- concentrations and θ_g observations taken on Oct-31 are illustrated in Figures 5.28, 5.29 and 5.30. These figures suggest in general that larger concentrations of Br^- were found at the 0-20 cm depth and progressively smaller Br^- concentration values were found in the 20-50cm depths. This finding indicated that the majority of Br^- applied remained in the 0-20 cm depth. Also, the observations of soil water content θ_g in the 0-10cm depth increment showed larger values than in the depth increments below probably due to a larger porosity in the 0-10 cm depth compartment as this compartment of the soil profile is the one mostly exposed to bioturbation processes and highest in soil organic matter content, causing the lowest dry bulk density.

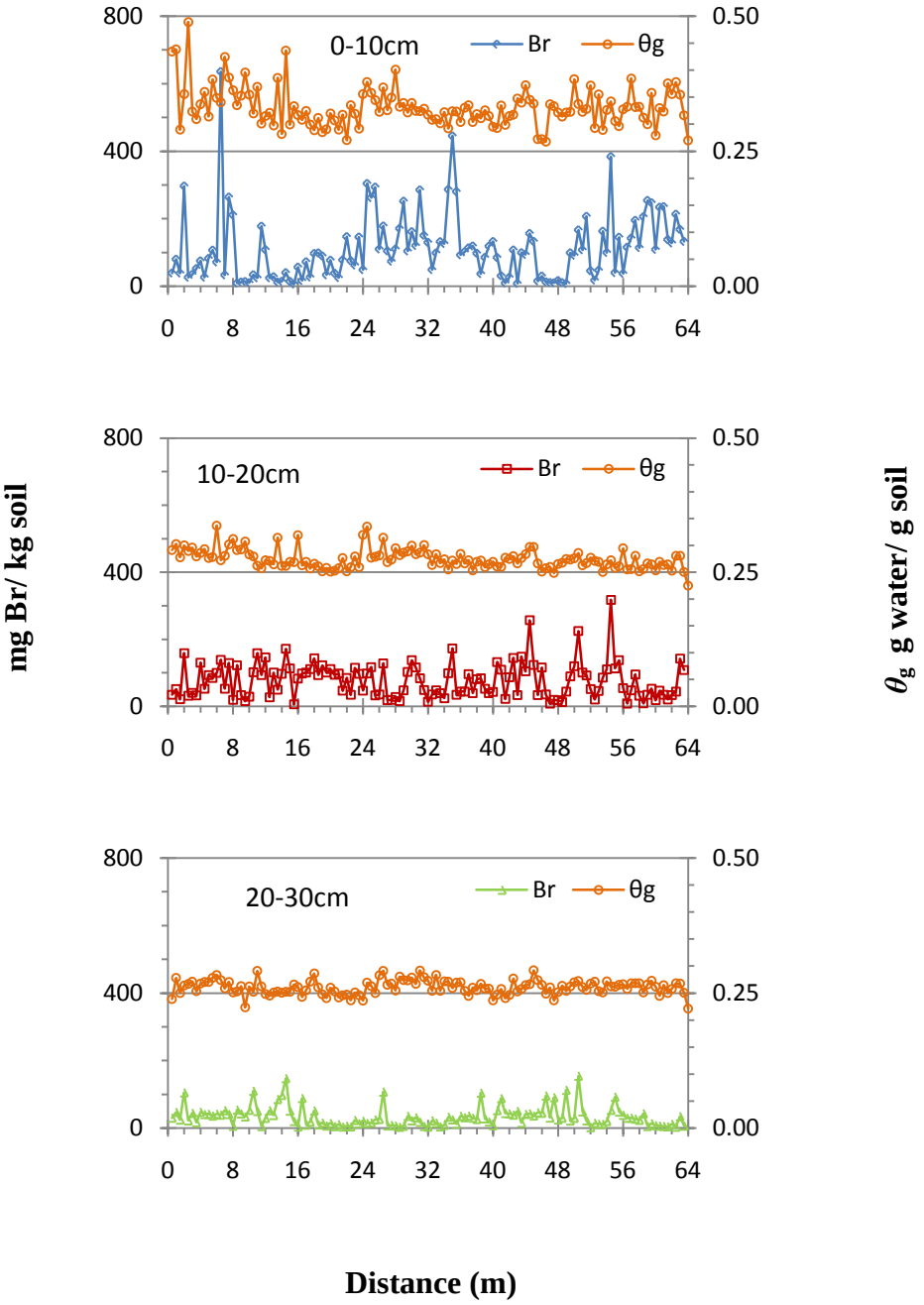

Figure 5.28. Bromide (Br) and gravimetric water content θ_g for the upper three depth compartments measured on Oct-31-08.

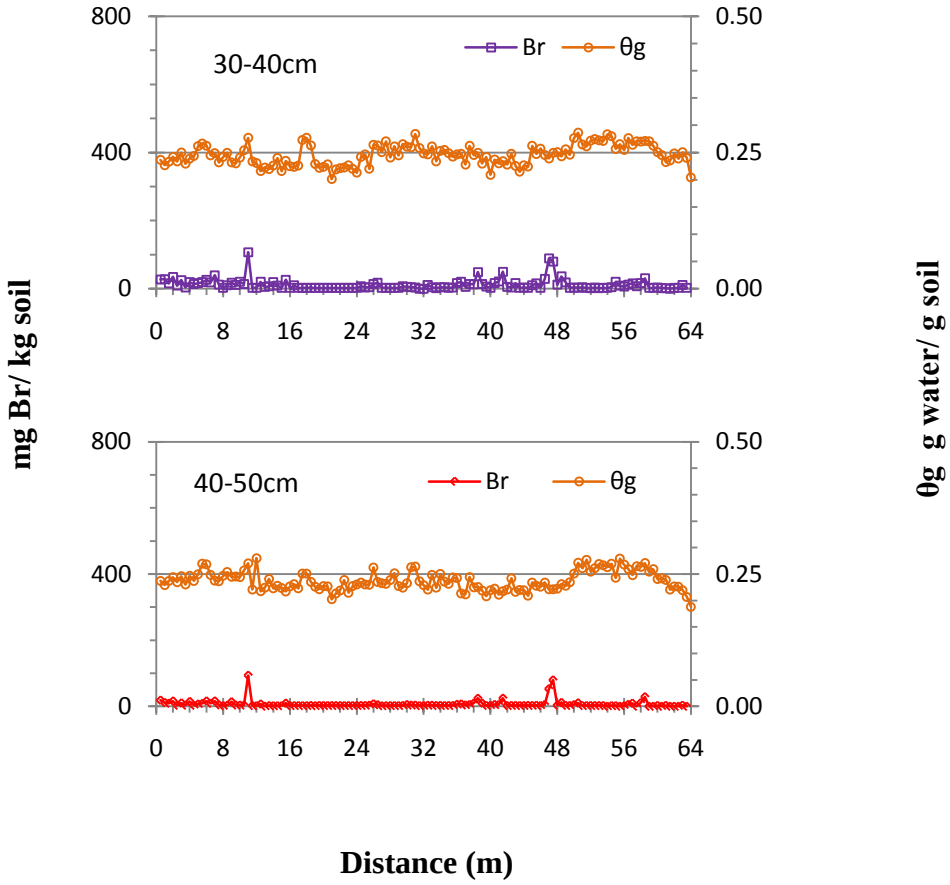

Figure 5.29. Bromide (Br) and gravimetric water content θ_g for the lower two depth increments measured on Oct-31-08.

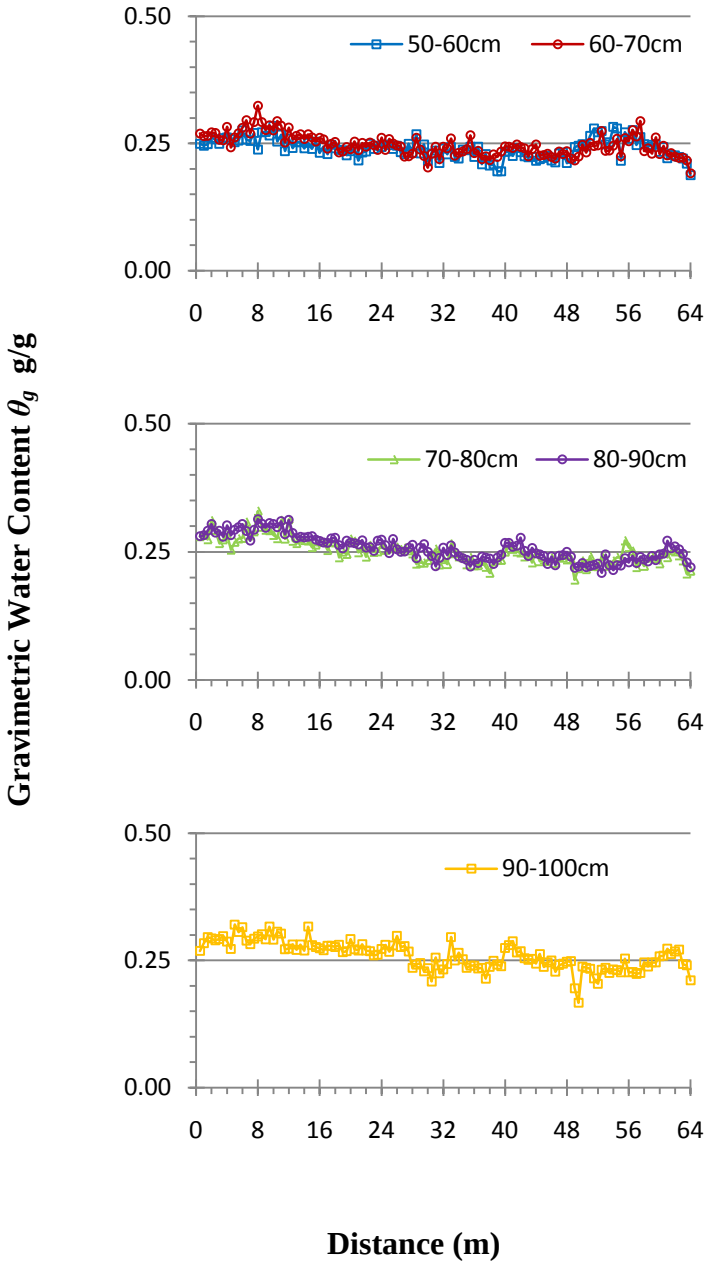

Figure 5.30. Gravimetric water content for lower depth compartments on Oct-31-08 for the main leaching study.

Following Br^- and soil water content analyses on Oct-31, the descriptive statistics for these variables at the moment of soil core sampling are shown in Table 5.3. In general, the mean and the variance of both series decrease with increasing depth down to 50 cm and the variability exhibited by the Br^- series is roughly 8 (0-10cm) to 24 times (40-50 cm) greater than the variability exhibited by soil water content manifested by their respective coefficients of variation CV (Table 5.3). The high CV observed for Br^- in the two lower depth compartments in Table 5.3 was a result of smaller Br^- concentrations found in these compartments. Furthermore, in the 40-50 cm depth compartment the mean Br^- concentration decreased while variance increased, probably as a result of eight non-quantifiable concentrations bdl that were consequently set to "0".

Table 5.3. Descriptive statistics of θ_g and Br on core samples taken on Oct-31-08.

	θ_g			Br		
Depth (cm)	Mean	Variance	CV	Mean	Variance	CV
	g/g	$(g/g)^2$	%	mg /kg soil	$(mg /kg soil)^2$	%
0 to 10	0.33	0.00135	11.09	111.3	9700	88.48
10 to 20	0.27	0.00033	6.65	76.5	2800.5	69.13
20 to 30	0.26	0.00018	5.12	34.4	902.3	87.21
30 to 40	0.25	0.00036	7.68	11.6	258.4	138.55
40 to 50	0.24	0.00033	7.71	6.6	156.2	187.29
50 to 60	0.24	0.00034	7.73			
60 to 70	0.25	0.00047	8.77			
70 to 80	0.25	0.00060	9.74			
80 to 90	0.26	0.00063	9.78			
90 to 100	0.26	0.00074	10.38			

5.2.7. Spatial structure of Br^- and soil water content on Oct-31-08

The objective of this section was to check if the sampling design used, i.e., core samples taken every 0.5 m intervals on a 64 m long transect was adequate to describe the autocovariance structure of Br^- and soil water content.

In Figure 5.31 for the 0-10cm depth increment, both Br^- and θ_g normalized semivariograms appear as pure nugget effect, i.e., the distribution of both series, for the given sampling design, is random and no spatial dependence between observations of Br^- and θ_g existed for the 0-10 cm depth.

Random distribution of Br^- and θ_g was also found in the 0-10 cm depth compartment in the Pilot leaching study of 2007 described under 5.1.2. And these findings are consistent with those of Netto et al. (1999) who reported no spatial autocorrelation for gravimetric water content and solute concentration for the 0-13 cm depth in a field study characterizing the spatial variability of solute transport in a fallow field. This lack of spatial correlation for water content and solute concentration could be attributed, perhaps, to the fact that all water and solute had to pass this first layer. Due to high biological activity soil structural macropores affected transport through this layer, and the retained water and solute is rather irregularly distributed.

In Figure 5.31, the identification of spatial structure over a range of 2 and 4 m for Br^- and θ_g in the 10-20 cm depth compartment suggests that the sampling design used was adequate to characterize the spatial behavior of the water and Br^- transport in the experiment. Also in Figure 5.31 for the 10-20 cm depth, it appears that the θ_g

semivariogram has three different plateaus at 4-18, 30-40 and 54-60 m lag distance indicating the spatial dependency of water content at different scales.

However, the nugget variance in the 10-20 cm depth compartment for Br^- and θ_g in Figure 5.31 indicates that approximately more than half of the variation for both variables at this depth increment was due to small scale variability or measurement error.

Also in Figure 5.31 for the 20-30 cm depth increment, spatial structure is identified over a 6 m range for both Br^- and θ_g confirming that the experimental sampling design was able to capture the spatial autocovariance structure for both variables. However, the nugget variance for both variables in the 20-30 cm depth increment depicted in Figure 5.31 represents more than 60 % of the total variance, suggesting that a closer sampling interval, larger sampling domain or maybe larger sample support volume would decrease this nugget variance in favor of spatially structured variation.

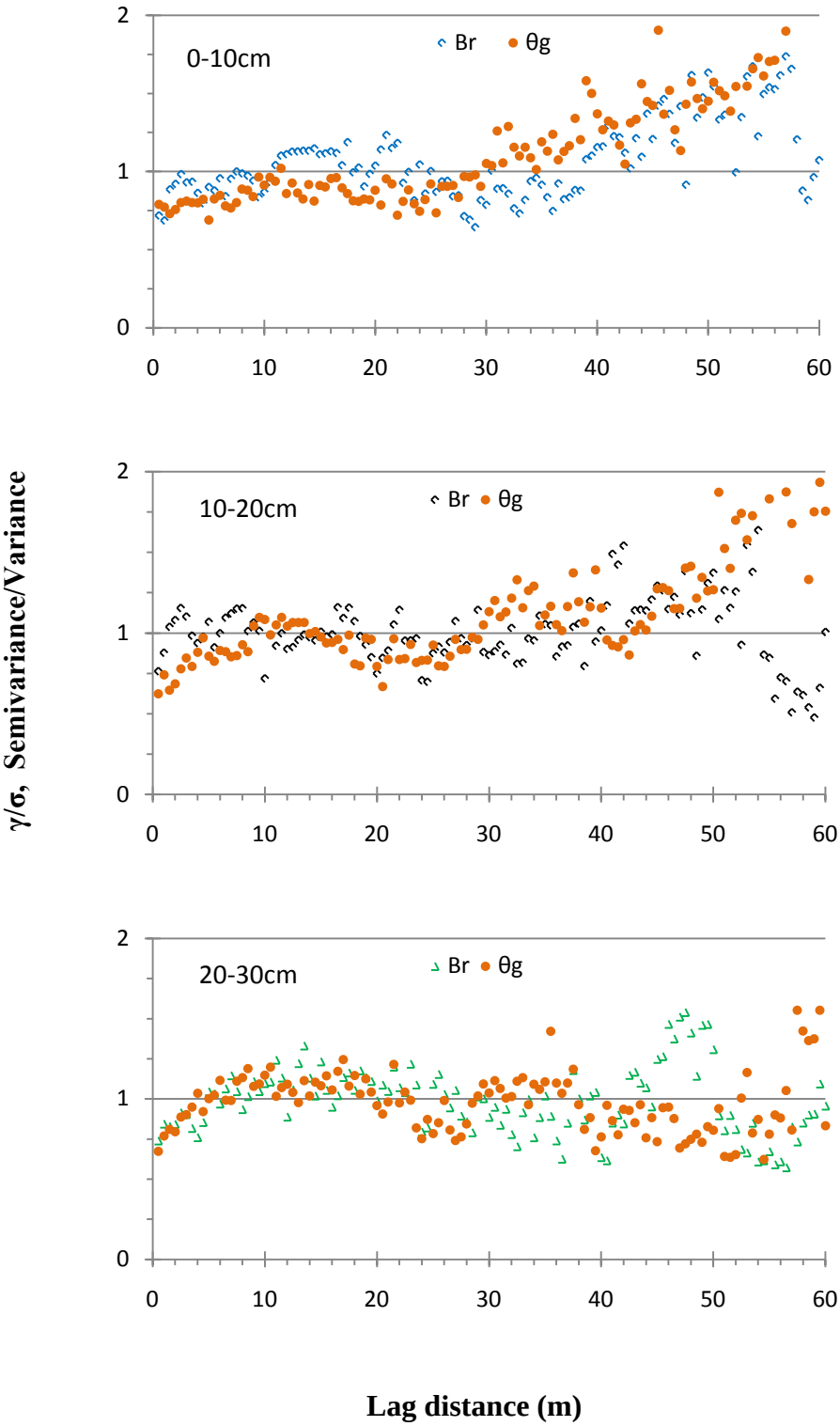

Figure 5.31. Bromide and θ_g normalized semivariograms for the 0-30 cm depth increments in Oct-31-08.

Deeper into the soil profile, the normalized semivariogram for the 30-40 cm depth increment in Figure 5.32 indicates spatial structure over 3 and 10 m ranges for Br^- and θ_g respectively, supporting the validity of the experimental sampling design used. Also, the nugget variance remained approximately the same for the Br^- observations at this depth, i.e., ≈ 60 % of the total variance when compared to depth compartments above. However, the nugget variance for the θ_g series at the 30-40 cm depth is dramatically reduced to ≈ 25 % of the total variance at this depth, in favor of a stronger spatial relationship at the 30-40 cm depth for θ_g due to a smaller local noise and smaller variance at this depth (Table 5.3).

For the second depth compartment in Figure 5.32, the 40-50 cm depth increment, spatial structure for Br^- could not be identified. However the θ_g series at the 40-50 cm depth was spatially correlated over 10 m distance and the nugget variance was ≈ 30% of the total variance at this depth.

In summary, Br^- observations presented spatial structure from 10 and up to 40 cm depth increments over short ranges (2–6 m) and with similar nugget variances of ≈ 60 % of the total variance. This finding suggests that despite the fact that ≈ 60 % of the total variance in Br^- concentration for the 10-40 cm depth increments was associated with small scale variability and measurement error, the experimental design used was able to characterize the spatially structured variation observed for Br^-. Also, by using normalized semivariograms to define the sill of the 10-20, 20-30 and 30-40 cm depths, it is concluded that the strength of the spatial relationship, as quantified by the nugget to sill ratio, did not change for these three depth compartments as the nugget variance remained nearly constant at ≈ 60 % of the total variance.

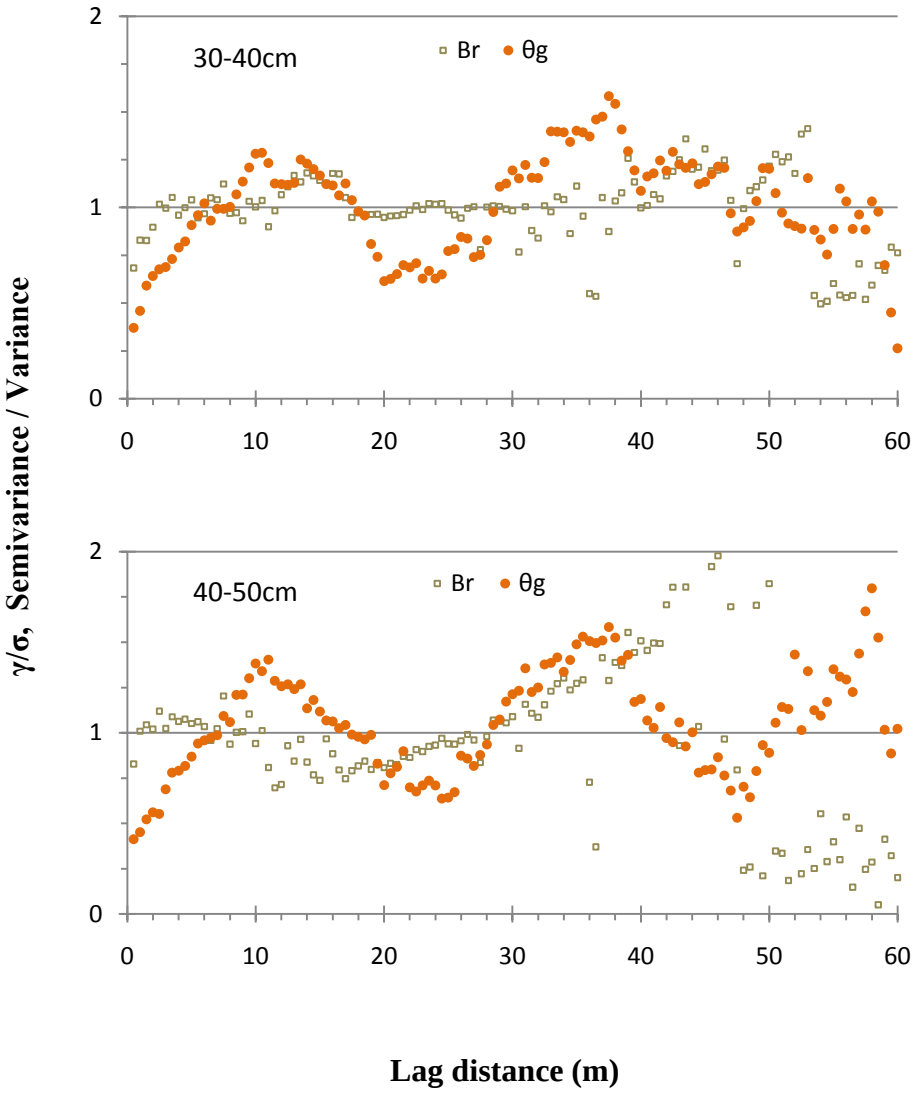

Figure 5.32. Bromide and θ_g normalized semivariograms for the 30-50cm depth increments in samples taken Oct-31-08.

Spatial structure was identified for θ_g over 10 m distance for the 50-60 cm depth compartment in Figure 5.33 with approximately 25 % of the total variation attributed to small scale variability. This finding supports the ability of the sampling design in capturing the spatially structured behavior of θ_g at this depth.

Deeper into the profile; however, from 60 -100 cm depth increments in Figure 5.33; the observations of θ_g presented only unbounded semivariograms suggesting that the variance of all observations within the domain was not constant (Nielsen and Wendroth, 2003).

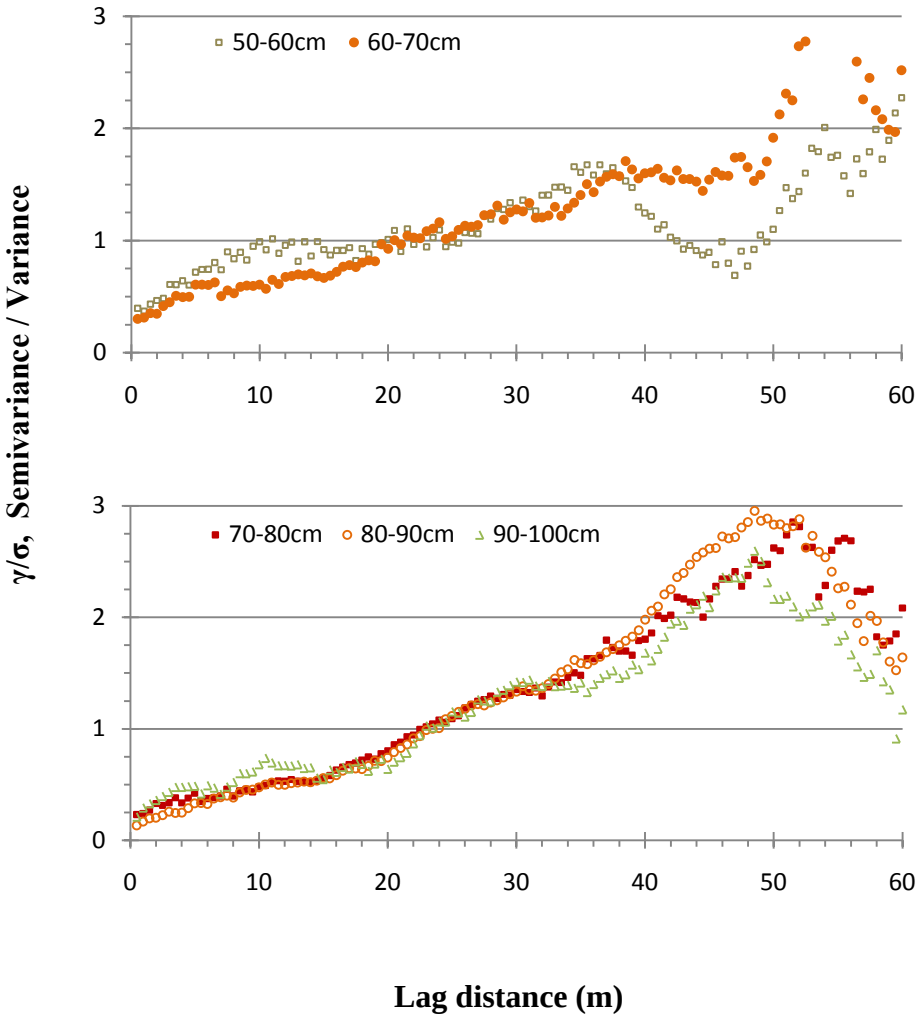

Figure 5.33. Normalized semivariograms of gravimetric water content for the 50-100 cm depth increments in samples taken on Oct-31-08.

5.2.8. Leaching Depth Estimated by Bromide Center of Mass

The main objectives of this research were to find out how the different transport causing factors, i.e., precipitation amount, precipitation intensity, and KBr application time delay affected the leaching depth of the Br^- tracer. In order to quantify the leaching depth, the Br^- center of mass was calculated to define the leaching depth, in length coordinates, to which half of the total solute mass for a given solute concentration profile has leached (Olson and Cassel 1999). The Br^- center of mass with the distribution of the different transport causing factors and their different levels are illustrated in Figure 5.34. The observations of the Br^- center of mass located at the boundary from one plot to another were are also clearly marked in Figure 5.34.

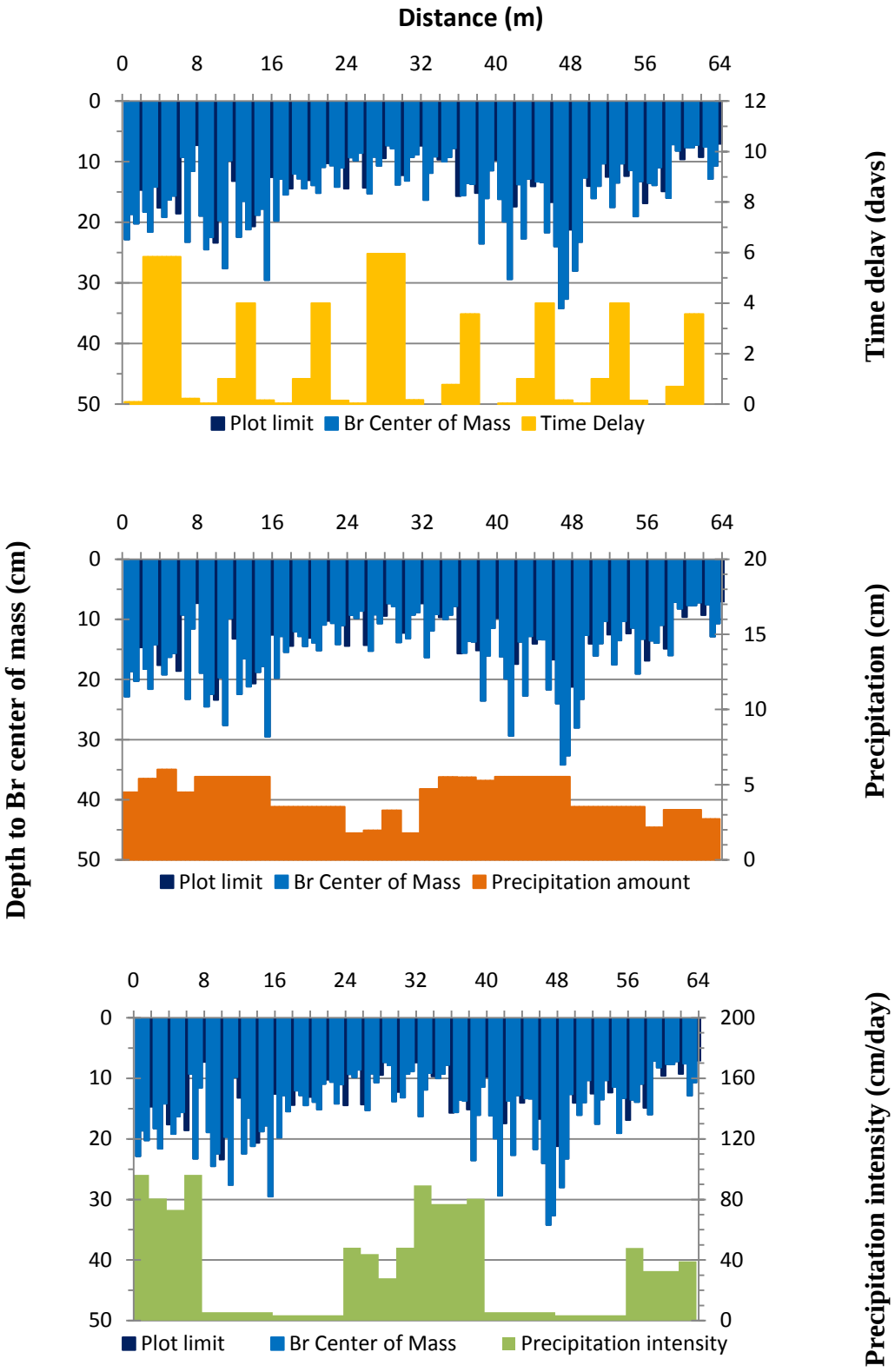

Figure 5.34. Bromide center of mass as a function of precipitation amount, intensity and Br- pulse time delay investigated in the main leaching study of 2008.

However, another way of visualizing the results was by creating four categories of precipitation amount, intensity and application time delay. This categorization might have been a better way to illustrate the effect of the different levels of transport causing factors on the Br^- centers of mass in Table 5.5. The plot average Bromide centers of mass in Table 5.5 were also categorized into 4 levels in order to construct such table.

Table 5.4. Categorization of transport causing factors.

Category	Precipitation amount (cm)	Precipitation intensity (cm/day)	Time delay (days)
1	$5.523 \leq X \leq 6.02$	$73.09 \leq X \leq 96.3$	$4 \leq X \leq 5.95$
2	$4.5 \leq X \leq 5.52$	$27.9 \leq X \leq 48.1$	$0.77 \leq X \leq 3.57$
3	3.523	5.523	$0.09375 \leq X \leq 0.694$
4	$1.7 \leq X \leq 3.32$	3.523	$0 \leq X \leq 0.41667$

Pronounced Br^- leaching was found where the highest precipitation amount of 5.52 cm was applied within one day (6 out of 8 plots) (Table 5.5). The high Br^- leaching also corresponded to the 3rd level of irrigation intensity applied (6 out of 8 plots), i.e., 5.52 cm/day and the two lower categories for time delay, i.e., from 0 to 0.42 days (Tables 5 and 6). Therefore, the greatest leaching depth in the experiment was found were the highest precipitation amount was applied with relatively low intensity. Moreover, looking into the effect of time delay in the high Br^- leaching group, it appeared that the shortest levels of time delay, i.e., 1 and 4 hour time delay caused a greater leaching of Br^- than the two longest time delay levels of 1 and 4 days, respectively.

These findings suggest that the larger the application time delay, i.e., the longer the time between the solute application and the following rainfall, the smaller or shallower the leaching depth of Br^-. This behavior could be a result of the greater time the solute is allowed to redistribute in the soil matrix and therefore, a portion of the solute mass could have entered a pore size domain that may not have been readily available for rapid convective Br^- transport as suggested by McLay et al. (1991). High leaching of Br^- in this experiment was observed with the shortest time delays, in agreement with findings of Evans et al. (1998), McLay et al. (1991), Shipitalo et al. (2000), and Walker et al. (2005) who described similar effects of the application time delay on the leaching depth of solutes.

It can also be seen in Table 5.5 that plots with low Br^- leaching were found where the lowest irrigation amounts, i.e., 1.77 to 3.32 cm and the second highest irrigation intensity, i.e., from 27.9 to 48.09 cm/day were applied. However for this low Br^- leaching category, the time delay effect was not clearly marked or could not be associated with the lowest leaching depth category since almost every category for the time delay was present for this group in Table 5.5.

It is interesting that plot 24, where the highest leaching depth was found according to Table 5.5, Br^- was leached approximately 1.37 times deeper than the 2^{nd} largest leaching depth found in plot 8. Both plots, 24 and 8, were treated under the same transport causing factors categories as can be observed in Table 5.5. The larger leaching depth observed for plot 24 when compared to the second largest leaching depth in plot 8 (Table 5.5), could be a result of the fast and abrupt temporal changes of $\Delta H/\Delta z$ in plot 24 taken between Oct-23 and Oct-24 and previously discussed under 5.2.3.

In summary, the leaching depth of Br^- is affected by the precipitation amount as a decrease in the amount of water applied, also decreases the Br^- leaching for all the categories presented in Table 5.5. The effect of the precipitation intensity, i.e., low precipitation intensities caused deeper Br^- leaching, appeared obvious in the highest and lowest Br^- leaching categories but not on the mid and mid to low leaching depth categories. Finally, the effect of the application time delay, i.e., shorter time delays caused high Br^- leaching, appeared to be easily distinguished when it was combined with a high precipitation amount and a low precipitation intensity.

Table 5.5. Categorical distribution of transport causing factors and plot average Br center of mass, Standard deviation and Coefficient of variation for the Br average center of mass.

Plot	P. Amount	P. Intensity	time delay	Center of Mass (cm)	Standard deviation	CV%
Category 1. High leaching						
24	1	3	3	30.28	5.49	18
8	1	3	3	22.04	6.51	30
5	1	3	4	21.96	2.81	13
21	1	3	4	21.82	6.81	31
25	3	4	4	21.30	7.87	37
1	2	1	3	20.58	2.12	10
7	1	3	1	20.05	3.11	16
6	1	3	2	19.04	8.92	47
Category 2. Mid leaching						
2	2	1	1	18.03	3.72	21
3	1	1	1	17.03	1.89	11
20	2	1	4	17.02	6.10	36
22	1	3	2	16.42	5.45	33
23	1	3	1	16.13	4.82	30
9	3	4	4	16.02	3.50	22
4	2	1	3	14.69	7.50	51
28	3	4	3	14.58	3.97	27
Category 3. Mid-Low leaching						
19	2	1	2	14.31	1.13	8
27	3	4	1	13.78	3.61	26
26	3	4	2	13.46	2.91	22
11	3	4	1	13.33	2.17	16
10	3	4	2	13.09	1.25	10
29	4	2	4	12.80	1.62	13
17	2	1	4	12.45	3.61	29
12	3	4	3	11.94	1.95	16
Category 4. Low leaching						
14	4	2	1	11.72	3.16	27
30	4	2	2	10.45	4.83	46
16	4	2	3	10.43	2.38	23
32	4	2	4	10.36	2.66	26
15	4	2	1	9.66	3.60	37
13	4	2	4	9.24	0.62	7
18	2	1	2	9.02	1.12	12
31	4	2	2	7.52	0.26	3

5.2.9. Spatial Statistical Analysis of Br^- Center of Mass

To investigate if both, the transport causing factors and the Br^- center of mass were correlated over the same distances, the analysis of the spatial autocovariance function using normalized semivariograms and crossvariograms for the Br^- center of mass and transport causing factors is presented in Figures 5.35 and 5.36. It is obvious that both the precipitation amount and intensity were correlated over 16 m distances with the Br center of mass, as can be inferred by the normalized semivariograms presented in Figure 5.35 and the crossvariogram in Figure 5.36.

The normalized semivariogram of time delay and crossvariogram of time delay vs. Br^- center of mass appeared to be correlated over 4 m distances (Figures 5.35 and 5.36). This 4 m range for the imposed pattern of time delay and its cyclic behavior could also be anticipated by looking at the separation distance over which pairs of imposed observations of time delay had their differences at a maximum in Figure 5.34.

Spectral analysis was included to find out the portion of the Br^- center of mass variation that could be attributed to the regular cyclic application pattern of the precipitation amount, intensity and especially time delay.

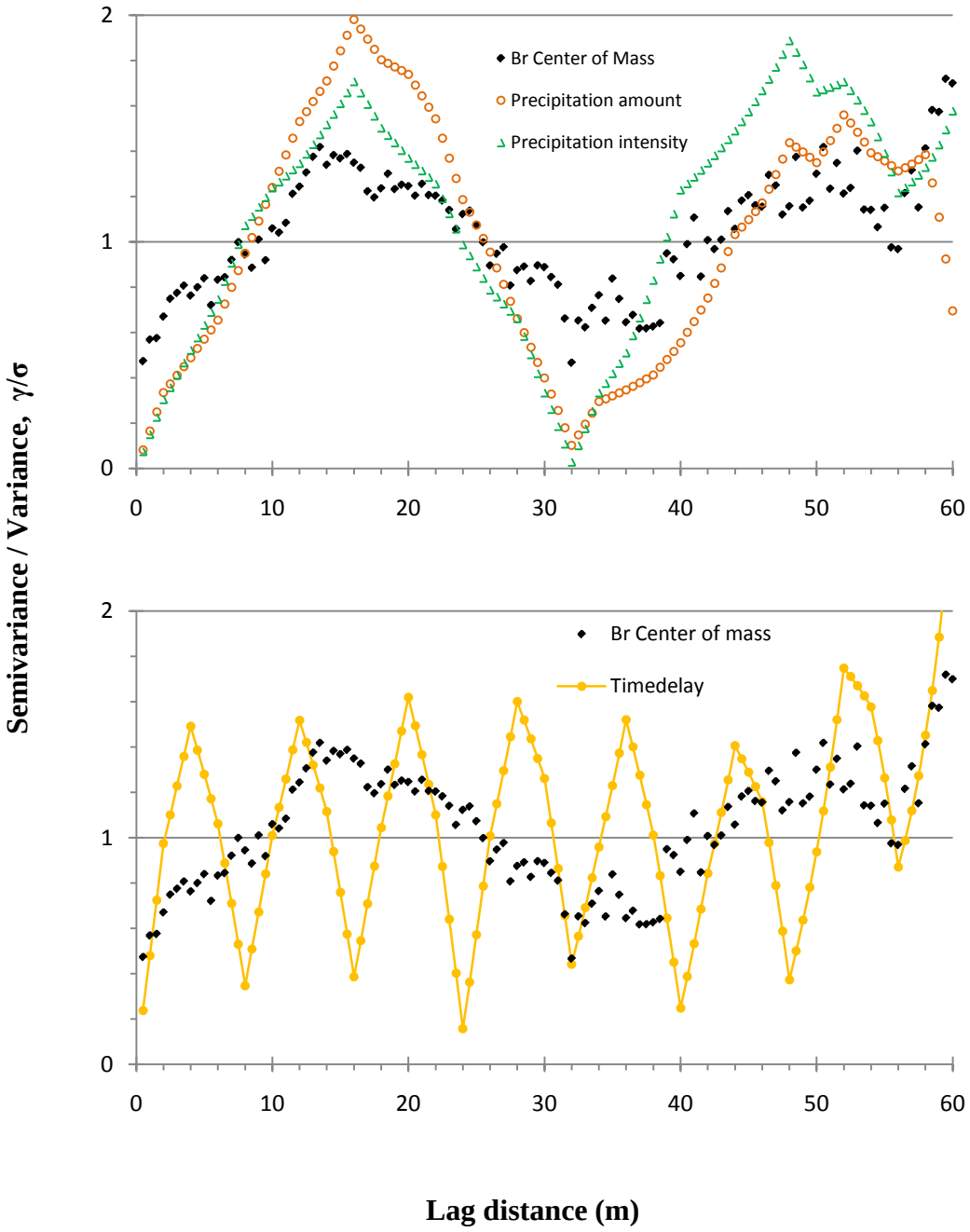

Figure 5.35. Spatial Structure of Bromide center of mass and transport causing factors for the main leaching study sampled in Oct-31-08.

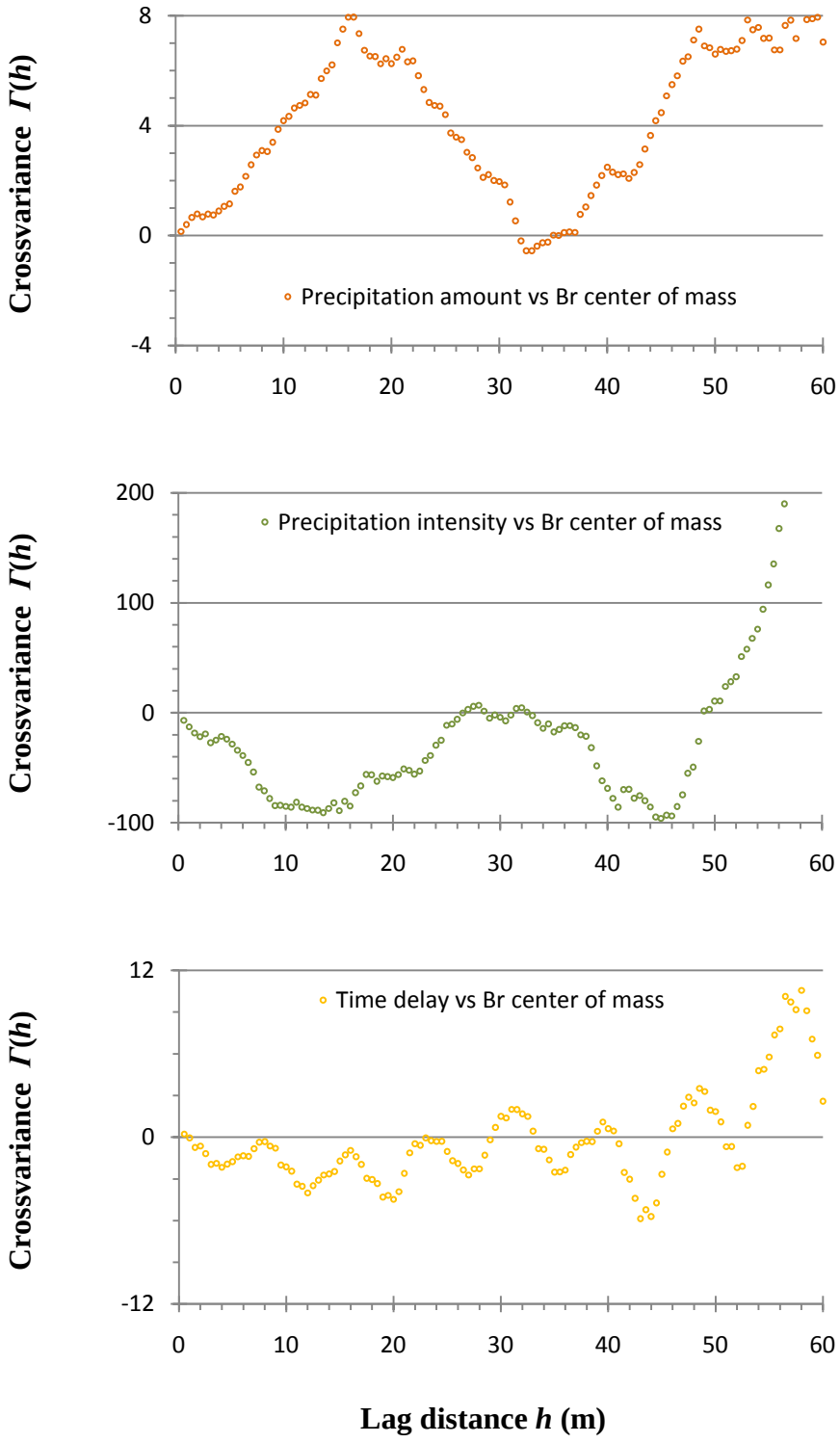

Figure 5.36. Crossvariograms of Bromide center of mass and transport causing factors in the main leaching study of 2008.

5.2.10. Cyclic Variation of Bromide Center of Mass and Transport Causing Factors.

The cyclic application pattern present every 32 m for the precipitation amount and intensity in Figure 5.34 was reflected by their spectral peaks at frequencies of 0.016 (0.5 m)$^{-1}$ frequency (Figure 5.37). The 0.016 (0.5 m)$^{-1}$ frequency corresponds exactly to the 32 m wavelength previously identified for the precipitation amount and intensity in Figure 5.34.

The time delay power spectrum in Figure 5.37 has three different peaks at 0.016, 0.063 and 0.19 (0.5m)$^{-1}$ frequencies corresponding to 32, 8 and 2.66 m wavelengths. The largest peak, however, is found for the 8 m wavelength component, in agreement with the spatial distribution of the time delay in Figure 5.34. The peak at 32 m wavelength for the time delay spectra in Figure 5.37 indicated, perhaps, the singular time delays registered for plots 3 and 15 (Figure 5.34) which may cause the identification of the cyclic pattern of 32 m wavelength on the time delay series (Figure 5.37). Lastly, the 2.66 m wavelength component in Figure 5.37 could not be associated with any cyclic variation pattern in the series of time delay in Figure 5.34.

The integer of the area underneath the power spectrum of the Br^- center of mass in Figure 5.37 is equal to the total variance of the Br^- center of mass series and suggests that the majority of the variability of the Br^- center of mass occurs in cycles of 32 m wavelengths and shows common cyclic variation with the precipitation amount and intensity spectra in Figure 5.37. Furthermore, the common cyclic variation at 32 m wavelength shared by the Br^- center of mass and precipitation amount and intensity, could also be seen in the pattern of their semi- and crossvariogram functions in Figures 5.35 and 5.36.

Finally, the Br^- center of mass spectrum also presented a smaller peak at 0.055 $(0.5\ m)^{-1}$ frequency or 9 m wavelength which could be associated with the 8 m wavelength cyclic variation imposed by the time delay factor.

In summary, the power spectrum of Br^- center of mass in Figure 5.37 indicates that the majority of the variation in the Br^- leaching depth occurred in common cycles with precipitation amount and intensity, and only a smaller fraction of the Br^- center of mass variability shares common cyclic variation with the time delay.

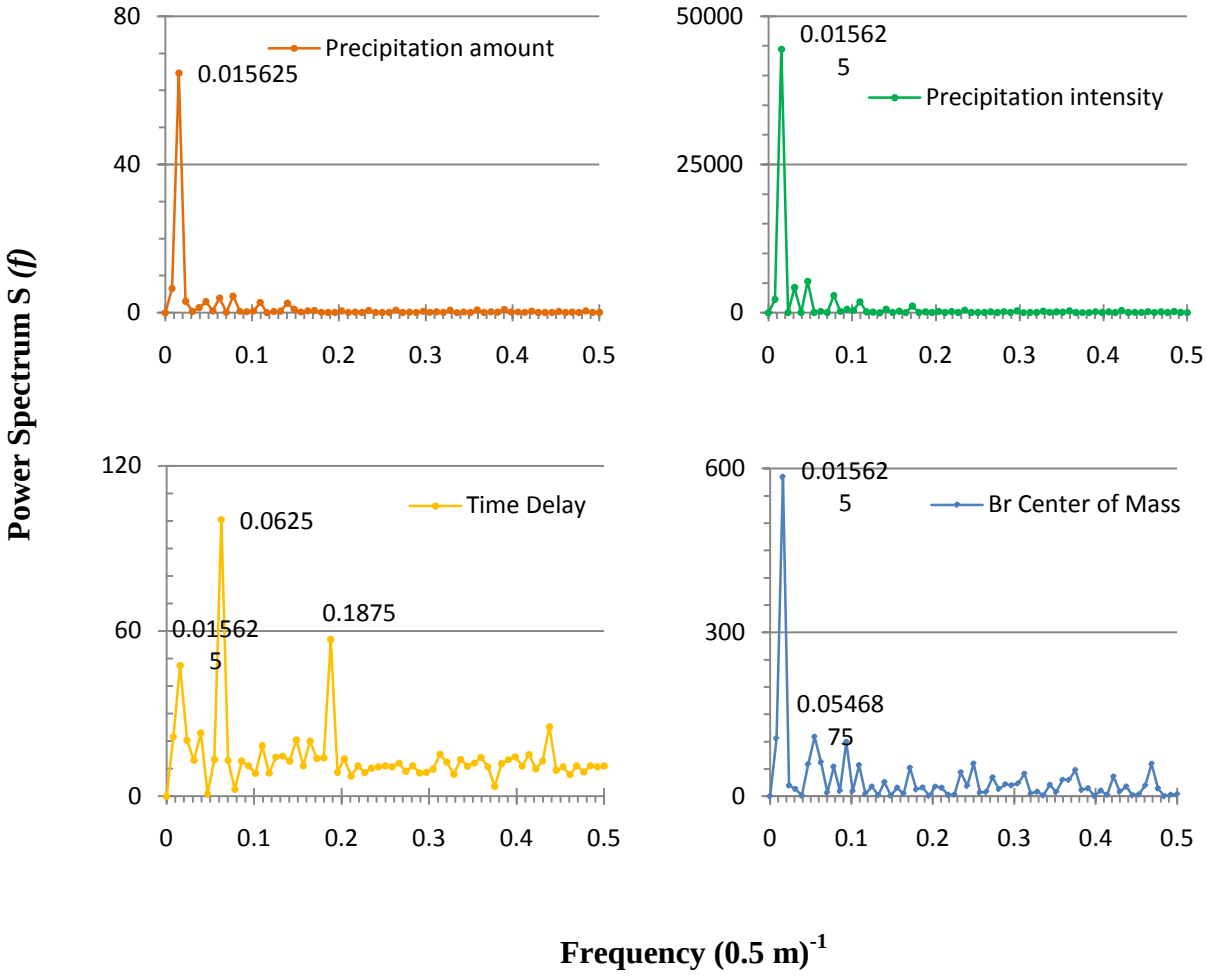

Figure 5.37. Spectral analysis of transport causing factors and Bromide center of mass investigated in the main leaching study of 2008.

The co- and quad-spectra of the different transport causing factors vs. the Br^- center of mass in Figure 5.38 indicated that the cyclic pattern of variation imposed by the precipitation amount, intensity and the time delay were correlated with the Br^- center of mass over 32, 32 and 8 m wavelengths, respectively, being the precipitation amount directly correlated with the Br^- center of mass whereas the precipitation intensity and the time delay are both inversely correlated with the Br^- center of mass. Therefore, Br^- leaching depth is directly correlated with precipitation amount and inversely correlated with precipitation intensity and time delay.

In conclusion, Br^- leaching was the highest when a large precipitation pulse was applied at a low intensity and when little time (time between solute application and following rainfall) was allowed for the solute to redistribute in the soil matrix. This conclusion could have been previously drawn for the precipitation amount and intensity by considering their common ranges of variation with the Br^- center of mass (Figures 5.35 and 5.36). However, the effect of the time delay factor was not clearly described by the semi- and crossvariograms in Figures 5.35 and 5.36 and the inclusion of the cross spectra of the time delay vs. the Br^- center of mass clearly identified the inverse nature of the correlation found in commonly occurring cycles of 8 m wavelengths for both time delay and Br leaching depth.

Lastly, the coherency spectrum, a measure of the goodness of the correlation between two sets of observations for various frequencies (Nielsen and Wendroth, 2003) indicated that, for 0.016 $(0.5\ m)^{-1}$ frequencies corresponding to 32 m wavelengths (Figure 5.38), there was a strong correlation (significant at the 95 % level) between precipitation amount and intensity vs. Br^- leaching depth.

The strength of the correlation of time delay vs. Br^- leaching depth appeared weak on the coherency spectrum in Figure 5.38, as no peak was identified at 0.063 $(0.5\ m)^{-1}$ frequency corresponding to 8 m wavelengths. This conclusion, however, must be considered carefully because it was demonstrated with Table 5.5, for the highest Br^- leaching category, that the majority of plots within this deep leaching category had the shortest time delays in the experiment. Therefore, we assume that the time delay effect had a stronger correlation with Br^- leaching depth when precipitation amount was highest and precipitation intensity was relatively low (Table 5.5) and that this pattern did not hold for the other treatment combinations in the experiment, giving rise to an overall weak correlation for the time delay effect on the coherency spectrum (Figure 5.38).

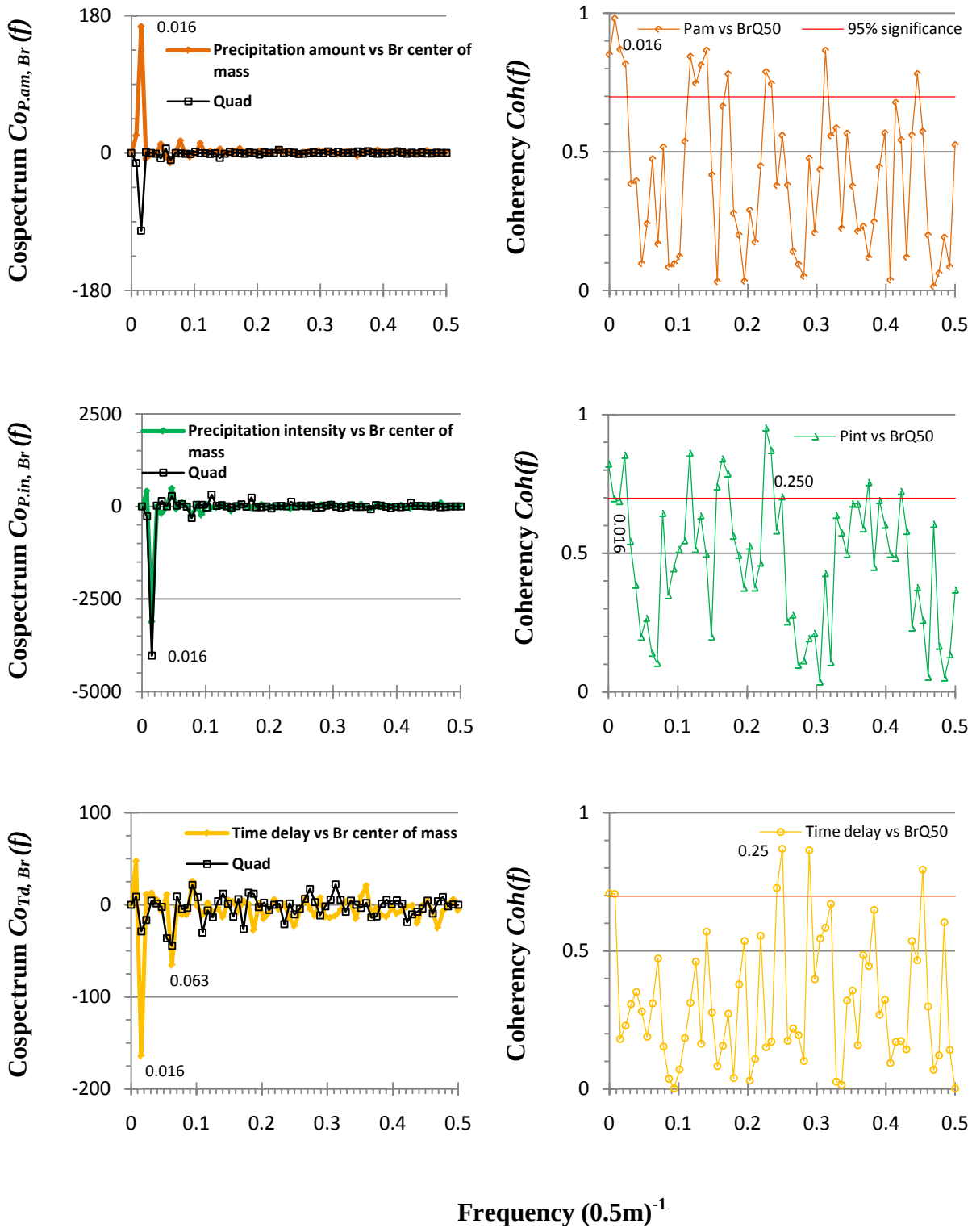

Figure 5.38. Co-, quadrature and coherency spectrum of transport causing factors vs. Br^- center of mass on the main leaching study of 2008.

Furthermore, to determine if the cyclic variation of the transport causing factors was in phase with the Br^- center of mass cyclic behavior, the phase spectrum was calculated (equation 8.4 in Nielsen and Wendroth, 2003) with the peaks observed for the quad- and co-spectrum for each pair of variables.

The phase spectrum indicated that the transport causing factors and the Br^- Center of mass were not in phase, and there was a lag of -5.6, +9.3, and +1.76 sampling intervals for the peaks observed at 0.016, 0.016 and 0.063 $(0.5\ m)^{-1}$ frequencies for the precipitation amount, intensity and time delay, respectively (Figure 5.38). Therefore, the phase lag was equivalent to -2.8, 4.65, and 0.88 m respectively (Figure 5.38), once the sampling interval of 0.5 m was multiplied by each phase lag distance.

The -2.8 m phase shift between the Precipitation amount and the Br^- center of mass indicated that Br^- Center of mass series was shifted 2.8 m to the right with respect to the precipitation amount series. This -2.8 m shift reflected the non symmetrical characteristic of the cross-correlation function, where the highest correlation between precipitation amount was associated with the Br^- center of mass not on the same sampling location, but 2.3 m to the right.

The 4.65 m phase shift between the precipitation intensity and the Br^- center of mass indicated that, both series being inversely correlated, a low precipitation intensity observation ws associated with a peak on the leaching depth of Br^- but not on the same location but 4.65 m to the left. This phase shift observed for the precipitation intensity and Br^- center of mass only reflected the asymmetrical nature of their cross-correlation.

For the time delay vs Br^- center of mass series, it could be assumed that there was no phase shift between the cyclic variation component of the time delay and the Br^- center of mass as the phase lag for the 8 m wavelength component of the variation was really close to 0 (phase lag = 0.075m). Therefore it is concluded that the cyclic variation of the time delay was in phase and proceeded synchronously with the cyclic variation of the Br^- center of mass.

5.2.11. Water Mass Balance for the Field Transect Investigated in 2008

The water mass balance for the duration of the experiment (Oct-19 to Oct-31-08) was calculated for each of the 128 locations sampled on Oct-31. The calculation steps were described in chapter 4.12. The water mass balances for the 128 profiles investigated in the field transect leaching study of 2008 are presented in Figure 5.39. An average water mass balance of 93 % was found over the 12 day period in which the experiment was carried out (Oct-19 to Oct-31-08) which indicates that the majority of the water applied in this leaching study remained in the soil profiles investigated. It also indicates that a small fraction of water, 7% left the soil profile through either downward flux out of the 100 cm depth soil profile or by means of lateral flux. Figure 5.39 shows that for distances between 16 and 44 m the mass balance is systematically lower than for other locations.

This could be, perhaps, a result of a steady decrease in the clay fraction accompanied by an increase on the silt fraction observed at the same distances at 27-33, 47-53 and 67-73 cm depth from the spatial analysis of soil textural classes (Figure 5.6) under chapter 5.2.1. The average decrease in clay of ≈ 10 % was accompanied by a 10 % increase of the

silt fraction. Therefore, if it can be assumed that the increase in the silt fraction (16-44 m distances) is accompanied by an increase in hydraulic conductivity, a localized area of enlarged drainage could be presumed responsible for this spatial behavior of the water mass balance.

Also in Figure 5.39, it can be seen that the variance of the mass balance of Br^- was 6 times larger than the variabiance of the mass balance of water as indicated by their CVs. This observation could indicate that water redistribution and equilibration proceeded, perhaps, more homogeneously than Br^- redistribution in the soil profile.

5.2.12. Bromide Mass Balance for Field Transect Investigated in 2008

The mass balance for Br^- was calculated with the method described in chapter 4.13 and the results are plotted in Figure 5.39. An average 104% Br mass balance indicated that all the solute applied was recovered from the soil profile at the moment of tracer sampling in Oct-31. The large spatial variability of this 104% mass balance with a 54% CV indicates that Br^- was more heterogeneously distributed than water.

Finally, the normalized semivariogram for the Br^- mass balance in Figure 5.40 indicated that Br^- mass was randomly distributed across space, and that the factors studied in this experiment had no spatially systematic effect on the spatial distribution on Br^- mass recovered at any location which is an encouraging result.

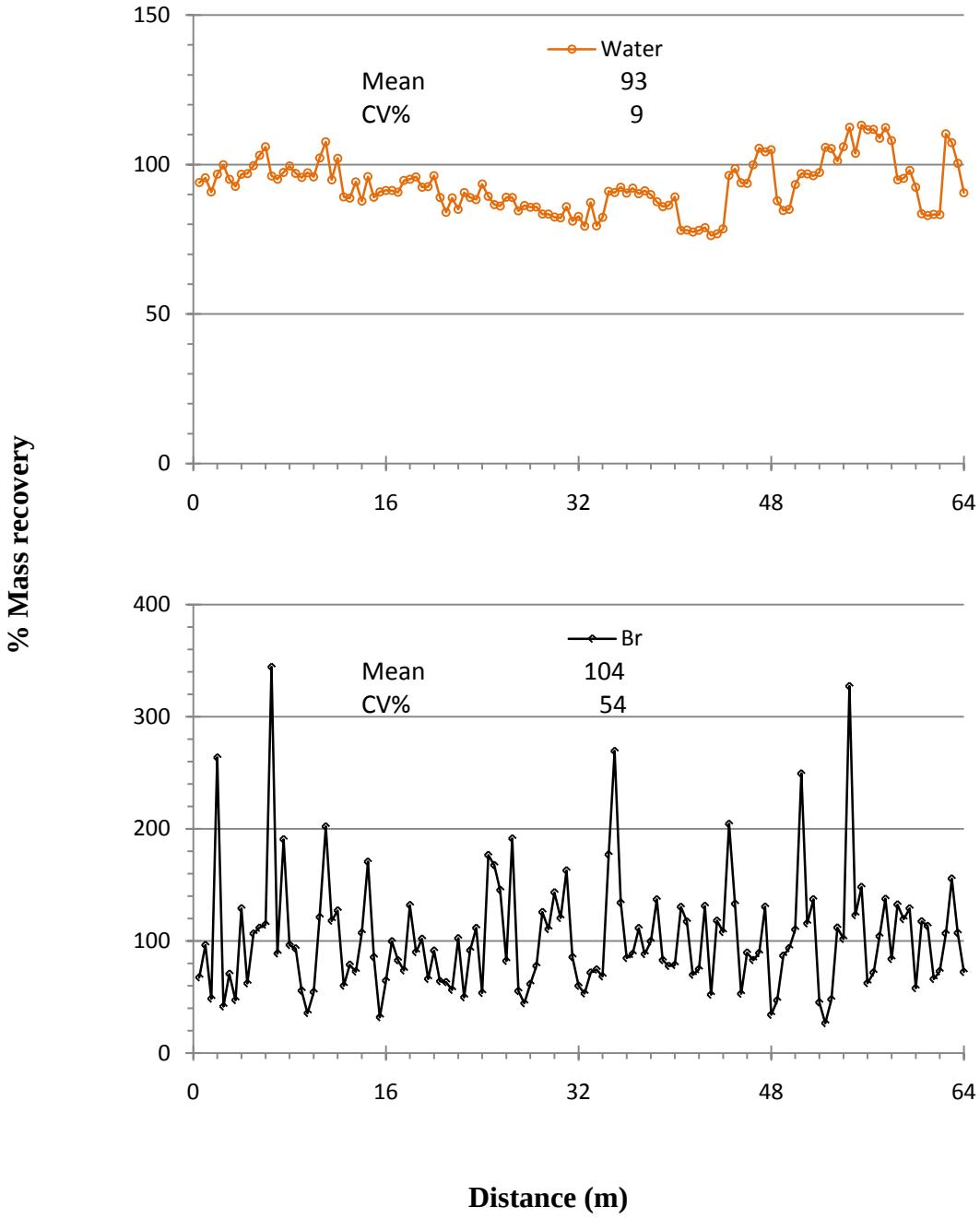

Figure 5.39. Mass balances of Water and Bromide for the field transect investigated in 2008 from Oct-19 to Oct-31.

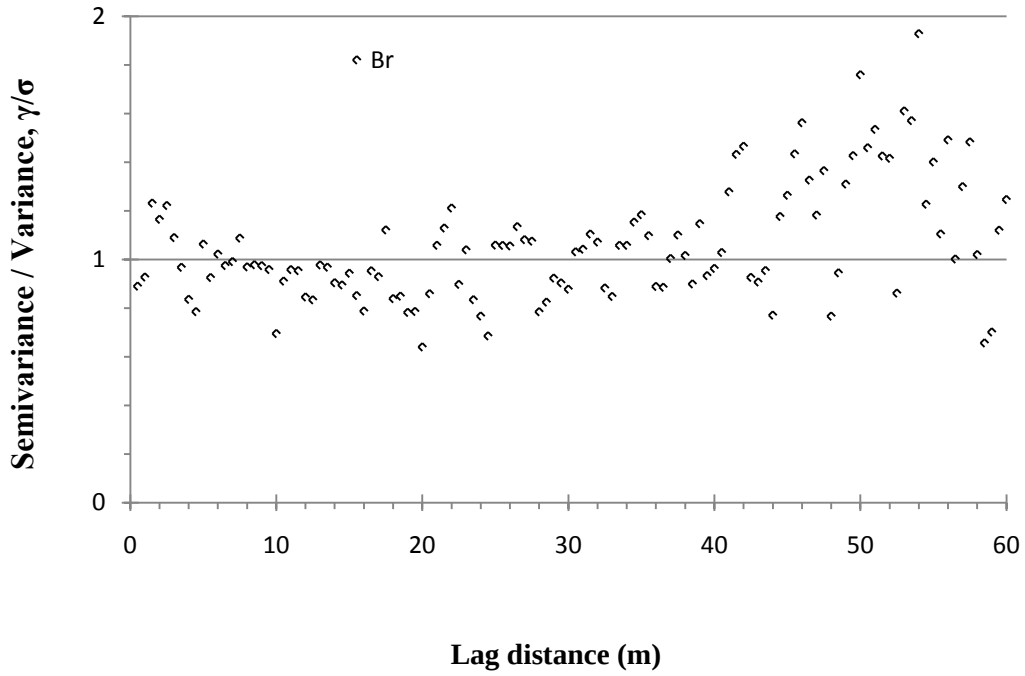

Figure 5.40. Spatial structure of Bromide mass balance for the field transect investigated in 2008.

5.2.13. Water and Bromide Transport Simulations

The main purpose of the Water and Br transport simulations was to determine if the field measurements of Br^- and ψ_m at the moment of tracer sampling, were in close agreement with their simulated values. In other words, this analysis should show how accurately the bromide transport and matric potential distribution was decribed by Hydrus1D based on the site specific parameterization and experimental upper boundary conditions.

5.2.13.1. Soil Information to the Model

The soil input information for the modelo was obtained from the intact soil cores investigated for soil hydraulic properties. There was one hydraulic property sample lost during the analysis due to various large tunnels carved by ants. This sample was taken on plot 5 at the 27-33cm depth. To overcome this problem, the soil hydraulic property parameters estimated for plot 1 at the 27-33cm depth were assumed to represent the parameters for plot 5 at the same depth interval. Moreover, it was assumed that the representation of each set of samples (7-13 and 27-33 cm depth) of soil hydraulic property parameters was four plots, i.e., samples taken in plot 1 represented plots 1-3, samples taken on plot 5 represented plots 4-7, samples taken in plot 9 represented plots 8-11, etc. The spatial representation of soil hydraulic property parameters along the transect is depicted in Table 5.6.

At last, the dispersivity parameter λ defined as the scale over which water flux and solute convection are averaged (Jury and Horton, 2004) was set to 10 cm for all three soil materials as suggested by Vanderborght and Vereecken (2007).

Table 5.6. Parameters for the Van Genuchten model of soil hydraulic properties on field transect investigated in 2008.

Plots	Depth cm	ρ_b (g/cm^3)	θr	θs	α	n	Ks (cm/day)	l
1, 2, 3	0-13.5	1.12	0.26	0.48	0.04	1.31	218.4	0.5
	15-49.5	1.35	0.3	0.43	0.15	1.38	1258	0.5
	51-150	1.5	0.078	0.43	0.036	1.56	24.96	0.5
4, 5, 6, 7	0-13.5	1.12	0.27	0.48	0.13	1.23	3094	0.5
	15-49.5	1.35	0.3	0.43	0.15	1.38	1258	0.5
	51-150	1.5	0.078	0.43	0.036	1.56	24.96	0.5
8, 9, 10, 11	0-13.5	1.12	0.05	0.47	0.17	1.08	9217	0.5
	15-49.5	1.35	0.26	0.43	0.23	1.33	3164	0.5
	51-150	1.5	0.078	0.43	0.036	1.56	24.96	0.5
12, 13, 14, 15	0-13.5	1.12	0.28	0.5	0.033	1.42	141	0.5
	15-49.5	1.35	0.23	0.45	0.16	1.24	1442	0.5
	51-150	1.5	0.078	0.43	0.036	1.56	24.96	0.5
16, 17, 18, 19	0-13.5	1.12	0.01	0.46	0.03	1.09	524	0.5
	15-49.5	1.35	0.18	0.44	0.08	1.2	1410	0.5
	51-150	1.5	0.078	0.43	0.036	1.56	24.96	0.5
20, 21, 22, 23	0-13.5	1.12	0.24	0.51	0.08	1.24	1223	0.5
	15-49.5	1.35	0.2	0.44	0.21	1.22	3961	0.5
	51-150	1.5	0.078	0.43	0.036	1.56	24.96	0.5
24, 25, 26, 27	0-13.5	1.12	0.25	0.5	0.046	1.28	327	0.5
	15-49.5	1.35	0.16	0.47	0.16	1.19	9216	0.5
	51-150	1.5	0.078	0.43	0.036	1.56	24.96	0.5
28, 29, 30, 31, 32	0-13.5	1.12	0.01	0.47	0.042	1.08	1132	0.5
	15-49.5	1.35	0.01	0.39	0.05	1.017	4059	0.5
	51-150	1.5	0.078	0.43	0.036	1.56	24.96	0.5

5.2.13.2. Measured and Simulated Bromide and Soil Water Matric Potential ψ_m

Measured and simulated Br^- concentrations for each 10 cm depth increment along the transect are depicted in Figures 5.41 and 5.42 for the moment of tracer sampling in Oct-31-08. In general, the simulated Br^- concentrations represented the average measured Br^- along the transect for the 0-10 depth (Figure 5.41). However, in the 10-20 cm depth, the Br^- concentrations were slightly underestimated by the model.

In the depth compartments between 20 and 50 cm depth simulated Br^- concentrations proceeded at a higher level than the measured concentrations (Figures 5.41 and 5.42), causing an overestimation of the Br^- leaching depth. However, the difference between simulated and measured Br^- concentrqations in the 30-50 cm depths (Figure 5.42) appeared smaller for those plots receiving lower irrigation amounts, i.e., plots 9-16 and 25-32 for transect distances of 16-32 and 48-64 m, respectively.

In conclusion, the simulated Br^- concentrations along the transect were in reasonably good agreement with measured values. Modeled Br^- profiles would have overestimated the measured leaching depth of Br^- in this experiment due to underestimation of Br^- concentrations in the 10-20 cm depth and overestimation of Br^-concentrations found in the 20-50 cm depths.

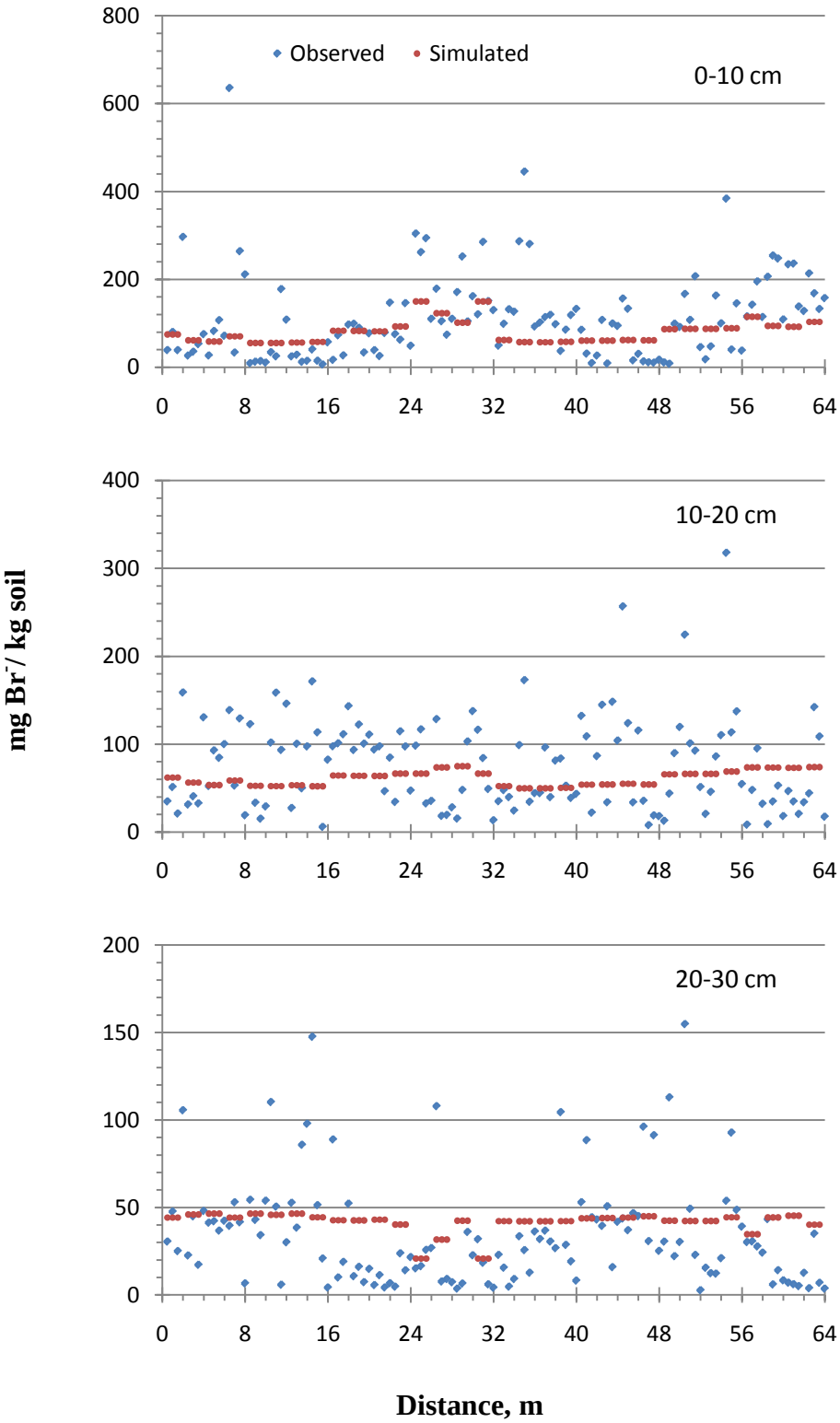

Figure 5.41. Measured and simulated Bromide concentrations in upper three depth compartments at tracer sampling in Oct-31-08.

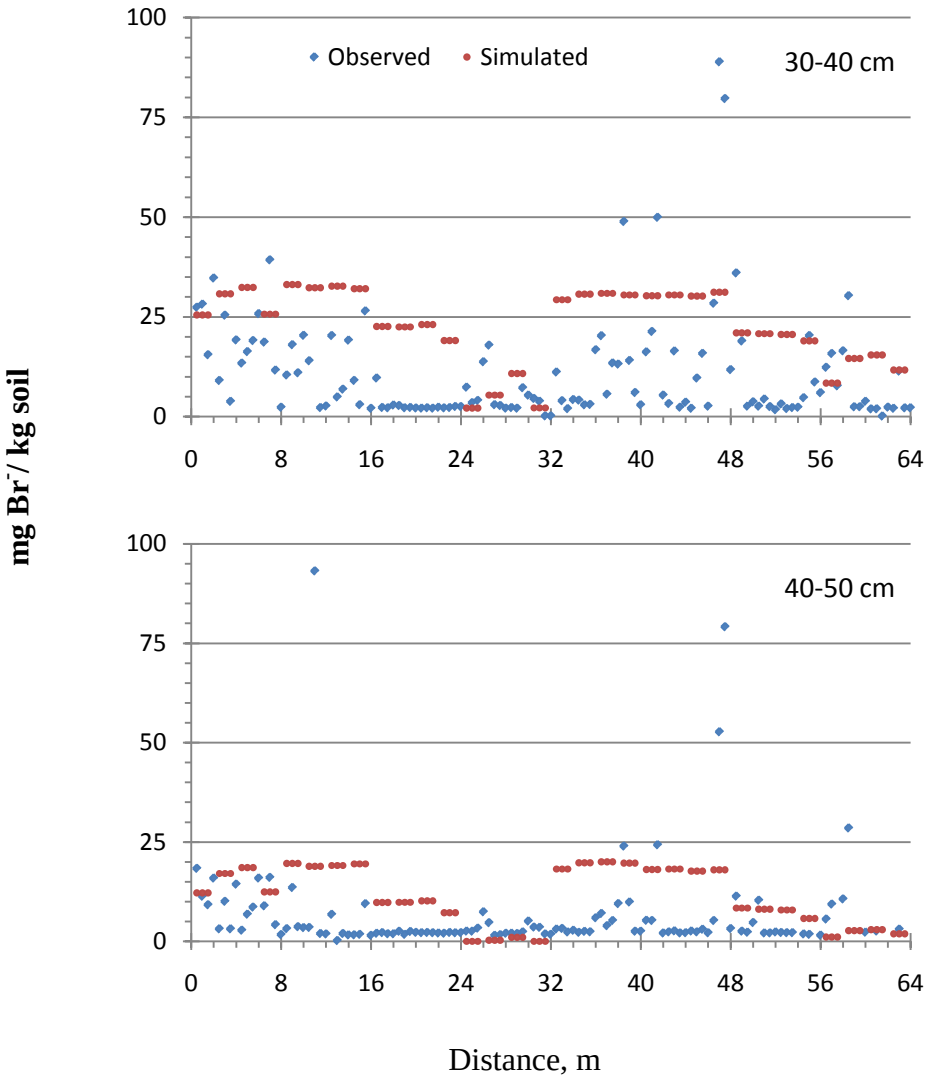

Figure 5.42. Measured and simulated Bromide concentrations in lower two depth compartments at tracer sampling in Oct-31-08.

The measured and simulated soil water matric potential (ψ_m) at the moment of tracer sampling is presented in Figures 5.43 and 5.44. In general, the simulated ψ_m for the upper three depths in Figure 5.43 were in reasonably good agreement with measured values. However, it appears that the simulated values for the upper three depths were in better agreement with measured ψ_m for transect distances > 32 m (Figure 5.43).

The simulated ψ_m values for the three lower depths shown in Figure 5.44 were consistently below the measured ψ_m. This indicates that the default parameters for a Loam soil assumed to represent the soil hydraulic properties at depths > 50 cm were probably not the best set of parameters to represent the hydraulic properties at these depths. Despite this consistent underestimation of ψ_m for the lower depths, simulated and measured values for all depths in Figures 5.43 and 5.44 were still in good agreement.

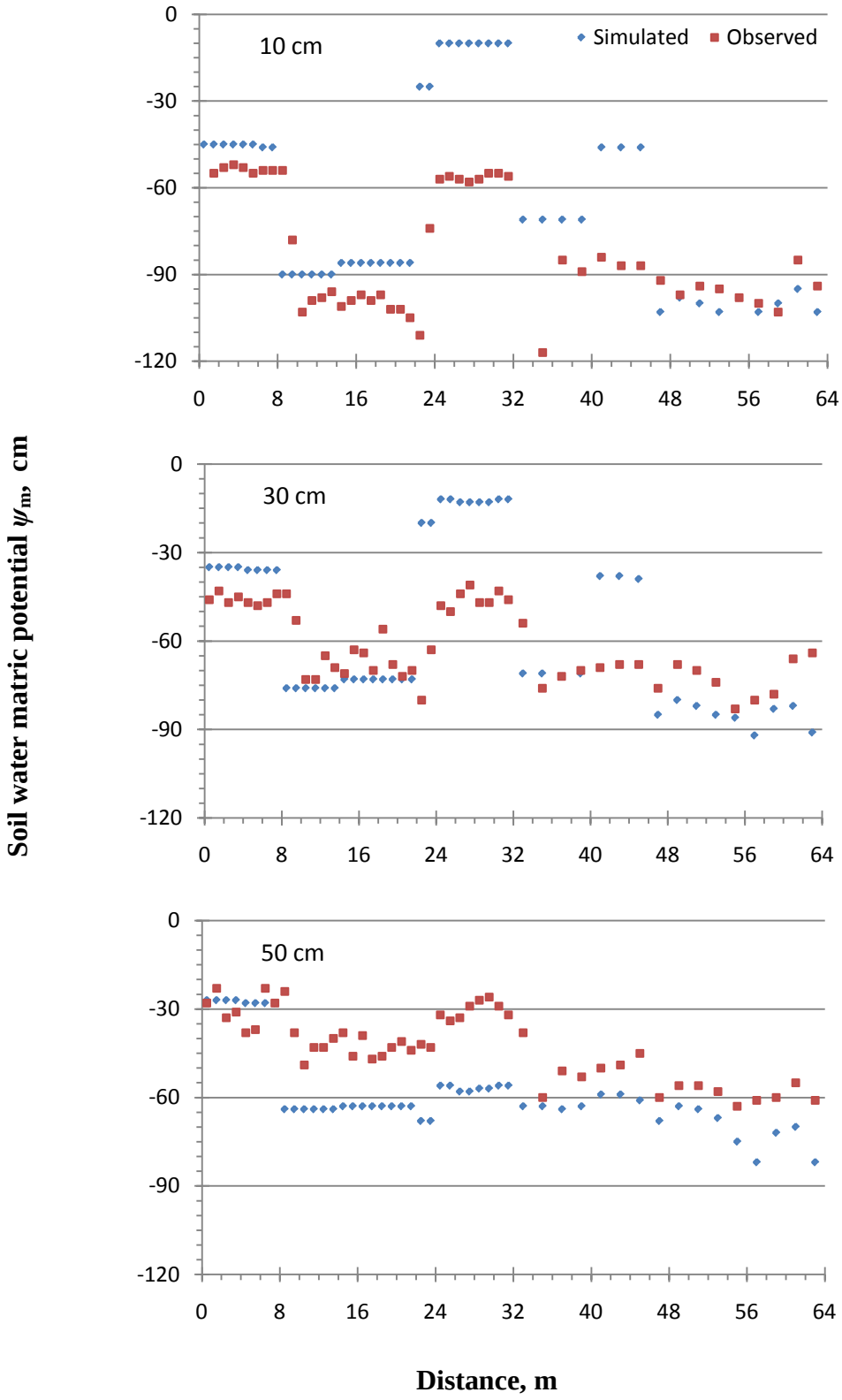

Figure 5.43. Measured and simulated soil water matric potential in upper three depths at tracer sampling in Oct-31-08.

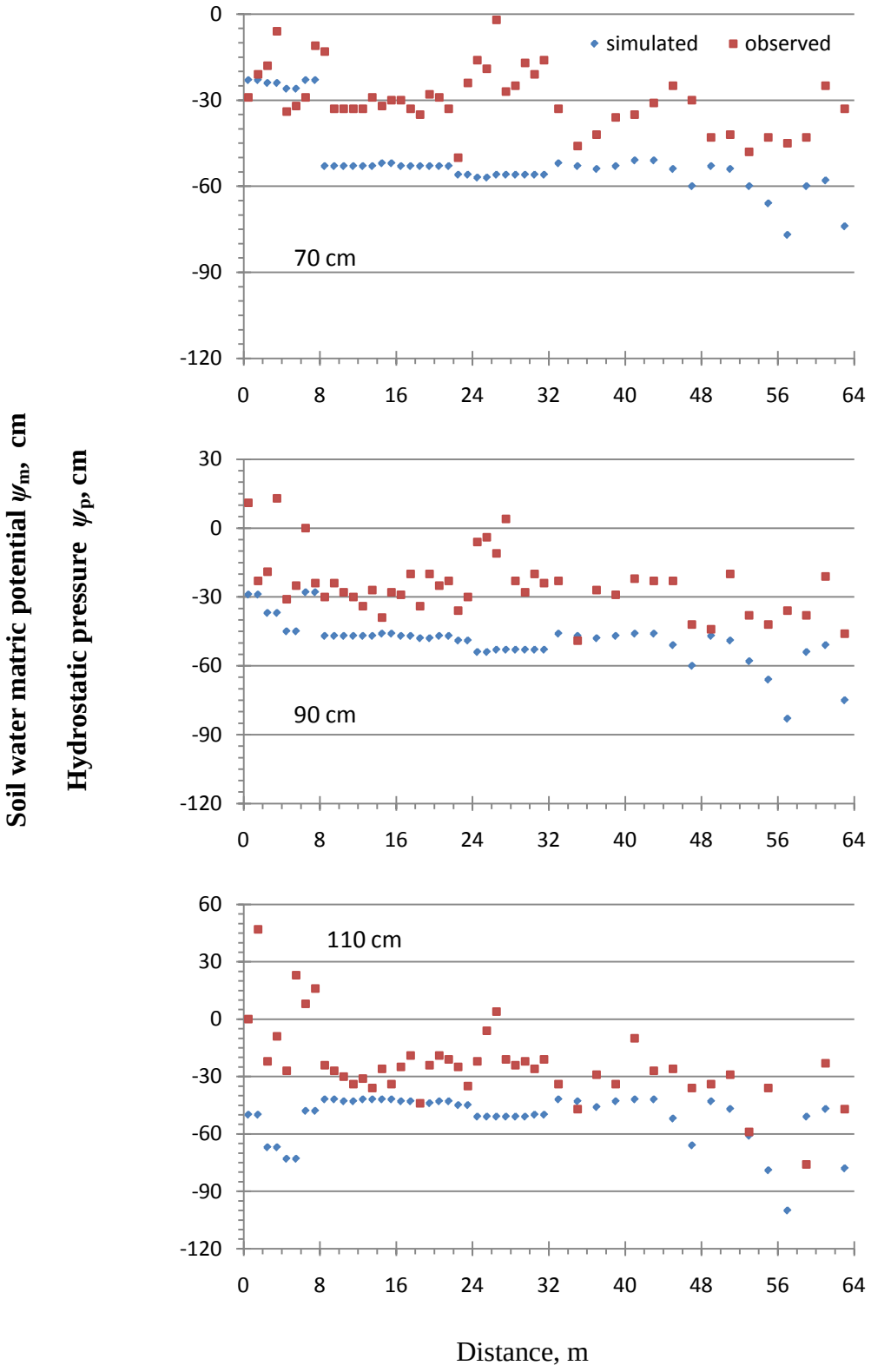

Figure 5.44. Measured and simulated soil water matric potential in lower three depths at tracer sampling in Oct-31-08.

6. General conclusions

- The field scale spatial variation scale of Br^- leaching was successfully identified.
- The same amount of rainfall caused deeper Br^- leaching when it occurred at a lower rainfall intensities
- Rainfall events occurring at short time intervals after solute application caused more rapid leaching than longer time intervals
- Rainfall amount had the greatest effect on the leaching depth of Br^- followed by the rainfall intensity and application time delay.
- The application time delay effect is greater when high amount, low intensity rainfalls coincide.
- Measured and simulated Br^- and ψ_m were in good agreement

Appendix

Appendix 1. Scheduled and executed Br pulse application and irrigation on main leaching study in Oct-2008.

	KBr Field spray application		Irrigations	
Plots	**Planned**	**Executed**	**Planned**	**Executed**
1	10/25/2008 11:00	10/30/2008 11:00	Oct/25/08 12:00	10/30/2008 13:15
2	10/24/2008 12:00	10/24/2008 12:00	Oct/25/08 12:00	10/30/2008 13:15
3	10/21/2008 12:00	10/21/2008 12:00	Oct/25/08 12:00	10/30/2008 13:15
4	10/25/2008 8:00	10/30/2008 8:00	Oct/25/08 12:00	10/30/2008 13:15
5	10/23/2008 12:00	10/23/2008 12:00	10/23/2008 13:00	10/23/2008 13:00
6	10/22/2008 13:00	10/22/2008 13:00	10/23/2008 13:00	10/23/2008 13:00
7	10/19/2008 13:00	10/19/2008 13:00	10/23/2008 13:00	10/23/2008 13:00
8	10/23/2008 9:00	10/23/2008 9:08	10/23/2008 13:00	10/23/2008 13:00
9	10/23/2008 11:30	10/23/2008 11:30	10/23/2008 12:30	10/23/2008 12:30
10	10/22/2008 12:30	10/22/2008 12:30	10/23/2008 12:30	10/23/2008 12:30
11	10/19/2008 12:30	10/19/2008 12:30	10/23/2008 12:30	10/23/2008 12:30
12	10/23/2008 8:30	10/23/2008 8:58	10/23/2008 12:30	10/23/2008 12:30
13	10/25/2008 15:00	10/30/2008 15:00	10/25/2008 16:00	10/30/2008 16:00
14	10/24/2008 16:00	10/24/2008 16:00	10/25/2008 16:00	10/30/2008 16:00
15	10/21/2008 16:00	10/21/2008 16:00	10/25/2008 16:00	10/30/2008 16:00
16	10/25/2008 12:00	10/30/2008 12:00	10/25/2008 16:00	10/30/2008 16:00
17	10/24/2008 13:00	10/24/2008 13:00	10/24/2008 14:00	10/24/2008 14:00
18	10/23/2008 14:00	10/23/2008 14:00	10/24/2008 14:00	10/24/2008 14:00
19	10/20/2008 14:00	10/20/2008 19:00	10/24/2008 14:00	10/24/2008 14:00
20	10/24/2008 10:00	10/24/2008 10:00	10/24/2008 14:00	10/24/2008 14:00
21	10/23/2008 11:45	10/23/2008 11:45	10/23/2008 12:45	10/23/2008 12:45
22	10/22/2008 12:45	10/22/2008 12:45	10/23/2008 12:45	10/23/2008 12:45
23	10/19/2008 12:45	10/19/2008 12:45	10/23/2008 12:45	10/23/2008 12:45
24	10/23/2008 8:45	10/23/2008 9:03	10/23/2008 12:45	10/23/2008 12:45
25	10/23/2008 11:15	10/23/2008 11:15	10/23/2008 12:15	10/23/2008 12:15
26	10/22/2008 12:15	10/22/2008 12:15	10/23/2008 12:15	10/23/2008 12:15
27	10/19/2008 12:15	10/19/2008 12:15	10/23/2008 12:15	10/23/2008 12:15
28	10/23/2008 8:15	10/23/2008 8:48	10/23/2008 12:15	10/23/2008 12:15
29	10/24/2008 15:00	10/24/2008 15:00	10/24/2008 16:00	10/24/2008 16:00
30	10/23/2008 16:00	10/23/2008 16:00	10/24/2008 16:00	10/24/2008 16:00
31	10/20/2008 16:00	10/20/2008 19:05	10/24/2008 16:00	10/24/2008 16:00
32	10/24/2008 12:00	10/24/2008 12:00	10/24/2008 16:00	10/24/2008 16:00

Appendix 2. Time variable boundary conditions on 0-32m distances for tracer experiment on 2008.

	Time interval		Precipitation intensity	
Plot	Planned	Executed	Planned	Executed
1	1 hr	2 hrs 15 min	4 cm/ hr	4.5 cm/67.3 min
2	1 day	5 days. 20 hrs 15 min	4 cm/ hr	4.5 cm/67.3 min
3	4 day	2 days 20 hrs 45 min: 5 days 20 hrs 15 min*	4 cm/ hr	1.52 cm/ 8.33 hrs: 4.5 cm/67.3 min
4	4 hr	5 hrs 15 min	4 cm/ hr	4.5 cm/67.3 min
5	1 hr	1 hr	4 cm/day	5.523 cm day-1
6	1 day	1 day	4 cm/day	5.523 cm day-1
7	4 day	4 day	4 cm/day	5.523 cm day-1
8	4 hr	3 hrs 52 min	4 cm/day	5.523 cm day-1
9	1 hr	1 hr	2 cm/day	3.523 cm day-1
10	1 day	1 day	2 cm/day	3.523 cm day-1
11	4 day	4 day	2 cm/day	3.523 cm day-1
12	4 hr	3.5 hrs	2 cm/day	3.523 cm day-1
13	1 hr	1hr	2 cm/ hr	1.77 cm 53 min-1
14	1 day	5 days 23 hours	2 cm/ hr	1.77 cm 53 min-1
15	4 day	2 days 16 hrs 40 min: 5 days 23 hours*	2 cm/ hr	1.52 cm/ 8.33 hrs + 1.77 cm/ 53 min
16	4 hr	4hrs	2 cm/ hr	1.77 cm/53 min

Appendix 3. Time variable boundary conditions tested on 2009 experiment for the 32-64m distances

	Time interval		Rainfall intensity	
Plot	Planned	Executed	Planned	Executed
17	1 hr	none, continuos flow	4 cm/ hr	0.8 cm/4.33 hr + Br + 0.18 cm/ hr + 4.18 cm/ hr +0.36 cm/2 hrs
18	1 day	18 hrs 40 min	4 cm/ hr	0.98 cm/ 5.33 hrs + 4.18 cm/hr + 0.36 cm/2hrs
19	4 day	3 days 13hrs 40 min	4 cm/ hr	0.96 cm/ 5.33 hr + 4.18 cm/ hr + 0.36 cm/ 2hrs
20	4 hr	none, continuos flow	4 cm/ hr	0.24 cm/1.33 hrs + Br + 0.73 cm /4 hr + 4 .18 cm/ hr + 0.36 cm/ 2 hrs
21	1 hr	1 hr	4 cm/day	5.523 cm day-1
22	1 day	1 day	4 cm/day	5.523 cm day-1
23	4 day	4 day	4 cm/day	5.523 cm day-1
24	4 hr	3 hrs 42 min	4 cm/day	5.523 cm day-1
25	1 hr	1 hr	2 cm/day	3.523 cm day-1
26	1 day	1 day	2 cm/day	3.523 cm day-1
27	4 day	4 day	2 cm/day	3.523 cm day-1
28	4 hr	3 hrs 27 min	2 cm/day	3.523 cm day-1
29	1 hr	none, continuos flow	2 cm/ hr	1.16cm/ 6.33 hrs + Br + 0.18cm/hr + 1.98 cm/55min
30	1 day	16h 40 min	2 cm/ hr	1.34cm/ 7.33 hrs + 1.98 cm/ 55 min
31	4 day	3 days 13 hrs 35 min	2 cm/ hr	1.34 cm/7.33hrs + 1.98 cm/ 55 min
32	4 hr	none, continuos flow	2 cm/ hr	0.61 cm /3.33hrs + Br + 0.73 cm/ 4hrs + 1.98 cm/ 55min

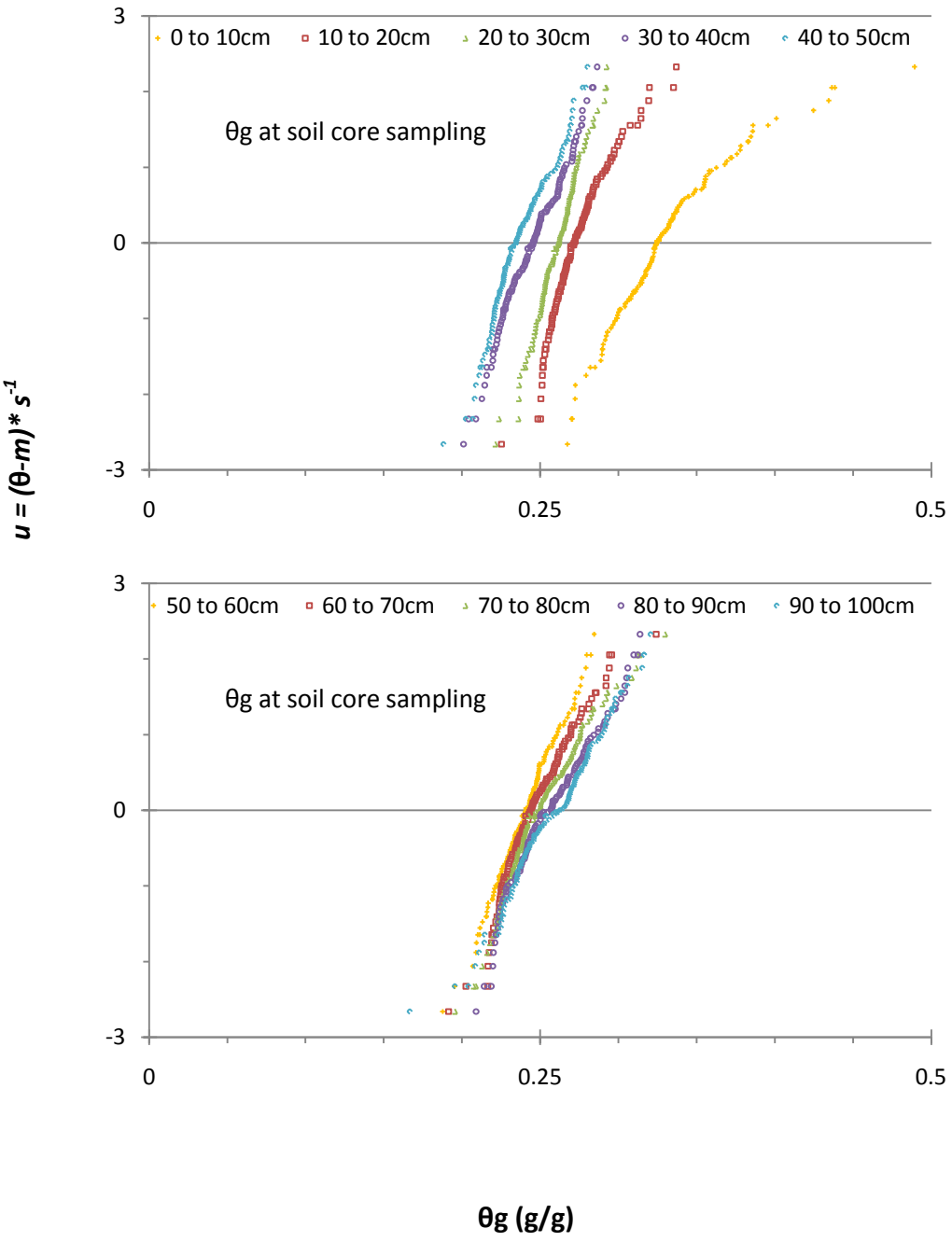

Appendix 4. Fractile diagram of soil water content measurements on main leaching study of 2008

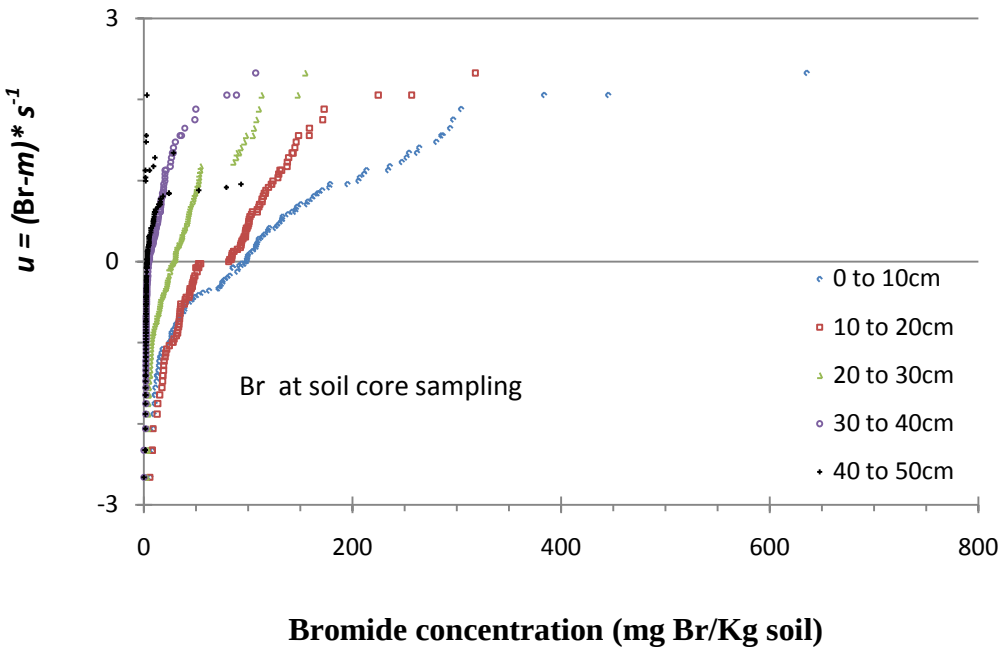

Appendix 5. Fractile diagram of Br concentrations on main leaching study of 2008.

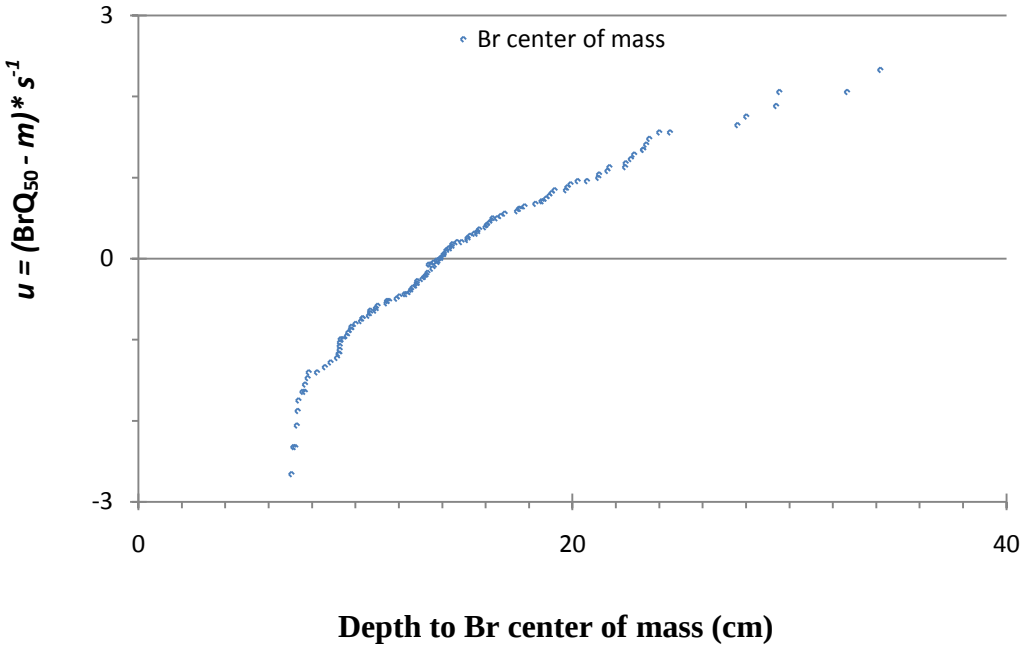

Appendix 6. Fractile diagram of the Br center of mass calculated for samples taken on Oct-31-08 for the main leaching study.

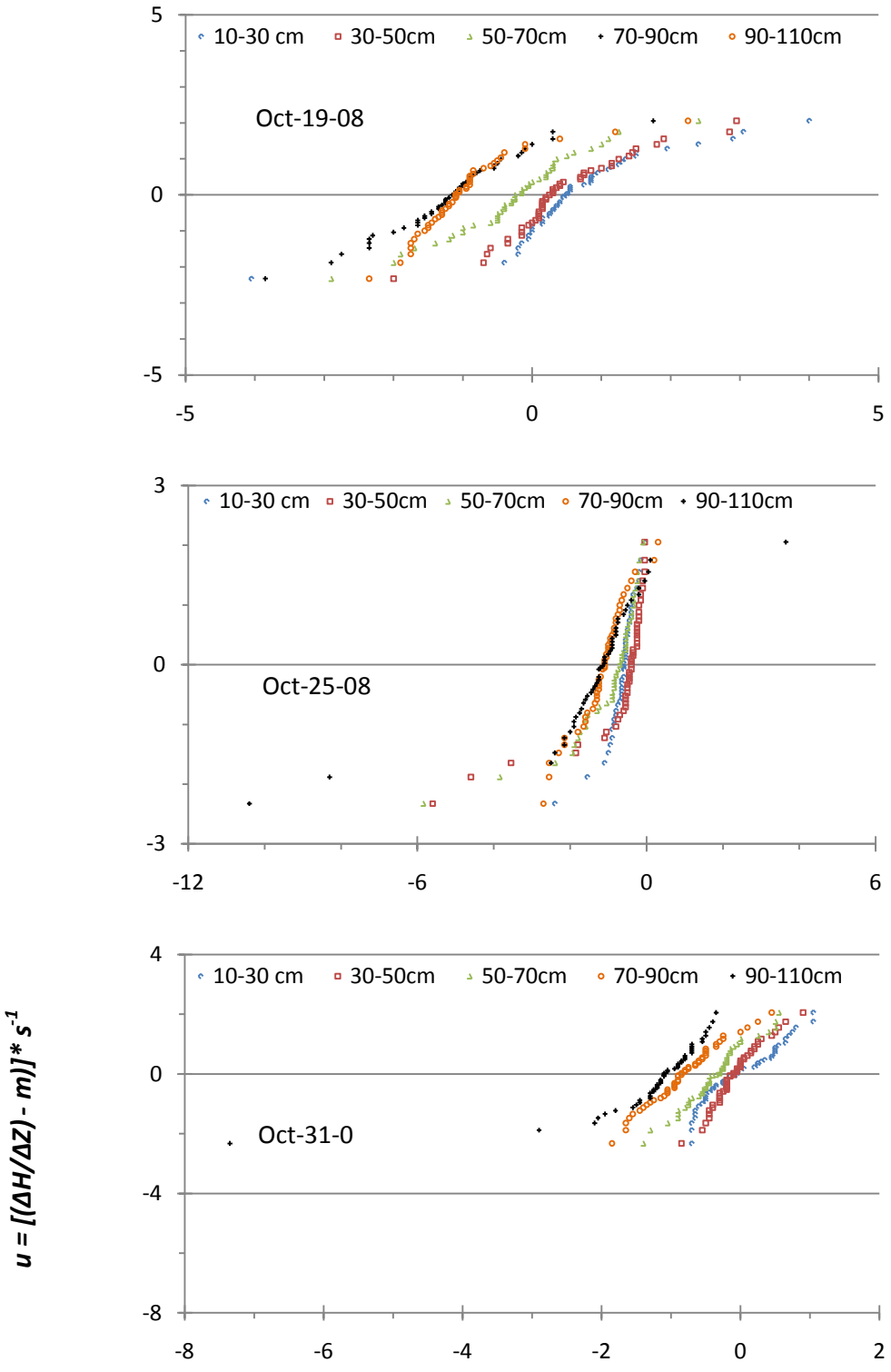

Appendix 7. Fractile diagram for hydraulic gradients at key moments during the main leaching study of 2008.

Appendix 8. Time variable boundary conditions for plots 1-4.

Plot 1

Date	**Time**	**Fluxtop**	**cTop**
M/D/Y hour	(days)	(cm)	(mmol/cm^3)
10/19/08 10:00	0		
10/24/08 8:40	4.94444	0	0
10/24/08 17:00	5.29167	-4.38624	0
10/30/08 11:00	11.0417	0	0
10/30/08 11:04	11.0444	-38.52	0.33617
10/30/08 13:15	11.1354	0	0
10/30/08 14:22	11.1822	-96	0
10/31/08 6:00	11.8333	0	0
10/31/2008 10:00	12	0	0

Plot 2

10/19/08 10:00	0		
10/24/08 8:40	4.94444	0	0
10/24/2008 11:59	5.08264	-4.38624	0
10/24/2008 12:00	5.08333	0	0
10/24/2008 12:04	5.08611	-38.52	0.33617
10/24/2008 12:05	5.08681	0	0
10/24/08 17:00	5.29167	-4.38624	0
10/30/08 13:15	11.1354	0	0
10/30/08 14:22	11.1822	-96	0

Plot 3			
10/19/08 10:00	0		
10/21/2008 12:00	2.08333	0	0
10/21/2008 12:04	2.08611	-38.52	0.33617
10/24/2008 8:40	4.94444	0	0
10/24/2008 17:00	5.29167	-4.386	0
10/30/2008 13:15	11.1354	0	0
10/30/2008 14:22	11.1822	-96	0
10/31/2008 6:00	11.8333	0	0
10/31/2008 10:00	12	0	0
Plot 4			
Oct/19/08 10:00	0		
10/24/2008 8:40	4.944444	0	0
10/24/2008 17:00	5.291667	-4.38634	0
10/30/2008 8:00	10.91667	0	0
10/30/2008 8:04	10.91944	-38.52	0.33617
10/30/2008 13:15	11.13542	0	0
10/30/2008 14:22	11.1822	-96	0
10/31/2008 6:00	11.83333	0	0
10/31/2008 10:00	12	0	0

Appendix 9. Time variable boundary conditions for Plots 5 and 6.

Plot 5 Date	**Time, day**	**Fluxtop, cm/ day**	**cTop, mmol**	**Plot 6 Date**	**Time, day**	**Fluxtop, cm/day**	**cTop, mmol**
10/19/08 10:00				10/19/08 10:00			
10/23/2008 12:00	4.083333	0	0	10/22/08 13:00	3.125	0	0
10/23/2008 12:04	4.086111	-38.52	0.33617	10/22/08 13:04	3.127778	-38.52	0.33617
10/23/2008 13:00	4.125	0	0	10/23/08 13:00	4.125	0	0
10/23/2008 13:05	4.128472	-48	0	10/23/08 13:05	4.128472	-48	0
10/23/2008 14:00	4.166667	0	0	10/23/08 14:00	4.166667	0	0
10/23/2008 14:05	4.170139	-48	0	10/23/08 14:05	4.170139	-48	0
10/23/2008 15:00	4.208333	0	0	10/23/08 15:00	4.208333	0	0
10/23/2008 15:05	4.211806	-48	0	10/23/08 15:05	4.211806	-48	0
10/23/2008 16:00	4.25	0	0	10/23/2008 16:00	4.25	0	0
10/23/2008 16:05	4.253472	-48	0	10/23/2008 16:05	4.253472	-48	0
10/23/2008 17:00	4.291667	0	0	10/23/2008 17:00	4.291667	0	0
10/23/2008 17:05	4.295139	-48	0	10/23/2008 17:05	4.295139	-48	0
10/23/2008 18:00	4.333334	0	0	10/23/2008 18:00	4.333334	0	0
10/23/2008 18:05	4.336806	-48	0	10/23/2008 18:05	4.336806	-48	0
10/23/2008 19:00	4.375	0	0	10/23/2008 19:00	4.375	0	0
10/23/2008 19:05	4.378472	-48	0	10/23/2008 19:05	4.378472	-48	0
10/23/2008 20:00	4.416667	0	0	10/23/2008 20:00	4.416667	0	0
10/23/2008 20:05	4.420139	-48	0	10/23/2008 20:05	4.420139	-48	0
10/23/2008 21:00	4.458334	0	0	10/23/2008 21:00	4.458334	0	0
10/23/2008 21:05	4.461806	-48	0	10/23/2008 21:05	4.461806	-48	0
10/23/2008 22:00	4.5	0	0	10/23/2008 22:00	4.5	0	0
10/23/2008 22:05	4.503472	-48	0	10/23/2008 22:05	4.503472	-48	0
10/23/2008 23:00	4.541667	0	0	10/23/2008 23:00	4.541667	0	0
10/23/2008 23:05	4.545139	-48	0	10/23/2008 23:05	4.545139	-48	0
10/24/2008 0:00	4.583334	0	0	10/24/2008 0:00	4.583334	0	0
10/24/2008 0:05	4.586806	-48	0	10/24/2008 0:05	4.586806	-48	0
10/24/2008 1:00	4.625001	0	0	10/24/2008 1:00	4.625001	0	0
10/24/2008 1:05	4.628472	-48	0	10/24/2008 1:05	4.628472	-48	0
10/24/2008 2:00	4.666667	0	0	10/24/2008 2:00	4.666667	0	0
10/24/2008 2:05	4.670139	-48	0	10/24/2008 2:05	4.670139	-48	0
10/24/2008 3:00	4.708334	0	0	10/24/2008 3:00	4.708334	0	0
10/24/2008 3:05	4.711806	-48	0	10/24/2008 3:05	4.711806	-48	0
10/24/2008 4:00	4.750001	0	0	10/24/08 4:00	4.750001	0	0
10/24/2008 4:05	4.753472	-48	0	10/24/08 4:05	4.753472	-48	0
10/24/2008 5:00	4.791668	0	0	10/24/08 5:00	4.791668	0	0
10/24/2008 5:05	4.795139	-48	0	10/24/08 5:05	4.795139	-48	0
10/24/2008 6:00	4.833334	0	0	10/24/08 6:00	4.833334	0	0
10/24/2008 6:05	4.836806	-48	0	10/24/08 6:05	4.836806	-48	0
10/24/2008 7:00	4.875001	0	0	10/24/08 7:00	4.875001	0	0
10/24/2008 7:05	4.878472	-48	0	10/24/08 7:05	4.878472	-48	0
10/24/2008 8:00	4.916668	0	0	10/24/08 8:00	4.916668	0	0
10/24/2008 8:05	4.920139	-48	0	10/24/08 8:05	4.920139	-48	0
10/24/2008 8:40	4.944444	0	0	10/24/08 8:40	4.944444	0	0
10/24/2008 9:00	4.958334	-4.38364	0	10/24/08 9:00	4.958334	-4.38364	0
10/24/2008 9:05	4.961806	-52.383648	0	10/24/08 9:05	4.961806	-52.3836	0
10/24/2008 10:00	5.000001	-4.38364	0	10/24/08 10:00	5.000001	-4.38364	0
10/24/2008 10:05	5.003472	-52.383648	0	10/24/08 10:05	5.003472	-52.3836	0
10/24/2008 11:00	5.041668	-4.38364	0	10/24/08 11:00	5.041668	-4.38364	0
10/24/2008 11:05	5.045139	-52.383648	0	10/24/08 11:05	5.045139	-52.3836	0
10/24/2008 12:00	5.083333	-4.38364	0	10/24/08 12:00	5.083333	-4.38364	0
10/24/2008 12:05	5.086806	-52.383648	0	10/24/08 12:05	5.086806	-52.3836	0
10/24/2008 17:00	5.291667	-4.38364	0	10/24/08 17:00	5.291667	-4.38364	0
10/31/2008 6:00	11.83333	0	0	10/31/08 6:00	11.83333	0	0
10/31/2008 10:00	12	0	0	10/31/2008 10:00	12	0	0

Appendix 10. Time variable boundary conditions for plots 7 and 8.

Plot 7 Date	Time	Fluxtop	cTop	Plot 8 Date	Time	Fluxtop	cTop
10/19/08 10:00				10/19/08 10:00			
10/19/08 13:00	0.125	0	0	10/23/08 9:08	3.963888889	0	0
10/19/08 13:04	0.127778	-38.52	0.33617	10/23/08 9:12	3.966666667	-38.52	0.33617
10/23/08 13:00	4.125	0	0	10/23/08 13:00	4.125	0	0
10/23/08 13:05	4.128472	-48	0	10/23/08 13:05	4.128472222	-48	0
10/23/08 14:00	4.166667	0	0	10/23/08 14:00	4.166666667	0	0
10/23/08 14:05	4.170139	-48	0	10/23/08 14:05	4.170138889	-48	0
10/23/08 15:00	4.208333	0	0	10/23/08 15:00	4.208333333	0	0
10/23/08 15:05	4.211806	-48	0	10/23/08 15:05	4.211805556	-48	0
10/23/2008 16:00	4.25	0	0	10/23/2008 16:00	4.250000116	0	0
10/23/2008 16:05	4.253472	-48	0	10/23/2008 16:05	4.253472222	-48	0
10/23/2008 17:00	4.291667	0	0	10/23/2008 17:00	4.29166684	0	0
10/23/2008 17:05	4.295139	-48	0	10/23/2008 17:05	4.295138889	-48	0
10/23/2008 18:00	4.333334	0	0	10/23/2008 18:00	4.333333565	0	0
10/23/2008 18:05	4.336806	-48	0	10/23/2008 18:05	4.336805556	-48	0
10/23/2008 19:00	4.375	0	0	10/23/2008 19:00	4.375000289	0	0
10/23/2008 19:05	4.378472	-48	0	10/23/2008 19:05	4.378472222	-48	0
10/23/2008 20:00	4.416667	0	0	10/23/2008 20:00	4.416667014	0	0
10/23/2008 20:05	4.420139	-48	0	10/23/2008 20:05	4.420138889	-48	0
10/23/2008 21:00	4.458334	0	0	10/23/2008 21:00	4.458333738	0	0
10/23/2008 21:05	4.461806	-48	0	10/23/2008 21:05	4.461805556	-48	0
10/23/2008 22:00	4.5	0	0	10/23/2008 22:00	4.500000463	0	0
10/23/2008 22:05	4.503472	-48	0	10/23/2008 22:05	4.503472222	-48	0
10/23/2008 23:00	4.541667	0	0	10/23/2008 23:00	4.541667187	0	0
10/23/2008 23:05	4.545139	-48	0	10/23/2008 23:05	4.545138889	-48	0
10/24/2008 0:00	4.583334	0	0	10/24/2008 0:00	4.583333912	0	0
10/24/2008 0:05	4.586806	-48	0	10/24/2008 0:05	4.586805556	-48	0
10/24/2008 1:00	4.625001	0	0	10/24/2008 1:00	4.625000637	0	0
10/24/2008 1:05	4.628472	-48	0	10/24/2008 1:05	4.628472222	-48	0
10/24/2008 2:00	4.666667	0	0	10/24/2008 2:00	4.666667361	0	0
10/24/2008 2:05	4.670139	-48	0	10/24/2008 2:05	4.670138889	-48	0
10/24/2008 3:00	4.708334	0	0	10/24/2008 3:00	4.708334086	0	0
10/24/2008 3:05	4.711806	-48	0	10/24/2008 3:05	4.711805556	-48	0
10/24/08 4:00	4.750001	0	0	10/24/08 4:00	4.75000081	0	0
10/24/08 4:05	4.753472	-48	0	10/24/08 4:05	4.753472222	-48	0
10/24/08 5:00	4.791668	0	0	10/24/08 5:00	4.791667535	0	0
10/24/08 5:05	4.795139	-48	0	10/24/08 5:05	4.795138889	-48	0
10/24/08 6:00	4.833334	0	0	10/24/08 6:00	4.833334259	0	0
10/24/08 6:05	4.836806	-48	0	10/24/08 6:05	4.836805556	-48	0
10/24/08 7:00	4.875001	0	0	10/24/08 7:00	4.875000984	0	0
10/24/08 7:05	4.878472	-48	0	10/24/08 7:05	4.878472222	-48	0
10/24/08 8:00	4.916668	0	0	10/24/08 8:00	4.916667708	0	0
10/24/08 8:05	4.920139	-48	0	10/24/08 8:05	4.920138889	-48	0
10/24/08 8:40	4.944444	0	0	10/24/08 8:40	4.944444444	0	0
10/24/08 9:00	4.958334	-4.38364	0	10/24/08 9:00	4.958334433	-4.38364	0
10/24/08 9:05	4.961806	-52.3836	0	10/24/08 9:05	4.961805556	-52.3836	0
10/24/08 10:00	5.000001	-4.38364	0	10/24/08 10:00	5.000001157	-4.38364	0
10/24/08 10:05	5.003472	-52.3836	0	10/24/08 10:05	5.003472222	-52.3836	0
10/24/08 11:00	5.041668	-4.38364	0	10/24/08 11:00	5.041667882	-4.38364	0
10/24/08 11:05	5.045139	-52.3836	0	10/24/08 11:05	5.045138889	-52.3836	0
10/24/08 12:00	5.083333	-4.38364	0	10/24/08 12:00	5.083333333	-4.38364	0
10/24/08 12:05	5.086806	-52.3836	0	10/24/08 12:05	5.086805556	-52.3836	0
10/24/08 17:00	5.291667	-4.38364	0	10/24/08 17:00	5.291666667	-4.38364	0
10/31/08 6:00	11.83333	0	0	10/31/08 6:00	11.83333333	0	0
10/31/08 10:00	12	0	0	10/31/08 10:00	12	0	0

Appendix 11. Time variable boundary conditions for plots 9 and 10

Plot 9 Date	Time	Fluxtop	cTop	Plot 10 Date	Time	Fluxtop	cTop
10/19/08 10:00				10/19/08 10:00			
10/23/08 11:30	4.0625	0	0	10/22/2008 12:30	3.104166667	0	0
10/23/08 11:34	4.065277778	-38.52	0.33617	10/22/2008 12:34	3.106944444	-38.52	0.33617
10/23/08 12:30	4.104166667	0	0	10/23/08 12:30	4.104166667	0	0
10/23/08 12:35	4.107638889	-24	0	10/23/08 12:35	4.107638889	-24	0
10/23/08 13:30	4.145833333	0	0	10/23/08 13:30	4.145833333	0	0
10/23/08 13:35	4.149305555	-24	0	10/23/08 13:35	4.149305555	-24	0
10/23/08 14:30	4.187499999	0	0	10/23/08 14:30	4.187499999	0	0
10/23/08 14:35	4.190972221	-24	0	10/23/08 14:35	4.190972221	-24	0
10/23/08 15:30	4.229166665	0	0	10/23/08 15:30	4.229166665	0	0
10/23/08 15:35	4.232638887	-24	0	10/23/08 15:35	4.232638887	-24	0
10/23/08 16:30	4.270833331	0	0	10/23/08 16:30	4.270833331	0	0
10/23/08 16:35	4.274305553	-24	0	10/23/08 16:35	4.274305553	-24	0
10/23/08 17:30	4.312499997	0	0	10/23/08 17:30	4.312499997	0	0
10/23/08 17:35	4.315972219	-24	0	10/23/08 17:35	4.315972219	-24	0
10/23/08 18:30	4.354166663	0	0	10/23/08 18:30	4.354166663	0	0
10/23/08 18:35	4.357638885	-24	0	10/23/08 18:35	4.357638885	-24	0
10/23/08 19:30	4.395833329	0	0	10/23/08 19:30	4.395833329	0	0
10/23/08 19:35	4.399305551	-24	0	10/23/08 19:35	4.399305551	-24	0
10/23/08 20:30	4.437499995	0	0	10/23/08 20:30	4.437499995	0	0
10/23/08 20:35	4.440972217	-24	0	10/23/08 20:35	4.440972217	-24	0
10/23/08 21:30	4.479166661	0	0	10/23/08 21:30	4.479166661	0	0
10/23/08 21:35	4.482638883	-24	0	10/23/08 21:35	4.482638883	-24	0
10/23/08 22:30	4.520833327	0	0	10/23/08 22:30	4.520833327	0	0
10/23/08 22:35	4.524305549	-24	0	10/23/08 22:35	4.524305549	-24	0
10/23/08 23:30	4.562499993	0	0	10/23/08 23:30	4.562499993	0	0
10/23/08 23:35	4.565972215	-24	0	10/23/08 23:35	4.565972215	-24	0
10/24/08 0:30	4.604166659	0	0	10/24/08 0:30	4.604166659	0	0
10/24/08 0:35	4.607638881	-24	0	10/24/08 0:35	4.607638881	-24	0
10/24/08 1:30	4.645833325	0	0	10/24/08 1:30	4.645833325	0	0
10/24/08 1:35	4.649305547	-24	0	10/24/08 1:35	4.649305547	-24	0
10/24/08 2:30	4.687499991	0	0	10/24/08 2:30	4.687499991	0	0
10/24/08 2:35	4.690972213	-24	0	10/24/08 2:35	4.690972213	-24	0
10/24/08 3:30	4.729166657	0	0	10/24/08 3:30	4.729166657	0	0
10/24/08 3:35	4.732638879	-24	0	10/24/08 3:35	4.732638879	-24	0
10/24/08 4:30	4.770833323	0	0	10/24/08 4:30	4.770833323	0	0
10/24/08 4:35	4.774305545	-24	0	10/24/08 4:35	4.774305545	-24	0
10/24/08 5:30	4.812499989	0	0	10/24/08 5:30	4.812499989	0	0
10/24/08 5:35	4.815972211	-24	0	10/24/08 5:35	4.815972211	-24	0
10/24/08 6:30	4.854166655	0	0	10/24/08 6:30	4.854166655	0	0
10/24/08 6:35	4.857638877	-24	0	10/24/08 6:35	4.857638877	-24	0
10/24/08 7:30	4.895833321	0	0	10/24/08 7:30	4.895833321	0	0
10/24/08 7:35	4.899305543	-24	0	10/24/08 7:35	4.899305543	-24	0
10/24/08 8:30	4.937499987	0	0	10/24/08 8:30	4.937499987	0	0
10/24/08 8:35	4.940972209	-24	0	10/24/08 8:35	4.940972209	-24	0
10/24/08 8:40	4.944444444	0	0	10/24/08 8:40	4.944444444	0	0
10/24/08 9:30	4.979166667	-4.38364	0	10/24/08 9:30	4.979166667	-4.38364	0
10/24/08 9:35	4.982638889	-28.38364	0	10/24/08 9:35	4.982638889	-28.38364	0
10/24/08 10:30	5.020833333	-4.38364	0	10/24/08 10:30	5.020833333	-4.38364	0
10/24/08 10:35	5.024305555	-28.38364	0	10/24/08 10:35	5.024305555	-28.38364	0
10/24/08 11:30	5.062499999	-4.38364	0	10/24/08 11:30	5.062499999	-4.38364	0
10/24/08 11:35	5.065972221	-28.38364	0	10/24/08 11:35	5.065972221	-28.38364	0
10/24/08 17:00	5.291666667	-4.38364	0	10/24/08 17:00	5.291666667	-4.38364	0
10/31/08 6:00	11.83333333	0	0	10/31/08 6:00	11.83333333	0	0
10/31/08 10:00	12	0	0	10/31/08 10:00	12	0	0

Appendix 12. Time variable boundary conditions for plots 11 and 12.

Plot 11 Date	Time	Fluxtop	cTop	Plot 12 Date	Time	Fluxtop	cTop
10/19/08 10:00				10/19/08 10:00			
10/19/08 12:30	0.10416666	0	0	10/23/08 8:58	3.95694	0	0
10/19/08 12:34	0.10694444	-38.52	0.33617	10/23/08 9:02	3.95972	-38.52	0.33617
10/23/08 12:30	4.10416666	0	0	10/23/08 12:30	4.10416	0	0
10/23/08 12:35	4.10763888	-24	0	10/23/08 12:35	4.10763	-24	0
10/23/08 13:30	4.14583333	0	0	10/23/08 13:30	4.14583	0	0
10/23/08 13:35	4.14930555	-24	0	10/23/08 13:35	4.14930	-24	0
10/23/08 14:30	4.18749999	0	0	10/23/08 14:30	4.18749	0	0
10/23/08 14:35	4.19097222	-24	0	10/23/08 14:35	4.19097	-24	0
10/23/08 15:30	4.22916666	0	0	10/23/08 15:30	4.22916	0	0
10/23/08 15:35	4.23263888	-24	0	10/23/08 15:35	4.23263	-24	0
10/23/08 16:30	4.27083333	0	0	10/23/08 16:30	4.27083	0	0
10/23/08 16:35	4.27430555	-24	0	10/23/08 16:35	4.27430	-24	0
10/23/08 17:30	4.31249999	0	0	10/23/08 17:30	4.31249	0	0
10/23/08 17:35	4.31597221	-24	0	10/23/08 17:35	4.31597	-24	0
10/23/08 18:30	4.35416666	0	0	10/23/08 18:30	4.35416	0	0
10/23/08 18:35	4.35763888	-24	0	10/23/08 18:35	4.35763	-24	0
10/23/08 19:30	4.39583332	0	0	10/23/08 19:30	4.39583	0	0
10/23/08 19:35	4.39930555	-24	0	10/23/08 19:35	4.39930	-24	0
10/23/08 20:30	4.43749999	0	0	10/23/08 20:30	4.43749	0	0
10/23/08 20:35	4.44097221	-24	0	10/23/08 20:35	4.44097	-24	0
10/23/08 21:30	4.47916666	0	0	10/23/08 21:30	4.47916	0	0
10/23/08 21:35	4.48263888	-24	0	10/23/08 21:35	4.48263	-24	0
10/23/08 22:30	4.52083332	0	0	10/23/08 22:30	4.52083	0	0
10/23/08 22:35	4.52430554	-24	0	10/23/08 22:35	4.52430	-24	0
10/23/08 23:30	4.56249999	0	0	10/23/08 23:30	4.56249	0	0
10/23/08 23:35	4.56597221	-24	0	10/23/08 23:35	4.56597	-24	0
10/24/08 0:30	4.60416665	0	0	10/24/08 0:30	4.60416	0	0
10/24/08 0:35	4.60763888	-24	0	10/24/08 0:35	4.60763	-24	0
10/24/08 1:30	4.64583332	0	0	10/24/08 1:30	4.64583	0	0
10/24/08 1:35	4.64930554	-24	0	10/24/08 1:35	4.64930	-24	0
10/24/08 2:30	4.68749999	0	0	10/24/08 2:30	4.68749	0	0
10/24/08 2:35	4.69097221	-24	0	10/24/08 2:35	4.69097	-24	0
10/24/08 3:30	4.72916665	0	0	10/24/08 3:30	4.72916	0	0
10/24/08 3:35	4.73263887	-24	0	10/24/08 3:35	4.73263	-24	0
10/24/08 4:30	4.77083332	0	0	10/24/08 4:30	4.77083	0	0
10/24/08 4:35	4.77430554	-24	0	10/24/08 4:35	4.77430	-24	0
10/24/08 5:30	4.81249998	0	0	10/24/08 5:30	4.81249	0	0
10/24/08 5:35	4.81597221	-24	0	10/24/08 5:35	4.81597	-24	0
10/24/08 6:30	4.85416665	0	0	10/24/08 6:30	4.85416	0	0
10/24/08 6:35	4.85763887	-24	0	10/24/08 6:35	4.85763	-24	0
10/24/08 7:30	4.89583332	0	0	10/24/08 7:30	4.89583	0	0
10/24/08 7:35	4.89930554	-24	0	10/24/08 7:35	4.89930	-24	0
10/24/08 8:30	4.93749998	0	0	10/24/08 8:30	4.93749	0	0
10/24/08 8:35	4.94097220	-24	0	10/24/08 8:35	4.94097	-24	0
10/24/08 8:40	4.94444444	0	0	10/24/08 8:40	4.94444	0	0
10/24/08 9:30	4.97916666	-4.38364	0	10/24/08 9:30	4.97916	-4.38364	0
10/24/08 9:35	4.98263888	-28.38364	0	10/24/08 9:35	4.98263	-28.38364	0
10/24/08 10:30	5.02083333	-4.38364	0	10/24/08 10:30	5.02083	-4.38364	0
10/24/08 10:35	5.02430555	-28.38364	0	10/24/08 10:35	5.02430	-28.38364	0
10/24/08 11:30	5.06249999	-4.38364	0	10/24/08 11:30	5.06249	-4.38364	0
10/24/08 11:35	5.06597222	-28.38364	0	10/24/08 11:35	5.06597	-28.38364	0
10/24/08 17:00	5.29166666	-4.38364	0	10/24/08 17:00	5.29166	-4.38364	0
10/31/08 6:00	11.8333333	0	0	10/31/08 6:00	11.8333	0	0
10/31/08 10:00	12	0	0	10/31/08 10:00	12	0	0

Appendix 13. Time variable boundary conditions for plots 13-16

Plot 13

Date	**Time**	**Fluxtop**	**cTop**
M/D/Y hour	(days)	(cm)	(mmol/cm^3)
10/19/08 10:00			
10/24/08 8:40	4.944444444	0	0
10/24/08 17:00	5.291666667	-4.38364	0
10/30/08 15:00	11.20833333	0	0
10/30/08 15:04	11.21111111	-38.52	0.33617
10/30/08 16:00	11.25	0	0
10/30/08 16:53	11.28691667	-48	0
10/31/08 6:00	11.83333333	0	0
10/31/08 10:00	12	0	0

Plot 14

10/19/08 10:00			
10/24/08 8:40	4.944444444	0	0
10/24/08 16:00	5.25	-4.38364	0
10/24/08 16:04	5.252777778	-38.52	0.33617
10/24/08 17:04	5.294444444	-4.38364	0
10/30/08 16:00	11.25	0	0
10/30/08 16:53	11.28691667	-48	0
10/31/08 6:00	11.83333333	0	0
10/31/08 10:00	12	0	0

Plot 15			
10/19/08 10:00			
10/21/08 16:00	2.25	0	0
10/21/08 16:04	2.252777778	-38.52	0.33617
10/24/08 8:40	4.944444444	0	0
10/24/08 17:00	5.291666667	-4.38364	0
10/30/08 16:00	11.25	0	0
10/30/08 16:53	11.28691667	-48	0
10/31/08 6:00	11.83333333	0	0
10/31/08 10:00	12	0	0
Plot 16			
10/19/08 10:00			
10/24/08 8:40	4.944444444	0	0
10/24/08 17:00	5.291666667	-4.38364	0
10/30/08 12:00	11.08333333	0	0
10/30/08 12:04	11.08611111	-38.52	0.33617
10/30/08 16:00	11.25	0	0
10/30/08 16:53	11.28691667	-48	0
10/31/08 6:00	11.83333333	0	0
10/31/08 10:00	12	0	0

Appendix 14. Time variable boundary conditions for plots 17-20.

Plot 17

Date	**Time**	**Fluxtop**	**cTop**
M/D/Y hour	(days)	(cm)	(mmol/cm^3)
10/19/08 10:00			
10/24/2008 8:40	4.944444444	0	0
10/24/2008 13:00	5.125	-4.38364	0
10/24/2008 13:04	5.127777778	-38.52	0.33617
10/24/2008 14:00	5.166666667	-4.38364	0
10/24/2008 15:00	5.208333333	-100.38364	0
10/24/2008 17:04	5.294444444	-4.38364	0
10/31/08 12:00	12.08333333	0	0
10/31/2008 18:00	12.33333333	0	0

Plot 18

10/19/08 10:00			
10/23/2008 14:00	4.166666667	0	0
10/23/2008 14:04	4.169444444	-38.52	0.33617
10/24/2008 8:40	4.944444444	0	0
10/24/2008 14:00	5.166666667	-4.38364	0
10/24/2008 15:00	5.208333333	-100.38364	0
10/24/2008 17:00	5.291666667	-4.38364	0
10/31/08 12:00	12.08333333	0	0
10/31/2008 18:00	12.33333333	0	0

Plot 19			
10/19/08 10:00			
10/20/2008 19:00	1.375	0	0
10/20/2008 19:04	1.377777778	-38.52	0.33617
10/24/2008 8:40	4.944444444	0	0
10/24/2008 14:00	5.166666667	-4.38364	0
10/24/2008 15:00	5.208333333	-100.38364	0
10/24/2008 17:00	5.291666667	-4.38364	0
10/31/08 12:00	12.08333333	0	0
10/31/2008 18:00	12.33333333	0	0
Plot 20			
10/19/08 10:00			
10/24/2008 8:40	4.944444444	0	0
10/24/2008 10:00	5	-4.38364	0
10/24/2008 10:04	5.002777778	-38.52	0.33617
10/24/2008 14:00	5.166666667	-4.38364	0
10/24/2008 15:00	5.208333333	-100.38364	0
10/24/2008 17:04	5.294444444	-4.38364	0
10/31/08 12:00	12.08333333	0	0
10/31/2008 18:00	12.33333333	0	0

Appendix 15. Time variable boundary conditions for plots 21 and 22.

Plot 21 Date	Time	Fluxtop	cTop	Plot 22 Date	Time	Fluxtop	cTop
10/19/08 10:00				10/19/08 10:00			
10/23/08 11:45	4.072916667	0	0	10/22/08 12:45	3.114583333	0	0
10/23/08 11:49	4.075694444	-38.52	0.33617	10/22/08 12:49	3.117361111	-38.52	0.33617
10/23/08 12:45	4.114583333	0	0	10/23/08 12:45	4.114583333	0	0
10/23/08 12:50	4.118055556	-48	0	10/23/08 12:50	4.118055556	-48	0
10/23/08 13:45	4.15625	0	0	10/23/08 13:45	4.15625	0	0
10/23/08 13:50	4.159722222	-48	0	10/23/08 13:50	4.159722222	-48	0
10/23/08 14:45	4.197916667	0	0	10/23/08 14:45	4.197916667	0	0
10/23/08 14:50	4.201388889	-48	0	10/23/08 14:50	4.201388889	-48	0
10/23/08 15:45	4.239583333	0	0	10/23/08 15:45	4.239583333	0	0
10/23/08 15:50	4.243055556	-48	0	10/23/08 15:50	4.243055556	-48	0
10/23/08 16:45	4.28125	0	0	10/23/08 16:45	4.28125	0	0
10/23/08 16:50	4.284722222	-48	0	10/23/08 16:50	4.284722222	-48	0
10/23/08 17:45	4.322916667	0	0	10/23/08 17:45	4.322916667	0	0
10/23/08 17:50	4.326388889	-48	0	10/23/08 17:50	4.326388889	-48	0
10/23/08 18:45	4.364583333	0	0	10/23/08 18:45	4.364583333	0	0
10/23/08 18:50	4.368055556	-48	0	10/23/08 18:50	4.368055556	-48	0
10/23/08 19:45	4.40625	0	0	10/23/08 19:45	4.40625	0	0
10/23/08 19:50	4.409722222	-48	0	10/23/08 19:50	4.409722222	-48	0
10/23/08 20:45	4.447916667	0	0	10/23/08 20:45	4.447916667	0	0
10/23/08 20:50	4.451388889	-48	0	10/23/08 20:50	4.451388889	-48	0
10/23/08 21:45	4.489583333	0	0	10/23/08 21:45	4.489583333	0	0
10/23/08 21:50	4.493055556	-48	0	10/23/08 21:50	4.493055556	-48	0
10/23/08 22:45	4.53125	0	0	10/23/08 22:45	4.53125	0	0
10/23/08 22:50	4.534722222	-48	0	10/23/08 22:50	4.534722222	-48	0
10/23/08 23:45	4.572916667	0	0	10/23/08 23:45	4.572916667	0	0
10/23/08 23:50	4.576388889	-48	0	10/23/08 23:50	4.576388889	-48	0
10/24/08 0:45	4.614583333	0	0	10/24/08 0:45	4.614583333	0	0
10/24/08 0:50	4.618055556	-48	0	10/24/08 0:50	4.618055556	-48	0
10/24/08 1:45	4.65625	0	0	10/24/08 1:45	4.65625	0	0
10/24/08 1:50	4.659722222	-48	0	10/24/08 1:50	4.659722222	-48	0
10/24/08 2:45	4.697916667	0	0	10/24/08 2:45	4.697916667	0	0
10/24/08 2:50	4.701388889	-48	0	10/24/08 2:50	4.701388889	-48	0
10/24/08 3:45	4.739583333	0	0	10/24/08 3:45	4.739583333	0	0
10/24/08 3:50	4.743055556	-48	0	10/24/08 3:50	4.743055556	-48	0
10/24/08 4:45	4.78125	0	0	10/24/08 4:45	4.78125	0	0
10/24/08 4:50	4.784722222	-48	0	10/24/08 4:50	4.784722222	-48	0
10/24/08 5:45	4.822916667	0	0	10/24/08 5:45	4.822916667	0	0
10/24/08 5:50	4.826388889	-48	0	10/24/08 5:50	4.826388889	-48	0
10/24/08 6:45	4.864583333	0	0	10/24/08 6:45	4.864583333	0	0
10/24/08 6:50	4.868055556	-48	0	10/24/08 6:50	4.868055556	-48	0
10/24/08 7:45	4.90625	0	0	10/24/08 7:45	4.90625	0	0
10/24/08 7:50	4.909722222	-48	0	10/24/08 7:50	4.909722222	-48	0
10/24/08 8:40	4.944444444	0	0	10/24/08 8:40	4.944444444	0	0
10/24/08 8:45	4.947916667	-4.38364	0	10/24/08 8:45	4.947916667	-4.38364	0
10/24/08 8:50	4.951388889	-52.38364	0	10/24/08 8:50	4.951388889	-52.38364	0
10/24/08 9:45	4.989583333	-4.38364	0	10/24/08 9:45	4.989583333	-4.38364	0
10/24/08 9:50	4.993055556	-52.38364	0	10/24/08 9:50	4.993055556	-52.38364	0
10/24/08 10:45	5.03125	-4.38364	0	10/24/08 10:45	5.03125	-4.38364	0
10/24/08 10:50	5.034722222	-52.38364	0	10/24/08 10:50	5.034722222	-52.38364	0
10/24/08 11:45	5.072916667	-4.38364	0	10/24/08 11:45	5.072916667	-4.38364	0
10/24/08 11:50	5.076388889	-52.38364	0	10/24/08 11:50	5.076388889	-52.38364	0
10/24/08 17:00	5.291666667	-4.38364	0	10/24/08 17:00	5.291666667	-4.38364	0
10/31/08 12:00	12.08333333	0	0	10/31/08 12:00	12.08333333	0	0
10/31/08 18:00	12.33333333	0	0	10/31/08 18:00	12.33333333	0	0

Appendix 16. Time variable boundary conditions for plots 23 and 24.

Plot 23 Date	Time	Fluxtop	cTop	Plot 24 Date	Time	Fluxtop	cTop
10/19/08 10:00				10/19/08 10:00			
10/19/08 12:45	0.114583333	0	0	10/23/08 9:03	3.960416667	0	0
10/19/08 12:49	0.117361111	-38.52	0.33617	10/23/08 9:07	3.963194444	-38.52	0.33617
10/23/08 12:45	4.114583333	0	0	10/23/08 12:45	4.114583333	0	0
10/23/08 12:50	4.118055556	-48	0	10/23/08 12:50	4.118055556	-48	0
10/23/08 13:45	4.15625	0	0	10/23/08 13:45	4.15625	0	0
10/23/08 13:50	4.159722222	-48	0	10/23/08 13:50	4.159722222	-48	0
10/23/08 14:45	4.197916667	0	0	10/23/08 14:45	4.197916667	0	0
10/23/08 14:50	4.201388889	-48	0	10/23/08 14:50	4.201388889	-48	0
10/23/08 15:45	4.239583333	0	0	10/23/08 15:45	4.239583333	0	0
10/23/08 15:50	4.243055556	-48	0	10/23/08 15:50	4.243055556	-48	0
10/23/08 16:45	4.28125	0	0	10/23/08 16:45	4.28125	0	0
10/23/08 16:50	4.284722222	-48	0	10/23/08 16:50	4.284722222	-48	0
10/23/08 17:45	4.322916667	0	0	10/23/08 17:45	4.322916667	0	0
10/23/08 17:50	4.326388889	-48	0	10/23/08 17:50	4.326388889	-48	0
10/23/08 18:45	4.364583333	0	0	10/23/08 18:45	4.364583333	0	0
10/23/08 18:50	4.368055556	-48	0	10/23/08 18:50	4.368055556	-48	0
10/23/08 19:45	4.40625	0	0	10/23/08 19:45	4.40625	0	0
10/23/08 19:50	4.409722222	-48	0	10/23/08 19:50	4.409722222	-48	0
10/23/08 20:45	4.447916667	0	0	10/23/08 20:45	4.447916667	0	0
10/23/08 20:50	4.451388889	-48	0	10/23/08 20:50	4.451388889	-48	0
10/23/08 21:45	4.489583333	0	0	10/23/08 21:45	4.489583333	0	0
10/23/08 21:50	4.493055556	-48	0	10/23/08 21:50	4.493055556	-48	0
10/23/08 22:45	4.53125	0	0	10/23/08 22:45	4.53125	0	0
10/23/08 22:50	4.534722222	-48	0	10/23/08 22:50	4.534722222	-48	0
10/23/08 23:45	4.572916667	0	0	10/23/08 23:45	4.572916667	0	0
10/23/08 23:50	4.576388889	-48	0	10/23/08 23:50	4.576388889	-48	0
10/24/08 0:45	4.614583333	0	0	10/24/08 0:45	4.614583333	0	0
10/24/08 0:50	4.618055556	-48	0	10/24/08 0:50	4.618055556	-48	0
10/24/08 1:45	4.65625	0	0	10/24/08 1:45	4.65625	0	0
10/24/08 1:50	4.659722222	-48	0	10/24/08 1:50	4.659722222	-48	0
10/24/08 2:45	4.697916667	0	0	10/24/08 2:45	4.697916667	0	0
10/24/08 2:50	4.701388889	-48	0	10/24/08 2:50	4.701388889	-48	0
10/24/08 3:45	4.739583333	0	0	10/24/08 3:45	4.739583333	0	0
10/24/08 3:50	4.743055556	-48	0	10/24/08 3:50	4.743055556	-48	0
10/24/08 4:45	4.78125	0	0	10/24/08 4:45	4.78125	0	0
10/24/08 4:50	4.784722222	-48	0	10/24/08 4:50	4.784722222	-48	0
10/24/08 5:45	4.822916667	0	0	10/24/08 5:45	4.822916667	0	0
10/24/08 5:50	4.826388889	-48	0	10/24/08 5:50	4.826388889	-48	0
10/24/08 6:45	4.864583333	0	0	10/24/08 6:45	4.864583333	0	0
10/24/08 6:50	4.868055556	-48	0	10/24/08 6:50	4.868055556	-48	0
10/24/08 7:45	4.90625	0	0	10/24/08 7:45	4.90625	0	0
10/24/08 7:50	4.909722222	-48	0	10/24/08 7:50	4.909722222	-48	0
10/24/08 8:40	4.944444444	0	0	10/24/08 8:40	4.944444444	0	0
10/24/08 8:45	4.947916667	-4.38364	0	10/24/08 8:45	4.947916667	-4.38364	0
10/24/08 8:50	4.951388889	-52.38364	0	10/24/08 8:50	4.951388889	-52.38364	0
10/24/08 9:45	4.989583333	-4.38364	0	10/24/08 9:45	4.989583333	-4.38364	0
10/24/08 9:50	4.993055556	-52.38364	0	10/24/08 9:50	4.993055556	-52.38364	0
10/24/08 10:45	5.03125	-4.38364	0	10/24/08 10:45	5.03125	-4.38364	0
10/24/08 10:50	5.034722222	-52.38364	0	10/24/08 10:50	5.034722222	-52.38364	0
10/24/08 11:45	5.072916667	-4.38364	0	10/24/08 11:45	5.072916667	-4.38364	0
10/24/08 11:50	5.076388889	-52.38364	0	10/24/08 11:50	5.076388889	-52.38364	0
10/24/08 17:00	5.291666667	-4.38364	0	10/24/08 17:00	5.291666667	-4.38364	0
10/31/08 12:00	12.08333333	0	0	10/31/08 12:00	12.08333333	0	0
10/31/08 18:00	12.33333333	0	0	10/31/08 18:00	12.33333333	0	0

Appendix 17. Time variable boundary conditions for plots 25 and 26.

Plot 25 Date	Time	Fluxtop	cTop	Plot 26 Date	Time	Fluxtop	cTop
10/19/08 10:00				10/19/08 10:00			
10/23/08 11:15	4.05208333	0	0	10/22/08 12:15	3.09375	0	0
10/23/08 11:19	4.05486111	-38.52	0.33617	10/22/08 12:19	3.09652	-38.52	0.33617
10/23/08 12:15	4.09375	0	0	10/23/08 12:15	4.09375	0	0
10/23/08 12:20	4.09722222	-24	0	10/23/08 12:20	4.09722	-24	0
10/23/08 13:15	4.13541666	0	0	10/23/08 13:15	4.13541	0	0
10/23/08 13:20	4.13888888	-24	0	10/23/08 13:20	4.13888	-24	0
10/23/08 14:15	4.17708333	0	0	10/23/08 14:15	4.17708	0	0
10/23/08 14:20	4.18055555	-24	0	10/23/08 14:20	4.18055	-24	0
10/23/08 15:15	4.21875	0	0	10/23/08 15:15	4.21875	0	0
10/23/08 15:20	4.22222222	-24	0	10/23/08 15:20	4.22222	-24	0
10/23/08 16:15	4.26041666	0	0	10/23/08 16:15	4.26041	0	0
10/23/08 16:20	4.26388888	-24	0	10/23/08 16:20	4.26388	-24	0
10/23/08 17:15	4.30208333	0	0	10/23/08 17:15	4.30208	0	0
10/23/08 17:20	4.30555555	-24	0	10/23/08 17:20	4.30555	-24	0
10/23/08 18:15	4.34375	0	0	10/23/08 18:15	4.34375	0	0
10/23/08 18:20	4.34722222	-24	0	10/23/08 18:20	4.34722	-24	0
10/23/08 19:15	4.38541666	0	0	10/23/08 19:15	4.38541	0	0
10/23/08 19:20	4.38888888	-24	0	10/23/08 19:20	4.38888	-24	0
10/23/08 20:15	4.42708333	0	0	10/23/08 20:15	4.42708	0	0
10/23/08 20:20	4.43055555	-24	0	10/23/08 20:20	4.43055	-24	0
10/23/08 21:15	4.46875	0	0	10/23/08 21:15	4.46875	0	0
10/23/08 21:20	4.47222222	-24	0	10/23/08 21:20	4.47222	-24	0
10/23/08 22:15	4.51041666	0	0	10/23/08 22:15	4.51041	0	0
10/23/08 22:20	4.51388888	-24	0	10/23/08 22:20	4.51388	-24	0
10/23/08 23:15	4.55208333	0	0	10/23/08 23:15	4.55208	0	0
10/23/08 23:20	4.55555555	-24	0	10/23/08 23:20	4.55555	-24	0
10/24/08 0:15	4.59375	0	0	10/24/08 0:15	4.59375	0	0
10/24/08 0:20	4.59722222	-24	0	10/24/08 0:20	4.59722	-24	0
10/24/08 1:15	4.63541666	0	0	10/24/08 1:15	4.63541	0	0
10/24/08 1:20	4.63888888	-24	0	10/24/08 1:20	4.63888	-24	0
10/24/08 2:15	4.67708333	0	0	10/24/08 2:15	4.67708	0	0
10/24/08 2:20	4.68055555	-24	0	10/24/08 2:20	4.68055	-24	0
10/24/08 3:15	4.71875	0	0	10/24/08 3:15	4.71875	0	0
10/24/08 3:20	4.72222222	-24	0	10/24/08 3:20	4.72222	-24	0
10/24/08 4:15	4.76041666	0	0	10/24/08 4:15	4.76041	0	0
10/24/08 4:20	4.76388888	-24	0	10/24/08 4:20	4.76388	-24	0
10/24/08 5:15	4.80208333	0	0	10/24/08 5:15	4.80208	0	0
10/24/08 5:20	4.80555555	-24	0	10/24/08 5:20	4.80555	-24	0
10/24/08 6:15	4.84375	0	0	10/24/08 6:15	4.84375	0	0
10/24/08 6:20	4.84722222	-24	0	10/24/08 6:20	4.84722	-24	0
10/24/08 7:15	4.88541666	0	0	10/24/08 7:15	4.88541	0	0
10/24/08 7:20	4.88888888	-24	0	10/24/08 7:20	4.88888	-24	0
10/24/08 8:15	4.92708333	0	0	10/24/08 8:15	4.92708	0	0
10/24/08 8:20	4.93055555	-24	0	10/24/08 8:20	4.93055	-24	0
10/24/08 8:40	4.94444444	0	0	10/24/08 8:40	4.94444	0	0
10/24/08 9:15	4.96875	-4.38364	0	10/24/08 9:15	4.96875	-4.38364	0
10/24/08 9:20	4.97222222	-28.38364	0	10/24/08 9:20	4.97222	-28.38364	0
10/24/08 10:15	5.01041666	-4.38364	0	10/24/08 10:15	5.01041	-4.38364	0
10/24/08 10:20	5.01388888	-28.38364	0	10/24/08 10:20	5.01388	-28.38364	0
10/24/08 11:15	5.05208333	-4.38364	0	10/24/08 11:15	5.05208	-4.38364	0
10/24/08 11:20	5.05555555	-28.38364	0	10/24/08 11:20	5.05555	-28.38364	0
10/24/08 17:00	5.29166666	-4.38364	0	10/24/08 17:00	5.29166	-4.38364	0
10/31/08 12:00	12.0833333	0	0	10/31/08 12:00	12.0833	0	0
10/31/08 18:00	12.3333333	0	0	10/31/08 18:00	12.3333	0	0

Appendix 18. Time variable boundary conditions for plots 27 and 28.

Plot 27 Date	Time	Fluxtop	cTop	Plot 28 Date	Time	Fluxtop	cTop
10/19/08 10:00				10/19/08 10:00			
10/19/08 12:15	0.09375	0	0	10/23/08 8:48	3.95	0	0
10/19/08 12:19	0.09652777	-38.52	0.33617	10/23/08 8:52	3.95277	-38.52	0.33617
10/23/08 12:15	4.09375	0	0	10/23/08 12:15	4.09375	0	0
10/23/08 12:20	4.09722222	-24	0	10/23/08 12:20	4.09722	-24	0
10/23/08 13:15	4.13541666	0	0	10/23/08 13:15	4.13541	0	0
10/23/08 13:20	4.13888888	-24	0	10/23/08 13:20	4.13888	-24	0
10/23/08 14:15	4.17708333	0	0	10/23/08 14:15	4.17708	0	0
10/23/08 14:20	4.18055555	-24	0	10/23/08 14:20	4.18055	-24	0
10/23/08 15:15	4.21875	0	0	10/23/08 15:15	4.21875	0	0
10/23/08 15:20	4.22222222	-24	0	10/23/08 15:20	4.22222	-24	0
10/23/08 16:15	4.26041666	0	0	10/23/08 16:15	4.26041	0	0
10/23/08 16:20	4.26388888	-24	0	10/23/08 16:20	4.26388	-24	0
10/23/08 17:15	4.30208333	0	0	10/23/08 17:15	4.30208	0	0
10/23/08 17:20	4.30555555	-24	0	10/23/08 17:20	4.30555	-24	0
10/23/08 18:15	4.34375	0	0	10/23/08 18:15	4.34375	0	0
10/23/08 18:20	4.34722222	-24	0	10/23/08 18:20	4.34722	-24	0
10/23/08 19:15	4.38541666	0	0	10/23/08 19:15	4.38541	0	0
10/23/08 19:20	4.38888888	-24	0	10/23/08 19:20	4.38888	-24	0
10/23/08 20:15	4.42708333	0	0	10/23/08 20:15	4.42708	0	0
10/23/08 20:20	4.43055555	-24	0	10/23/08 20:20	4.43055	-24	0
10/23/08 21:15	4.46875	0	0	10/23/08 21:15	4.46875	0	0
10/23/08 21:20	4.47222222	-24	0	10/23/08 21:20	4.47222	-24	0
10/23/08 22:15	4.51041666	0	0	10/23/08 22:15	4.51041	0	0
10/23/08 22:20	4.51388888	-24	0	10/23/08 22:20	4.51388	-24	0
10/23/08 23:15	4.55208333	0	0	10/23/08 23:15	4.55208	0	0
10/23/08 23:20	4.55555555	-24	0	10/23/08 23:20	4.55555	-24	0
10/24/08 0:15	4.59375	0	0	10/24/08 0:15	4.59375	0	0
10/24/08 0:20	4.59722222	-24	0	10/24/08 0:20	4.59722	-24	0
10/24/08 1:15	4.63541666	0	0	10/24/08 1:15	4.63541	0	0
10/24/08 1:20	4.63888888	-24	0	10/24/08 1:20	4.63888	-24	0
10/24/08 2:15	4.67708333	0	0	10/24/08 2:15	4.67708	0	0
10/24/08 2:20	4.68055555	-24	0	10/24/08 2:20	4.68055	-24	0
10/24/08 3:15	4.71875	0	0	10/24/08 3:15	4.71875	0	0
10/24/08 3:20	4.72222222	-24	0	10/24/08 3:20	4.72222	-24	0
10/24/08 4:15	4.76041666	0	0	10/24/08 4:15	4.76041	0	0
10/24/08 4:20	4.76388888	-24	0	10/24/08 4:20	4.76388	-24	0
10/24/08 5:15	4.80208333	0	0	10/24/08 5:15	4.80208	0	0
10/24/08 5:20	4.80555555	-24	0	10/24/08 5:20	4.80555	-24	0
10/24/08 6:15	4.84375	0	0	10/24/08 6:15	4.84375	0	0
10/24/08 6:20	4.84722222	-24	0	10/24/08 6:20	4.84722	-24	0
10/24/08 7:15	4.88541666	0	0	10/24/08 7:15	4.88541	0	0
10/24/08 7:20	4.88888888	-24	0	10/24/08 7:20	4.88888	-24	0
10/24/08 8:15	4.92708333	0	0	10/24/08 8:15	4.92708	0	0
10/24/08 8:20	4.93055555	-24	0	10/24/08 8:20	4.93055	-24	0
10/24/08 8:40	4.94444444	0	0	10/24/08 8:40	4.94444	0	0
10/24/08 9:15	4.96875	-4.38364	0	10/24/08 9:15	4.96875	-4.38364	0
10/24/08 9:20	4.97222222	-28.38364	0	10/24/08 9:20	4.97222	-28.38364	0
10/24/08 10:15	5.01041666	-4.38364	0	10/24/08 10:15	5.01041	-4.38364	0
10/24/08 10:20	5.01388888	-28.38364	0	10/24/08 10:20	5.01388	-28.38364	0
10/24/08 11:15	5.05208333	-4.38364	0	10/24/08 11:15	5.05208	-4.38364	0
10/24/08 11:20	5.05555555	-28.38364	0	10/24/08 11:20	5.05555	-28.38364	0
10/24/08 17:00	5.29166666	-4.38364	0	10/24/08 17:00	5.29166	-4.38364	0
10/31/08 12:00	12.0833333	0	0	10/31/08 12:00	12.0833	0	0
10/31/08 18:00	12.3333333	0	0	10/31/08 18:00	12.3333	0	0

Appendix 19. Time variable boundary conditions for plots 29-32.

Plot 29

Date	**Time**	**Fluxtop**	**cTop**
M/D/Y hour	(days)	(cm)	(mmol/cm^3)
10/19/08 10:00			
10/24/08 8:40	4.944444	0	0
10/24/2008 15:00	5.208333	-4.38364	0
10/24/2008 15:04	5.211111	-38.52	0.33617
10/24/08 16:00	5.250000	-4.38364	0
10/24/08 16:55	5.288194	-52.38364	0
10/24/08 17:04	5.294444	-4.38364	0
10/31/08 12:00	12.083333	0	0
10/31/08 18:00	12.333333	0	0

Plot 30

10/19/08 10:00			
10/23/2008 16:00	4.250000	0	0
10/23/2008 16:04	4.252778	-38.52	0.33617
10/24/08 8:40	4.944444	0	0
10/24/08 16:00	5.250000	-4.38364	0
10/24/08 16:55	5.288194	-52.38364	0
10/24/08 17:00	5.291667	-4.38364	0
10/31/08 12:00	12.083333	0	0
10/31/08 18:00	12.333333	0	0

Plot 31			
Date	**Time**	**Fluxtop**	**cTop**
M/D/Y hour	(days)	(cm)	(mmol/cm^3)
10/20/08 19:05	1.378472	0	0
10/20/08 19:09	1.381250	-38.52	0.33617
10/24/08 8:40	4.944444	0	0
10/24/08 16:00	5.250000	-4.38364	0
10/24/08 16:55	5.288194	-52.38364	0
10/24/08 17:00	5.291667	-4.38364	0
10/31/08 12:00	12.083333	0	0
10/31/08 18:00	12.333333	0	0
Plot 32			
10/19/08 10:00			
10/24/08 8:40	4.944444444	0	0
10/24/2008 12:00	5.083333333	-4.38364	0
10/24/2008 12:04	5.086111111	-38.52	0.33617
10/24/08 16:00	5.25	-4.38364	0
10/24/08 16:55	5.288194444	-52.38364	0
10/24/08 17:04	5.294444444	-4.38364	0
10/31/08 12:00	12.08333333	0	0
10/31/08 18:00	12.33333333	0	0

References

APHA. (1989). Automated ferricyanide method for chloride determination in "Standard methods for examination of water and wastewater".

Beven, K., Germann, P. (1982) Macropores and water flow in soils. Water Resources Res. 18:1311-1325.

Brady N.C., Weil R.R. (2003). Elements of the nature and properties of soils 2nd Edition. Upper Saddle River, NJ: Prentic-Hall, Inc.

Caron J., Ben Jemia S., Gallichand J., Trepanier L. (1999). Field bromide transport under transient-state: Monitoring with Time Domain Reflectometry and porous cup. Soil Sci. Soc. Am. J. 63:1544–1553

Ehlers W. (1975). Observations on earthworm channels and infiltration on tilled and untilled loess soil. Soil Sci. Soc. Am. J. 119:242-249.

Ellsworth T.R., Boast C.W. (1996). Spatial structure of solute transport variability in an unsaturated field soil. Soil Sci. Soc. Am. J. 60:1355-1367.

Evans J.R., Edwards D.R., Workman S.R., Williams R.M. (1998). Response of runoff diazinon concentration to formulation and post applied irrigation. Transactions of the ASABE 41:1323-1329.

Hassan, H.M., Warrick,A.W., Amoozegar F. (1983). Sampling volume effects on determining salt in a soil profile. Soil Sci. Soc. Am. J. 47:1265-1267

Hosang J. (1993) Field-scale solute transport – spatially interpolating the parameters of a transfer function model. Geoderma 60:119-133.

Jiang Z., Wu Q.J., Brown L.C., Workman S.R. (1997) Water table depth and rainfall timing effect on Br^- and NO_3^- transport. Journal of Irrigation and Drainage Engineering 123:279-284.

Journel, A.G., and Huijbregts Ch. J. (1991). Mining geostatistics. Academic Press, London, 600 pp.

Jury W.A., and Horton R. (2004). Soil Physics. 6th Ed. Published by John Wiley and sons. Inc.

Kazemi H.V., Anderson S.H., Goyne K.W., Gantzer C.J. (2008). Spatial variability of bromide and atrazine transport parameters for a Udipsamment. Geoderma 144:545-556.

Kung K.-J.S., Kladivko E.J., Gish T.J., Steenhuis T.S., Bubenzer G., Helling C.S. (2000a). Quantifying preferential flow by breakthrough of sequentially applied tracers: Silt loam soil. Soil Sci. Soc. Am. J. 64:1296-1304.

Kung K.-J.S., Steenhuis T.S., Kladivko E.J., Gish T.J., Bubenzer G., Helling C.S. (2000b). Impact of preferential flow on the transport of adsorbing and non-adsorbing tracers. Soil Sci. Soc. Am. J. 64:1290-1296.

Legout A., Legout C., Nys C., Dambrine E. (2009). Preferential flow and slow convective chloride transport through the soil of a forested landscape (Fougères, France). Geoderma 151:179-190.

McLay C.D.A., Cameron K.C., McLaren R.G. (1991). Effect of time of application and continuity of rainfall on leaching of surface applied chemicals. Australian Journal of Soil Research. 29:1-9

Netto A.M., Pieritz R.A., Gaudet J.P. (1999) Field study on the local variability of soil water content and solute concentration. Journal of Hydrology 215:23-37.

Nielsen, D.R., Wendroth, O. 2003. Spatial and temporal statistics. Catena Verlag GMBH, 35447 Reiskirchen, Germany.

Olson G.L., Cassel D.K. (1999) Bromide leaching on a Piedmont toposequence. Soil Sci. Soc. Am. J. 63:1319-1326.

Reichardt K., Osny O.S., Villagra M.M., Turatti A.L., Pedrosa Z.O. (1993) Hydraulic variability in space and time in a dark red latosol of the tropics. Geoderma 60:159-168.

Sander, Kip Warren (1990). Movement of atrazine, cyanazine, and simazine in conventional and conservation tillage. Ph.D. dissertation, University of Kentucky, United States -- Kentucky. Retrieved June 30, 2010, from Dissertations & Theses @ University of Kentucky.(Publication No. AAT 9025255).

Shipitalo M.J., Dick W.A., Edwards W.M. (2000) Conservation tillage and macropore factors that affect water movement and the fate of chemicals. Soil and Tillage Research. 53:167-183

Shumway, R.H., Stoffer, D.S. 2000. Time series analysis and its applications. Springer-Verlag New York, Inc.

Šimůnek, J., Huang K., and van Genuchten, M. Th. (1998). The HYDRUS code for simulating the one-dimensional movement of water, heat, and multiple solutes in variably-saturated media. Version 6.0, Research Report No. 144, U.S. Salinity Laboratory, USDA, ARS, Riverside, California, 164 pp

Ünlü K., Nielsen D.R., Biggar J.W., Morkoc F. (1990) Statistical parameters characterizing the spatial variability of selected soil hydraulic properties. Soil Sci. Soc. Am. J. 54:1537-1547.

Vanderborght J., and Vereecken H. (2007) Review of dispersivities for transport modeling in soils. Vadose Zone J 6:29-52

van Genuchten, M. Th. (1980) A closed-form equation for predicting
the hydraulic conductivity of unsaturated soils. Soil Sci. Soc. Am. J. 44:892-898.

van Genuchten, M. Th., Leij f.J., and Yates S.R. (1991) The RETC Code for quantifying the hydraulic functions of unsaturated soils, Version 1.0. EPA Report 600/2-91/065, U.S. Salinity Laboratory, USDA, ARS, Riverside, California.

Walker A., Rodriguez-Cruz M.S., Mitchel M.J. (2005) Influence of ageing of residues on the availability of herbicides for leaching. Env. Pollution 133:43-51.

Wendroth O., Koszinski S., Pena-Yewtukhiv E. (2006) Spatial association among soil hydraulic properties, soil texture, and geoelectrical resistivity. Vadose Zone J. 5:341-355. DOI: 10.2136/vzj2005.0026.

Wendroth O., Pohl W., Koszinski S., Rogasik H., Ritsema C.J., Nielsen D.R. (1999a) Spatio-temporal patterns and covariance structures of soil water status in two Northeast-German field sties. Journal of Hydrology. 215:38-58.

Wendroth O., Rogasik H., Koszinski S., Ritsema C.J., Dekker L.W., and Nielsen D.R. (1999b) State-space prediction of field-scale soil water content time series in a sandy loam. Soil and Tillage Research 50:85-93.

Wendroth, O. and J. Simunek. 1999. Soil hydraulic properties determined from evaporation and tension infiltration experiments and their use for modeling field moisture status. In: Van Genuchten, mTh. And F.J. Leij (Eds). Proc. Int. Workshop on "Characterization and measurement of the hydraulic properties of unsaturated porous media", Riverside, California, pp. 737-748.

Wendroth, O., and N. Wypler. 2007. Unsaturated hydraulic properties: Laboratory evaporation. In: M.R. Carter and E.G. Gregorich (Eds.) Soil sampling and methods of analysis. Canadian Society of Soil Science, 2nd ed., CRC Press, Boca Raton, FL, pp. 1089-1106.

Wind, G.P. 1968. Capillary conductivity data estimated by a simple method. p 181-191.In P.E. Rijtema and H. Wassink (ed.) Water in the unsaturated Zone. Proc. Wageningen Symp. June 1966.Vol.1, IASAH, Gentbrugge.

Zhang, R., Warrick, A.W., and Myers, D.E. (1990) Variance as function of sample support size. Mathematical Geology, Vol. 22, No.1.

Zhang, R., Warrick, A.W., and Myers, D.E. (1994) Heterogeneity, plot shape effect and optimum plot size. Geoderma, 62:183-197

VITA

Name: Vicente Vasquez

Date and place of birth: Nov. 21, 1979, Quito, Ecuador

University Education:

Pan American School of Agriculture. Honduras, Central America. BS degree in Agronomy.

Professional positions held:

2002-2005: Sunrite Farm Holdings, Quito, Ecuador. Oil Palm Industry

2005-2010: University of Kentucky, Graduate Student Assistantship

Currently: PhD student at Aarhus University, Denmark, Hydrological observatory HOBE

Professional publications:

Wendroth, O. and V. Vasquez. 2010. Field-scale bromide transport as a function of rainfall amount, intensity and application time delay. Abstracts, IUSS, Brisbane, Australia.

Wendroth, O., S. Koszinski, and V. Vasquez. 2011. Soil spatial variability. In: Huang, P.M., Y.C. Li, and M.E. Sumner (Eds.) Handbook of Soil Science, 2nd ed., CRC Press. (in press).

Contributions to Scientific Meetings and conferences:

Wendroth, O., C.J. Matocha, and V. Vasquez. 2010. Field-Scale Bromide Transport as a Function of Rainfall Amount, Intensity and Application Time Delay. Poster. 19th World Congress of Soil Science, IUSS, Brisbane, Australia, Aug. 01-06, 2010.

Wendroth, O., V. Vasquez, and C.J. Matocha. 2010. Impact of rainfall amount, intensity, and time lag on leaching behavior of a surface-applied Bromide tracer. Oral Presentation. Kentucky Water Resources Annual Symposium, March 22, 2010, Griffin Gate Marriott Resort, Lexington, KY

Vasquez, V., and O. Wendroth. 2008. Spatial scale of bromide leaching into initially dry and wet soil. Poster, Annual Meeting, ASA-CSSA-SSSA, Oct. 5-9, 2008, Houston, TX.

Wendroth, O, V. Vasquez, and C.J. Matocha. 2010. Spatial Variation Scales of Rainfall Characteristics and Bromide Leaching. American Geophysical Union Fall Meeting, San Franscisco, CA.

Vicente Vasquez